



CMAP, Jeudi 29 Juin 2017, l'X

Numerical implementation of functional algorithms for 2D and 3D acoustic tomography problems

Andrey S. Shurup
Laboratory of inverse problems in acoustics



Faculty of Physics,
Acoustics Department,
M.V. Lomonosov Moscow State University

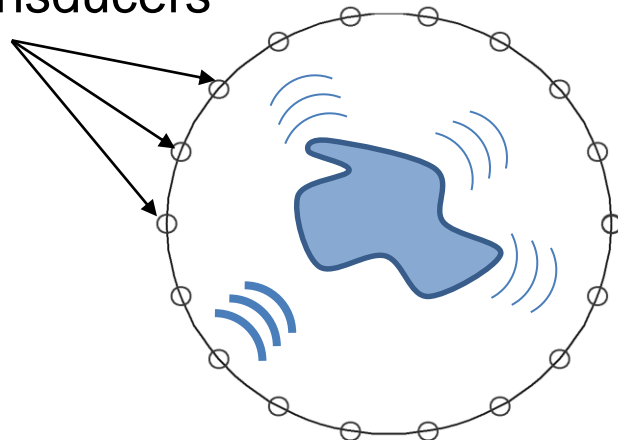


Acoustic tomography is a powerful tool for studying natural media that are transparent to acoustic waves; it is employed when direct measurement of medium characteristics is difficult or impossible.

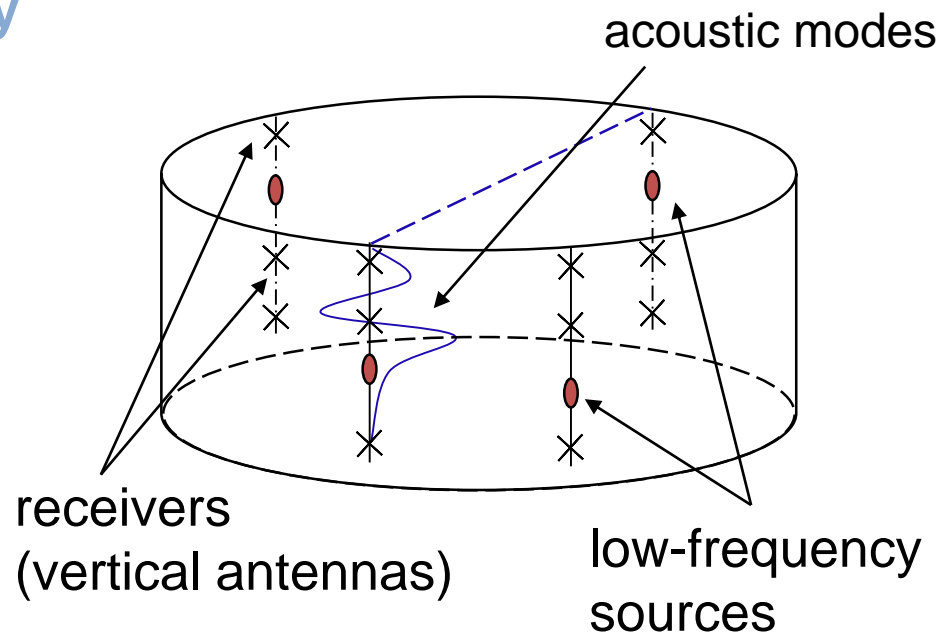
Medical diagnostics, geophysical researches and ocean tomography are the main areas of acoustic tomography application.

Ultrasound medical tomography

Transmitting-receiving transducers

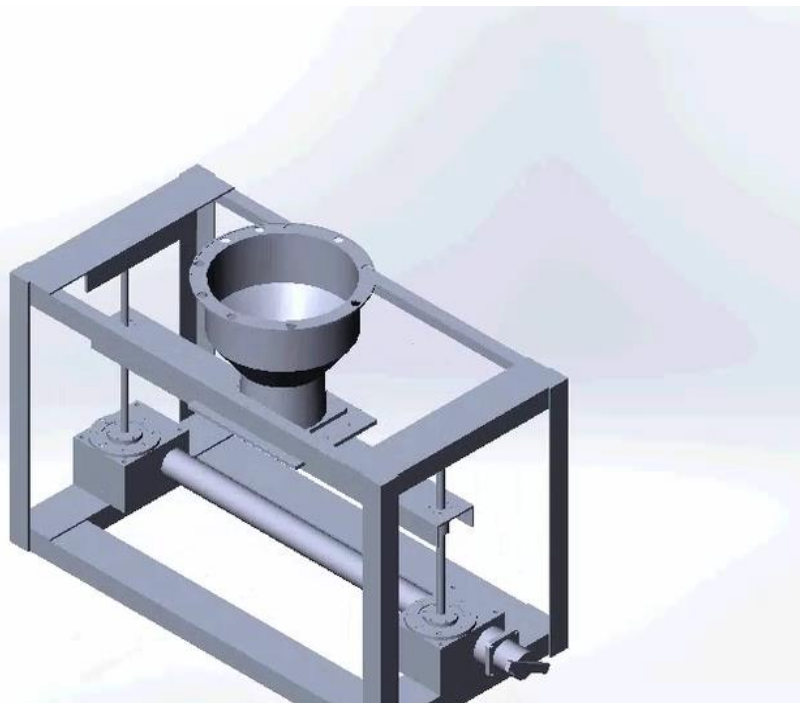


Ocean mode tomography



**Acoustic Tomograph
developing at Faculty of Physics,
Acoustics Department, MSU,
for the reconstruction of sound speed,
absorption and blood flow in the soft
biological tissues (first of all in the breast)
for the cancer diagnostic purposes.**

Top view



General view

The circular rotating antenna with the uniquely distributed 26 emitting-receiving transducers are equivalent to a fixed multi-element antenna with 256 transducers.

The main characteristics of a medium which influence the propagation of acoustic waves are space distributions of

sound speed $c(\mathbf{r})$,

density $\rho(\mathbf{r})$,

amplitude attenuation coefficient $\alpha(\mathbf{r}, \omega)$,

and vector field of flows $\mathbf{v}(\mathbf{r})$,

here – ω is cycle frequency.

For the solution of inverse scattering problems in acoustical applications it is perspective to use algorithms, which allow to reconstruct all the mentioned above properties of a medium for a wide class of scatterers in a joint tomography scheme.

Motivation

The known methods for the solution of acoustic tomography problems are **approximate**. The linear approximation is generally applied with iteration procedures and regularizations. The general perturbation theory is also considered.

There are quite **mathematically rigorous** (at least, for a rather wide class of scatterers) functional-analytical methods for solving the inverse problems, which were initially developed in quantum mechanics. Since the Schrödinger equation in the monochromatic (isoenergetic) case is the same as the Helmholtz equation up to notation, it gives the idea to apply these methods for acoustic applications. But the detail investigations are required based on numerical modeling to understand applicability of these methods for acoustics inverse problems.

In this report possibilities of the functional algorithm [1-4] for the reconstruction of both scalar and vector inhomogeneities for the purposes of 2D and 3D acoustic tomography are discussed.

1. Novikov R.G. *The inverse scattering problem on a fixed energy level for the two-dimensional Schrödinger operator* // *Journal of Functional Analysis*. 1992. V. 103. N 2. P. 409–463.
2. Novikov R.G., Santacesaria M. *Monochromatic reconstruction algorithms for two-dimensional multi-channel inverse problems* // *International Mathematics Research Notices*. 2013. V. 2013. N 6. P. 1205–1229.
3. Agaltsov A.D., Novikov R.G. *Riemann–Hilbert problem approach for two-dimensional flow inverse scattering* // *J. Math. Phys.* 2014. V. 55. N 10. P. 103502-1–103502-25.
4. Agaltsov A.D. *On the reconstruction of parameters of a moving fluid from the Dirichlet-to-Neumann map* // *Eurasian Journal of Mathematical and Computer Applications*. 2016. V. 4. N 1. P. 4–11.

Structure of report:

- Statement of 2D problem
- Reconstruction algorithm
- Numerical modeling
- Very recent results for 3D inverse problem
- Conclusions / Perspectives

Statement of 2D problem

It is assumed that the investigated area is surrounded over perimeter by the quasi-point transducers emitting and receiving acoustic fields $p(\mathbf{r}; \omega)$.

In the tomographic area there are an unknown **vector inhomogeneity**

$$\mathbf{A}(\mathbf{r}, \omega_j) = \omega_j \frac{\mathbf{v}(\mathbf{r})}{c^2(\mathbf{r})} + i\nabla \ln \sqrt{\rho(\mathbf{r})}, \quad \mathbf{r} \in V_\gamma$$

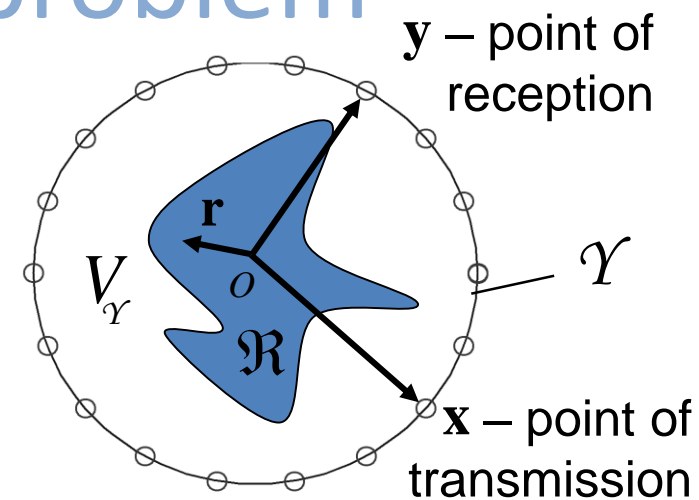
and an unknown **scalar inhomogeneity**

$$v(\mathbf{r}, \omega_j) = \omega_j^2 \left(\frac{1}{c_0^2} - \frac{1}{c^2(\mathbf{r})} \right) - 2i \omega_j \frac{\alpha(\mathbf{r}, \omega_j)}{c(\mathbf{r})},$$

ω_j – circular frequency, c_0 – known background sound speed value.

$\mathbf{v}(\mathbf{r})$ – flow velocity, $c(\mathbf{r})$ – sound speed,

$\alpha(\mathbf{r}, \omega_j)$ – absorption, $\rho(\mathbf{r})$ – density.



How to reconstruct these quantities, if we know acoustic fields $p(\mathbf{y}; \omega)$?

Solution of 2D problem

Acoustic fields in the considered area satisfy Helmholtz equation :

$$\nabla^2 p(\mathbf{r}; \omega_j) + \frac{\omega_j^2}{c_0^2} p(\mathbf{r}; \omega_j) = v(\mathbf{r}, \omega_j) p(\mathbf{r}; \omega_j) - 2i \mathbf{A}(\mathbf{r}, \omega_j) \nabla p(\mathbf{r}; \omega_j),$$

where index j corresponds to the particular frequency in the considered frequency range. The algorithm how to get the approximate solution of this equation is regarded in (*). By using this algorithm we can get estimates of the inhomogeneities $\mathbf{A}(\mathbf{r}, \omega_j)$, $v(\mathbf{r}, \omega_j)$ in the form:

$$\mathbf{A}^{\text{div}} = \mathbf{A} + \nabla \Phi, \quad v^{\text{div}} = v - i\Delta \Phi + (\nabla \Phi)^2 + 2\mathbf{A} \nabla \Phi.$$

$$\begin{cases} \Delta \Phi(\mathbf{r}, \omega_j) = -\text{div } \mathbf{A}(\mathbf{r}, \omega_j), \\ \Phi(\mathbf{r}, \omega_j) \xrightarrow[|\mathbf{r}| \rightarrow \infty} 0. \end{cases} \implies \mathbf{A} = \mathbf{A}^{\text{div}} - \nabla \Phi$$

Solenoidal component

unknown function

Potential (irrotational) component

$\text{div } \mathbf{A}^{\text{div}} = 0$

$\text{rot } (-\nabla \Phi) = 0$

(*). Agaltsov A.D., Novikov R.G. Riemann–Hilbert problem approach for two-dimensional flow inverse scattering // J. Math. Phys. 2014. N 55. 103502.

Reconstruction algorithm that uses data from a quasi-point transducers

Step 1. Calculation of operator $(\mathcal{F} - \mathcal{F}_0)(\mathbf{y}, \mathbf{x}; \omega_j)$

$$\frac{\partial u}{\partial n}\Big|_{\gamma} = \hat{\mathcal{F}}(\omega_j)\left(u\Big|_{\gamma}\right), \frac{\partial u_0}{\partial n}\Big|_{\gamma} = \hat{\mathcal{F}}_0(\omega_j)\left(u_0\Big|_{\gamma}\right), \nabla^2 u_0 + k_{0j}^2 u_0 = 0, \quad k_{0j} = \frac{\omega_j}{c_0}.$$

Step 2. Estimation of Faddeev generalized scattering amplitude $h^\pm(\omega_j)$ from $(\mathcal{F} - \mathcal{F}_0)(\mathbf{y}, \mathbf{x}; \omega_j)$

Step 3. Reconstruction of inhomogeneities $\mathbf{A}^{\text{div}}(\mathbf{r}, \omega_j)$, $\nu^{\text{div}}(\mathbf{r}, \omega_j)$ from $h^\pm(\omega_j)$, via solving some Riemann–Hilbert problem on Faddeev eigenfunctions.

Step 4. Reconstruction of medium properties $c(\mathbf{r})$, $\mathbf{v}(\mathbf{r})$, $\alpha(\mathbf{r}, \omega_j)$, $\rho(\mathbf{r})$ from $\mathbf{A}^{\text{div}}(\mathbf{r}, \omega_j)$, $\nu^{\text{div}}(\mathbf{r}, \omega_j)$.

Reconstruction algorithm.

Step 1. Estimation of operator

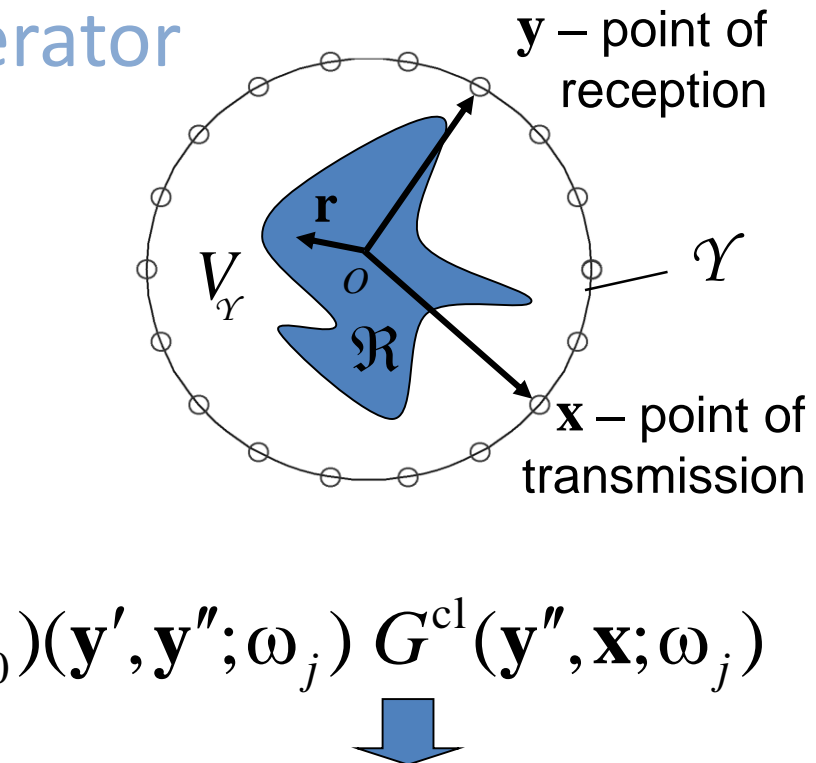
$$(F - F_0)(\mathbf{y}, \mathbf{x}; \omega_j).$$

System of linear equations

$$G^{\text{cl}}(\mathbf{y}, \mathbf{x}; \omega_j) = G_0^{\text{cl}}(\mathbf{y} - \mathbf{x}; \omega_j) +$$

$$\int_{\gamma} d\mathbf{y}' \int_{\gamma} d\mathbf{y}'' G_0^{\text{cl}}(\mathbf{y} - \mathbf{y}'; \omega_j) (F - F_0)(\mathbf{y}', \mathbf{y}''; \omega_j) G^{\text{cl}}(\mathbf{y}'', \mathbf{x}; \omega_j)$$

Green's function of medium without scatterer is calculated analytically.



Green's function of medium with scatterer is estimated in experiment.

$$G_0^{\text{cl}}(\mathbf{y} - \mathbf{x}; \omega_j) = -\frac{i}{4} H_0^{(1)}(k_{0j} |\mathbf{y} - \mathbf{x}|)$$

Reconstruction algorithm.

Step 1. Estimation of $(\tilde{F} - \tilde{F}_0)(\mathbf{y}, \mathbf{x}; \omega_j)$

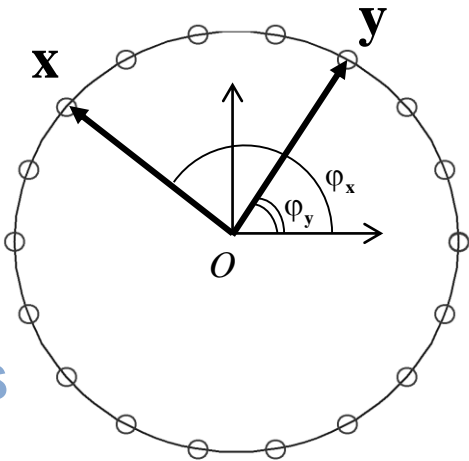
$$\mathbf{x} = (R_0, \varphi_x) \quad \mathbf{y} = (R_0, \varphi_y)$$

$$G(\varphi_y, \varphi_x; \omega_j) = \sum_{q_y=-\infty}^{\infty} \sum_{q_x=-\infty}^{\infty} \tilde{\tilde{G}}(q_y, q_x; \omega_j) \exp(i q_x \varphi_x) \cdot \\ \cdot \exp(i q_y \varphi_y)$$

angular
harmonics

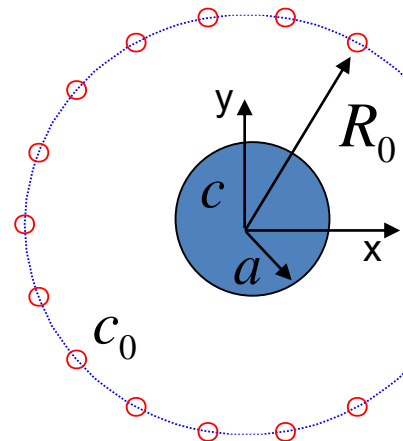
$$(2\pi R_0)^2 \sum_{q'_y=-\infty}^{\infty} \sum_{q'_x=-\infty}^{\infty} \tilde{\tilde{G}}_0^{\text{cl}}(q_y, -q'_y; \omega_j) (\tilde{\tilde{F}} - \tilde{\tilde{F}}_0)(q'_y, q'_x; \omega_j) \tilde{\tilde{G}}^{\text{cl}}(q'_x, -q_x; \omega_j) = \\ = \tilde{\tilde{G}}^{\text{cl}}(q_y, q_x; \omega_j) - \tilde{\tilde{G}}_0^{\text{cl}}(q_y, q_x; \omega_j); \quad q_x, q_y \in \mathbb{Z}$$

$$\tilde{\tilde{G}}_0^{\text{cl}}(q_y, q_x; \omega_j) = -\frac{i}{4} \delta_{q_x, -q_y} H_{q_y}^{(1)}(k_{0j} R_0) J_{q_y}(k_{0j} R_0)$$



system of the
linear equations
for estimating
 $(\tilde{\tilde{F}} - \tilde{\tilde{F}}_0)(q_y, q_x; \omega_j)$

Some numerical results

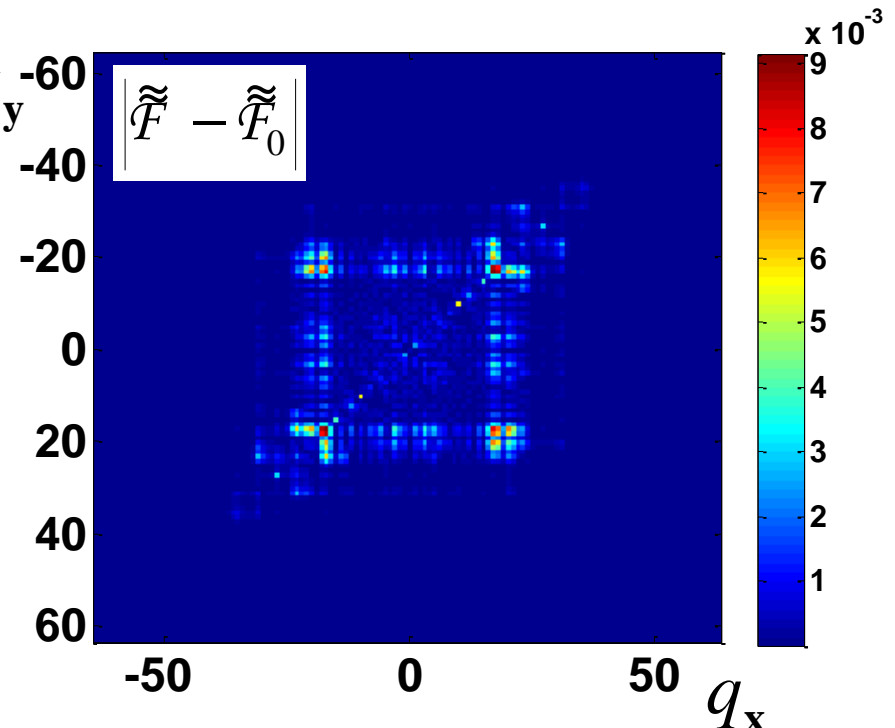
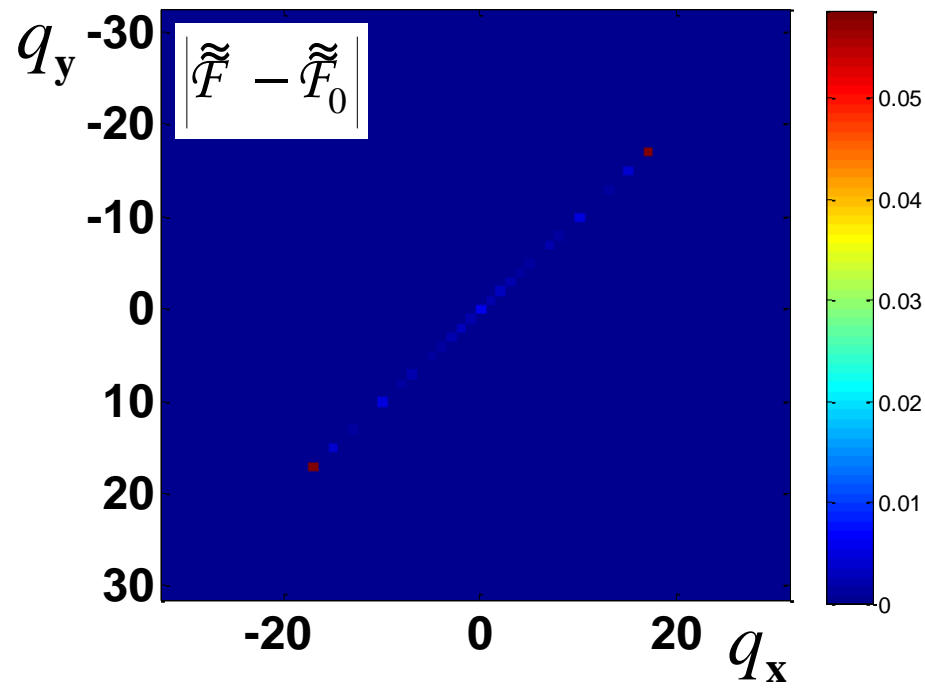
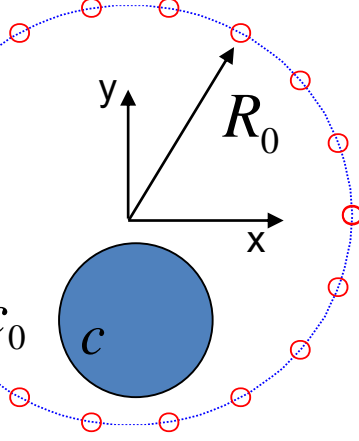


Symmetric
cylindrical
scatterer

$$R_0 \approx 6.7 \lambda \quad c_0/c = 0.75$$

Not symmetric
cylindrical
scatterer

$$a = 3 \lambda \quad \begin{cases} x_0 = 0 \\ y_0 = -3 \lambda \end{cases} \quad \lambda = 15 \text{ m}$$



Reconstruction algorithm.

Step 2. Estimation of $h^\pm(\varphi, \varphi'; \omega_j)$.

$$h^\pm(\mathbf{k}, \mathbf{l}; \omega_j) =$$

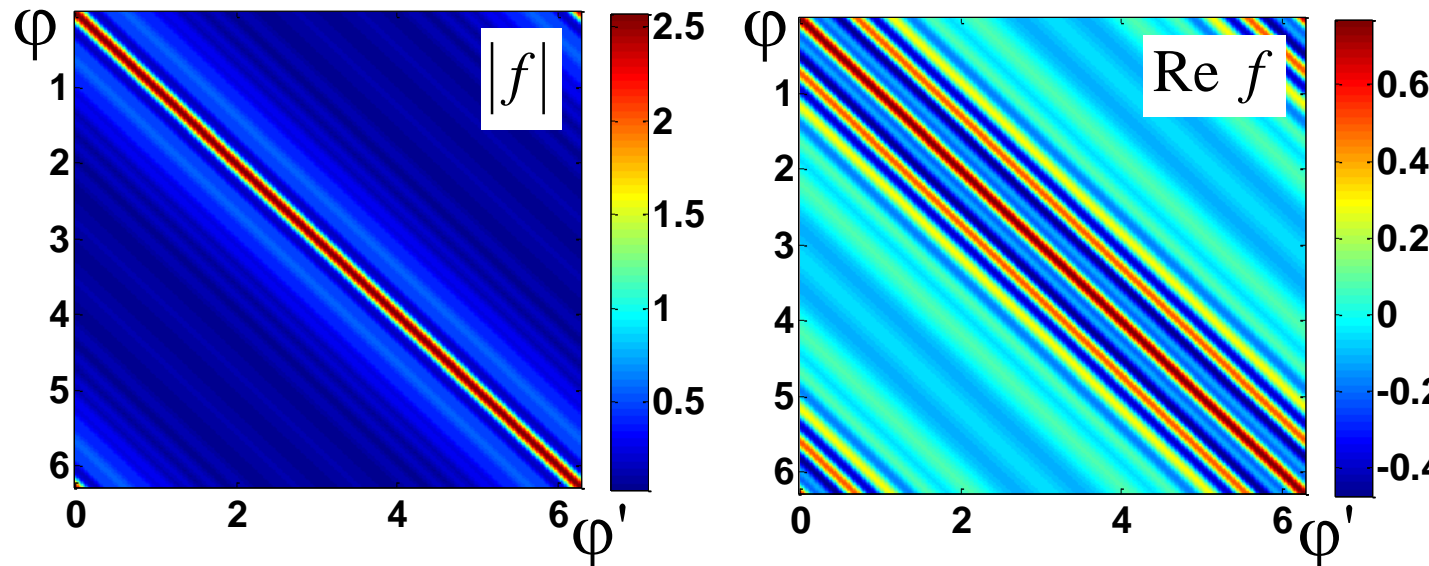
$$= \frac{1}{(2\pi)^2} \int_{\mathcal{Y}} d\mathbf{y}' \int_{\mathcal{Y}} d\mathbf{y}'' \exp(-i \mathbf{l} \mathbf{y}') (F - F_0)(\mathbf{y}', \mathbf{y}''; \omega_j) \Psi^\pm(\mathbf{y}'', \mathbf{k}; \omega_j),$$

$$\Psi^\pm(\mathbf{y}, \mathbf{k}; \omega_j) = \exp(i \mathbf{k} \mathbf{y}) + \int_{\mathcal{Y}} A^\pm(\mathbf{y}, \mathbf{y}'', \mathbf{k}; \omega_j) \Psi^\pm(\mathbf{y}'', \mathbf{k}; \omega_j) d\mathbf{y}'',$$

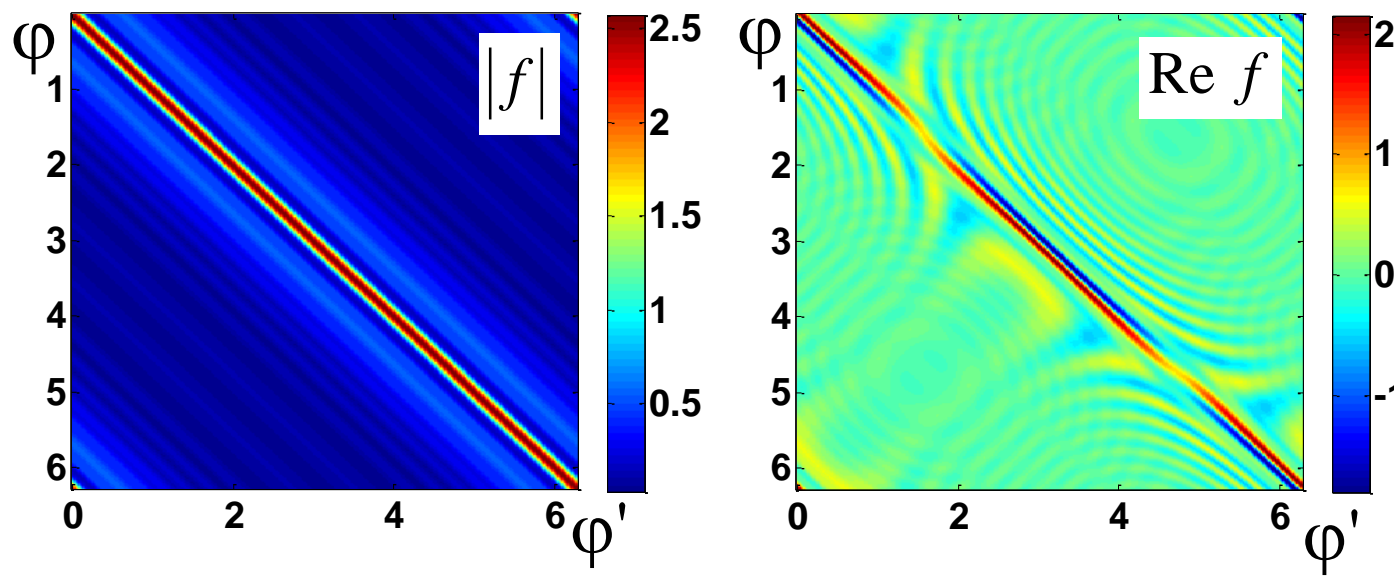
$$A^\pm(\mathbf{y}, \mathbf{y}'', \mathbf{k}; \omega_j) = \int_{\mathcal{Y}} G_{\text{Fad}}^\pm(\mathbf{y} - \mathbf{y}', \mathbf{k}; \omega_j) (F - F_0)(\mathbf{y}', \mathbf{y}''; \omega_j) d\mathbf{y}',$$

$$\mathbf{k} = \{k_{0j}, \varphi\}, \quad \mathbf{l} = \{k_{0j}, \varphi'\}, \quad \mathbf{y} \in \mathcal{Y}.$$

Some numerical results



Symmetric
cylindrical
scatterer



Not
symmetric
cylindrical
scatterer

Reconstruction algorithm.

Step 3. Reconstruction of
inhomogeneities $\mathbf{A}^{\text{div}}(\mathbf{r}, \omega_j)$, $v^{\text{div}}(\mathbf{r}, \omega_j)$.

$$h^\pm(\mathbf{k}, \mathbf{l}; \omega_j) \equiv h^\pm(\varphi, \varphi'; \omega_j), \quad \mathbf{r} = \{x, y\},$$

$$\begin{aligned} 1. \quad Q^\pm(\mathbf{r}, \varphi, \varphi'; \omega_j) &\equiv \\ &\equiv h^\pm(\varphi, \varphi'; \omega_j) \exp[\underline{i k_0 j \{x(\cos \varphi' - \cos \varphi) + y(\sin \varphi' - \sin \varphi)\}}] \cdot \\ &\quad \cdot \theta[\pm \sin(\varphi' - \varphi)], \end{aligned}$$

$$\begin{aligned} 2. \quad B(\mathbf{r}, \varphi, \varphi'; \omega) &= \frac{i}{2} \int_0^{2\pi} Q^-(\mathbf{r}, \varphi'', \varphi'; \omega) \chi^+(\varphi - \varphi'') d\varphi'' - \\ &- \frac{i}{2} \int_0^{2\pi} Q^+(\mathbf{r}, \varphi'', \varphi'; \omega) \chi^-(\varphi - \varphi'') d\varphi'', \quad \chi^\pm(\varphi) = 1/[1 - (1 \mp 0) \exp(i\varphi)]. \end{aligned}$$

Reconstruction algorithm.

**Step 3. Reconstruction of
inhomogeneities** $\mathbf{A}^{\text{div}}(\mathbf{r}, \omega_j)$, $v^{\text{div}}(\mathbf{r}, \omega_j)$.

$$3. \quad \mu^{\text{cl}}(\mathbf{r}, \varphi; \omega_j) + \int_0^{2\pi} B(\mathbf{r}, \varphi, \varphi'; \omega_j) \mu^{\text{cl}}(\mathbf{r}, \varphi'; \omega_j) d\varphi' = 1$$

$$\mu^{\text{cl}}(\mathbf{r}, \varphi; \omega_j) \equiv \exp[-ik_{0j}\{x \cos \varphi + y \sin \varphi\}] u(\mathbf{r}, \varphi; \omega_j)$$

$$4. \quad \mu^-(\mathbf{r}, \varphi; \omega_j) = \mu^{\text{cl}}(\mathbf{r}, \varphi; \omega_j) + \pi i \int_0^{2\pi} Q^-(\mathbf{r}, \varphi, \varphi'; \omega_j) \mu^{\text{cl}}(\mathbf{r}, \varphi'; \omega_j) d\varphi'$$

$$\mu^+(\mathbf{r}, \varphi; \omega_j) = \mu^{\text{cl}}(\mathbf{r}, \varphi; \omega_j) + \pi i \int_0^{2\pi} Q^+(\mathbf{r}, \varphi, \varphi'; \omega_j) \mu^{\text{cl}}(\mathbf{r}, \varphi'; \omega_j) d\varphi'$$

Reconstruction algorithm.

**Step 3. Reconstruction of
inhomogeneities** $\mathbf{A}^{\text{div}}(\mathbf{r}, \omega_j)$, $v^{\text{div}}(\mathbf{r}, \omega_j)$.

$$V^-(\mathbf{r}, \omega_j) = \frac{k_{0j}}{2\pi} \left(i \frac{\partial}{\partial x} + \frac{\partial}{\partial y} \right) \int_0^{2\pi} \mu^-(\mathbf{r}, \varphi; \omega_j) \exp(i\varphi) d\varphi$$

$$V^+(\mathbf{r}, \omega_j) = k_{0j} \left(i \frac{\partial}{\partial x} - \frac{\partial}{\partial y} \right) \left[\frac{\int_0^{2\pi} \mu^+(\mathbf{r}, \varphi; \omega_j) \exp(-i\varphi) d\varphi}{\int_0^{2\pi} \mu^+(\mathbf{r}, \varphi; \omega_j) d\varphi} \right]$$

$$a^-(\mathbf{r}, \omega_j) = 2 \left(\frac{\partial}{\partial x} + i \frac{\partial}{\partial y} \right) \ln \left\{ \int_0^{2\pi} \mu^+(\mathbf{r}, \varphi; \omega_j) d\varphi \right\}$$

$$a^+(\mathbf{r}, \omega_j) = -2 \left(\frac{\partial}{\partial x} - i \frac{\partial}{\partial y} \right) \ln \left\{ \int_0^{2\pi} \mu^+(\mathbf{r}, \varphi; \omega_j) d\varphi \right\}$$

Reconstruction algorithm.

**Step 3. Reconstruction of
inhomogeneities** $\mathbf{A}^{\text{div}}(\mathbf{r}, \omega_j)$, $v^{\text{div}}(\mathbf{r}, \omega_j)$.

$$v^{\text{div}}(\mathbf{r}, \omega_j) \equiv \frac{1}{2} [V^-(\mathbf{r}, \omega_j) + V^+(\mathbf{r}, \omega_j)] - \frac{1}{8} a^+(\mathbf{r}, \omega_j) a^-(\mathbf{r}, \omega_j)$$

$$\mathbf{A}^{\text{div}}(\mathbf{r}, \omega) = \{A_x^{\text{div}}(\mathbf{r}, \omega), A_y^{\text{div}}(\mathbf{r}, \omega)\},$$

$$A_x^{\text{div}}(\mathbf{r}, \omega_j) \equiv \frac{i}{8} [a^-(\mathbf{r}, \omega_j) + a^+(\mathbf{r}, \omega_j)] = -\frac{1}{2} \frac{\partial}{\partial y} \ln \left\{ \int_0^{2\pi} \mu^+(\mathbf{r}, \varphi; \omega_j) d\varphi \right\}$$

$$A_y^{\text{div}}(\mathbf{r}, \omega_j) \equiv \frac{1}{8} [a^-(\mathbf{r}, \omega_j) - a^+(\mathbf{r}, \omega_j)] = \frac{1}{2} \frac{\partial}{\partial x} \ln \left\{ \int_0^{2\pi} \mu^+(\mathbf{r}, \varphi; \omega_j) d\varphi \right\}$$

Attractive features of steps 1-3 of Algorithm

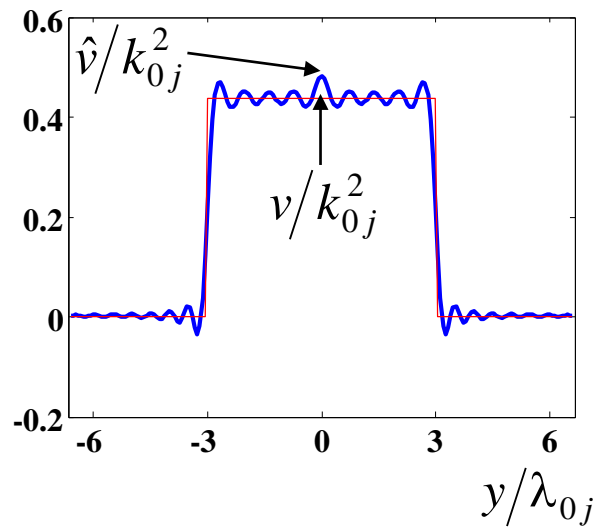
1. Linear integral equations - **no iterations** are required to solve inverse problem.
2. **Multiple scattering processes** are taken into account that allows to reconstruct scatterers beyond the Born's approximation.
3. Scatterer functions can be found for each point \mathbf{r} independently – **high speed of numerical realization**.
4. Generalization to the multi-frequency regime of sounding, i.e. **high noise stability**.
5. Possibility for the **joint reconstruction of scalar-vector inhomogeneities**.
6. Similar integral equations for 2D and 3D tomography.

Limitation of Algorithm

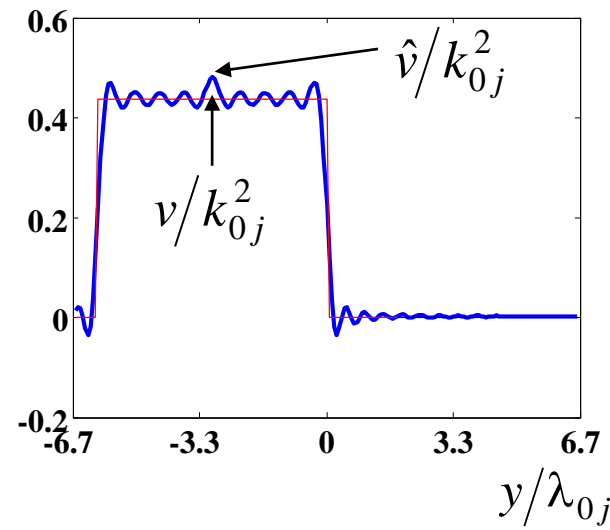
Space-spectrum components ξ of scatterers can be reconstructed **only in circle** $|\xi| < 2k_{0j}$.

Reconstruction results

Symmetric cylindrical scatterer



Not symmetric cylindrical scatterer



Reconstruction algorithm.

Step 4. Joint reconstruction of $c(\mathbf{r})$, $\mathbf{v}(\mathbf{r})$, $\alpha(\mathbf{r}, \omega)$, $\rho(\mathbf{r})$.

$$\mathbf{F}(\mathbf{r}) \equiv \frac{1}{\omega_j} \operatorname{rot} \mathbf{A}^{\operatorname{div}}(\mathbf{r}, \omega_j) = \operatorname{rot} \frac{\mathbf{v}(\mathbf{r})}{c^2(\mathbf{r})},$$

There are no needs
to estimate $\nabla \Phi$.

$$Q(\mathbf{r}, \omega_j) \equiv v^{\operatorname{div}} - \mathbf{A}^{\operatorname{div}}(\mathbf{r}, \omega_j) \cdot \mathbf{A}^{\operatorname{div}}(\mathbf{r}, \omega_j) =$$

$$= f_1 - \omega_j^2 f_2 + i \omega_j f_3 - 2i \omega_j \left(\frac{\omega_j}{\omega_0} \right)^{\zeta(\mathbf{r})} \frac{\alpha_0(\mathbf{r})}{c(\mathbf{r})}, \quad \alpha(\mathbf{r}, \omega_j) = \left(\frac{\omega_j}{\omega_0} \right)^{\zeta(\mathbf{r})} \alpha_0(\mathbf{r}).$$

$$\operatorname{Re} Q(\mathbf{r}, \omega) \rightarrow f_1 = \sqrt{\rho(\mathbf{r})} \nabla \frac{1}{\sqrt{\rho(\mathbf{r})}}, \quad f_2 = \frac{1}{c^2(\mathbf{r})} - \frac{1}{c_0^2} + \frac{\mathbf{v}(\mathbf{r})}{c^2(\mathbf{r})} \cdot \frac{\mathbf{v}(\mathbf{r})}{c^2(\mathbf{r})} \cong \frac{1}{c^2(\mathbf{r})} - \frac{1}{c_0^2},$$

$$\operatorname{Im} Q(\mathbf{r}, \omega) \rightarrow f_3 = \nabla \cdot \frac{\mathbf{v}(\mathbf{r})}{c^2(\mathbf{r})} - \frac{\mathbf{v}(\mathbf{r}) \cdot \nabla \ln \rho(\mathbf{r})}{c^2(\mathbf{r})}, \quad \zeta(\mathbf{r}), \quad \alpha_0(\mathbf{r}).$$

Reconstruction algorithm.

Step 4. Joint reconstruction of $c(\mathbf{r})$, $\mathbf{v}(\mathbf{r})$, $\alpha(\mathbf{r}, \omega)$, $\rho(\mathbf{r})$.

General case

$$\begin{cases} \operatorname{Re} Q(\mathbf{r}, \omega_1) = f_1 - \omega_1^2 f_2, \\ \operatorname{Re} Q(\mathbf{r}, \omega_2) = f_1 - \omega_2^2 f_2, \\ \dots \end{cases} \quad \xrightarrow{\hspace{1cm}} \quad f_1, \ f_2 \quad \xrightarrow{\hspace{1cm}} \quad c(\mathbf{r}), \ \rho(\mathbf{r})$$

$$\begin{cases} \operatorname{Im} Q(\mathbf{r}, \omega_1) = \omega_1 f_3 - 2 \omega_1 \left(\frac{\omega_1}{\omega_0} \right)^{\zeta(\mathbf{r})} \frac{\alpha_0(\mathbf{r})}{c(\mathbf{r})}, \\ \operatorname{Im} Q(\mathbf{r}, \omega_2) = \omega_2 f_3 - 2 \omega_2 \left(\frac{\omega_2}{\omega_0} \right)^{\zeta(\mathbf{r})} \frac{\alpha_0(\mathbf{r})}{c(\mathbf{r})}, \\ \dots \end{cases} \quad \xrightarrow{\hspace{1cm}} \quad \mathbf{v}(\mathbf{r}), \ \zeta(\mathbf{r}), \ \alpha_0(\mathbf{r}),$$

Particular case

Reconstruction of $\rho(\mathbf{r})$, $c(\mathbf{r})$, $\alpha(\mathbf{r}, \omega)$, without flows $\mathbf{v}(\mathbf{r})$.

V. A. Burov, A.L. Konyushkin and O. D. Rumyantseva, Acoustical Physics, 43, 4 (1997)

$$\begin{cases} \operatorname{Re} Q(\mathbf{r}, \omega_1) = f_1 - \omega_1^2 f_2, \\ \operatorname{Re} Q(\mathbf{r}, \omega_2) = f_1 - \omega_2^2 f_2, \\ \dots \end{cases} \quad \xrightarrow{\hspace{1cm}} \quad f_1, f_2 \quad \xrightarrow{\hspace{1cm}} \quad c(\mathbf{r}), \rho(\mathbf{r})$$

$$\operatorname{Im} Q(\mathbf{r}, \omega_j) = 2\omega_j \left(\frac{\omega_j}{\omega_0} \right)^{\zeta(\mathbf{r})} \frac{\alpha_0(\mathbf{r})}{c(\mathbf{r})}, \quad \xrightarrow{\hspace{1cm}} \quad \ln \left(\frac{\omega_j}{\omega_k} \right) [\zeta(\mathbf{r}) + 1] = \ln \left(\frac{\operatorname{Im} Q(\mathbf{r}, \omega_j)}{\operatorname{Im} Q(\mathbf{r}, \omega_k)} \right),$$

LSM estimation of $\zeta(\mathbf{r})$.

$$\xrightarrow{\hspace{1cm}} \zeta(\mathbf{r}) \quad \xrightarrow{\hspace{1cm}} \alpha_0(\mathbf{r}) = \frac{c(\mathbf{r})}{2\omega_j} \operatorname{Im} Q(\mathbf{r}, \omega_j) \left(\frac{\omega_0}{\omega_j} \right)^{\zeta(\mathbf{r})}$$

Reconstruction of attenuation power index $\zeta(\mathbf{r})$ when $\mathbf{v}(\mathbf{r}) \neq 0$

$$-2 \frac{\omega_j^{\zeta(\mathbf{r})+1}}{\omega_0^{\zeta(\mathbf{r})}} \frac{\alpha(\mathbf{r}, \omega_0)}{c(\mathbf{r})} + \omega_j \operatorname{div} \left\{ \frac{\mathbf{v}(\mathbf{r})}{c^2(\mathbf{r})} \right\} = \operatorname{Im} v^{\text{div}}(\mathbf{r}, \omega_j)$$

$$\frac{\frac{1}{\omega_2} \operatorname{Im} v^{\text{div}}(\mathbf{r}, \omega_2) - \frac{1}{\omega_1} \operatorname{Im} v^{\text{div}}(\mathbf{r}, \omega_1)}{\frac{1}{\omega_3} \operatorname{Im} v^{\text{div}}(\mathbf{r}, \omega_3) - \frac{1}{\omega_1} \operatorname{Im} v^{\text{div}}(\mathbf{r}, \omega_1)} = \begin{cases} \left(\frac{\omega_2}{\omega_1} \right)^{\zeta(\mathbf{r})} - 1 & 0.1 \leq \zeta(\mathbf{r}) \leq 3 \\ \left(\frac{\omega_3}{\omega_1} \right)^{\zeta(\mathbf{r})} - 1 & \omega_1 < \omega_2 < \omega_3 \end{cases}$$

The possible multi frequency generalization:

$$\prod_{\{j1, j2, j3\}} \frac{\frac{1}{\omega_{j2}} \operatorname{Im} v^{\text{div}}(\mathbf{r}, \omega_{j2}) - \frac{1}{\omega_{j1}} \operatorname{Im} v^{\text{div}}(\mathbf{r}, \omega_{j1})}{\frac{1}{\omega_{j3}} \operatorname{Im} v^{\text{div}}(\mathbf{r}, \omega_{j3}) - \frac{1}{\omega_{j1}} \operatorname{Im} v^{\text{div}}(\mathbf{r}, \omega_{j1})} = \prod_{\{j1, j2, j3\}} \frac{\left(\frac{\omega_{j2}}{\omega_{j1}} \right)^{\zeta(\mathbf{r})} - 1}{\left(\frac{\omega_{j3}}{\omega_{j1}} \right)^{\zeta(\mathbf{r})} - 1}$$

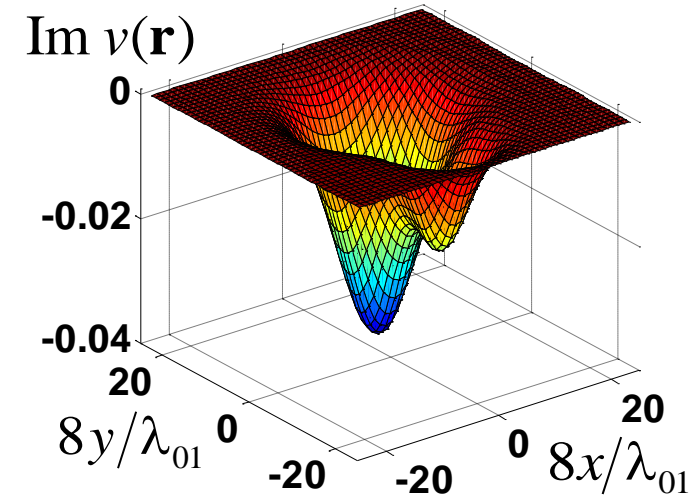
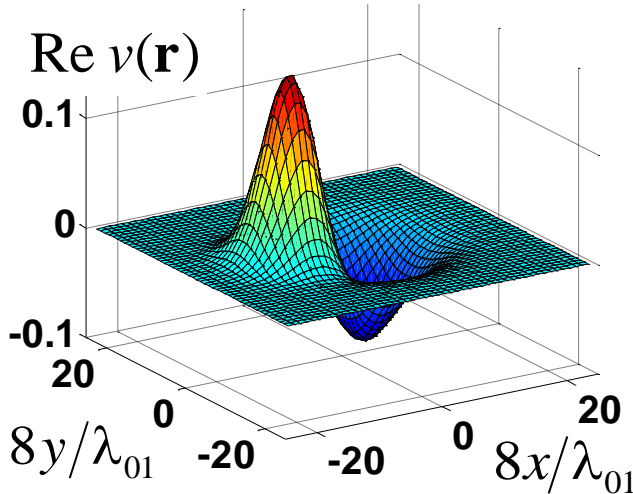
$\omega_{j1} < \omega_{j2} < \omega_{j3}$

Reconstruction of scalar inhomogeneity

Scalar inhomogeneity of sound speed and attenuation

$$\mathbf{A}(\mathbf{r}, \omega_j) \equiv 0$$

$$\text{Re } v(\mathbf{r}, \omega_j) = \omega_j^2 \left(\frac{1}{c_0^2} - \frac{1}{c^2(\mathbf{r})} \right), \quad \text{Im } v(\mathbf{r}, \omega_j) = -2 \omega_j \frac{\alpha(\mathbf{r}, \omega_j)}{c(\mathbf{r})}.$$

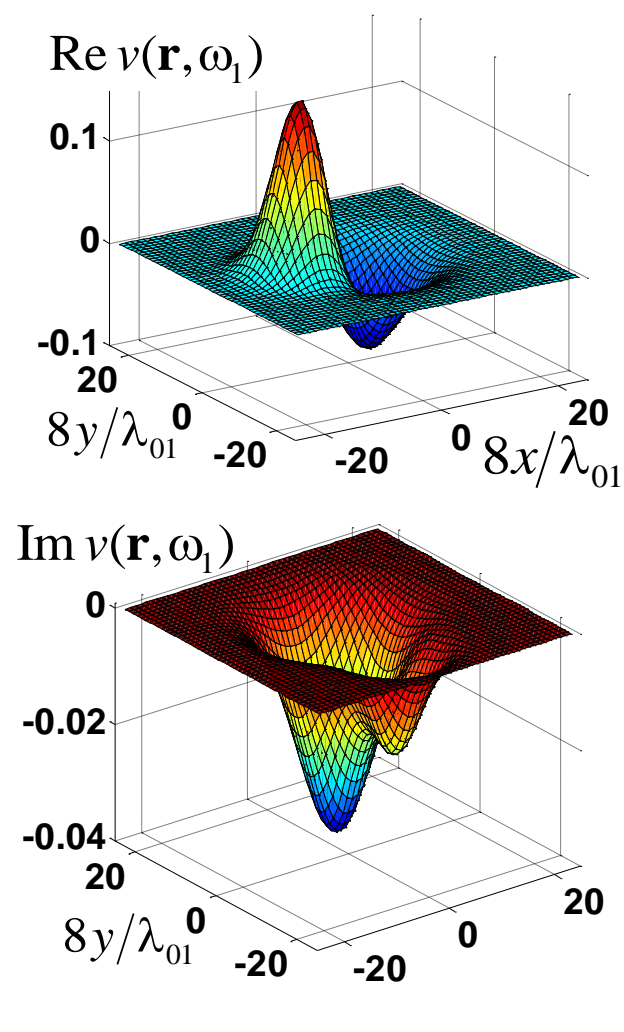


This is scatterer of medium strength:

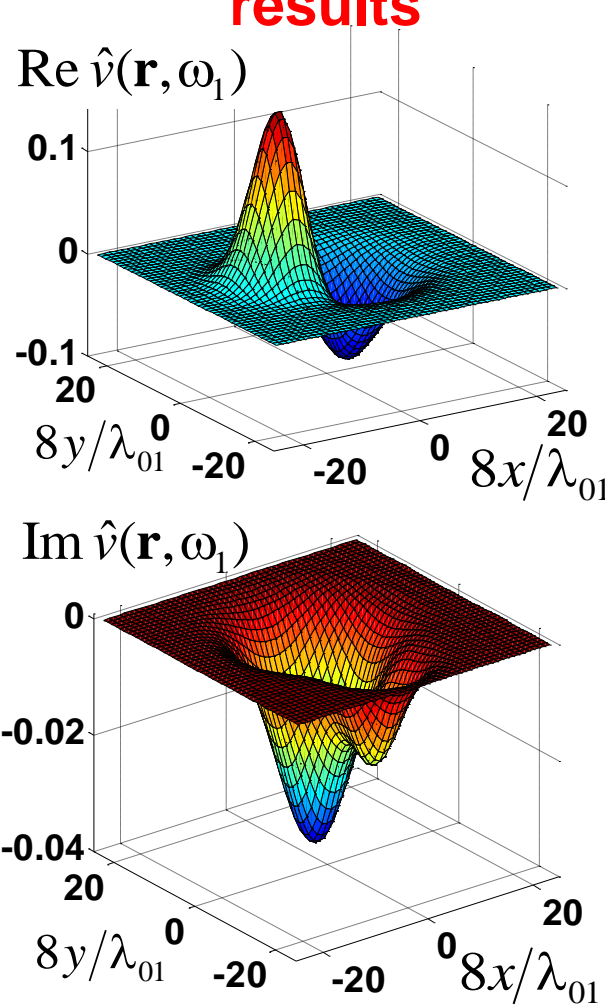
Additional phase shift along OX axis: for positive velocity contrast ($\text{Re } v > 0$) $\Delta\psi_{\text{pos}} \approx 0.3\pi$, for negative velocity contrast ($\text{Re } v < 0$) $\Delta\psi_{\text{neg}} \approx -0.18\pi$; amplitude attenuation coefficient is ≈ 1.4 (times).
 The similar parameters along OY axis: $\Delta\psi_{\text{pos}} \approx 0$, $\Delta\psi_{\text{neg}} \approx -0.21\pi$; amplitude attenuation is ≈ 1.6 (times).

Reconstruction results from the considered algorithm

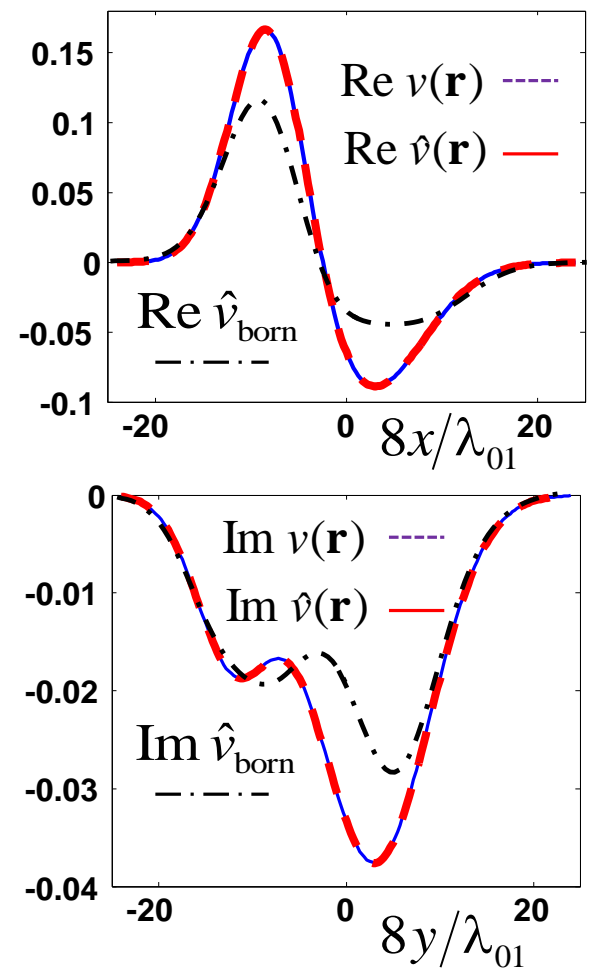
Model



Reconstruction results

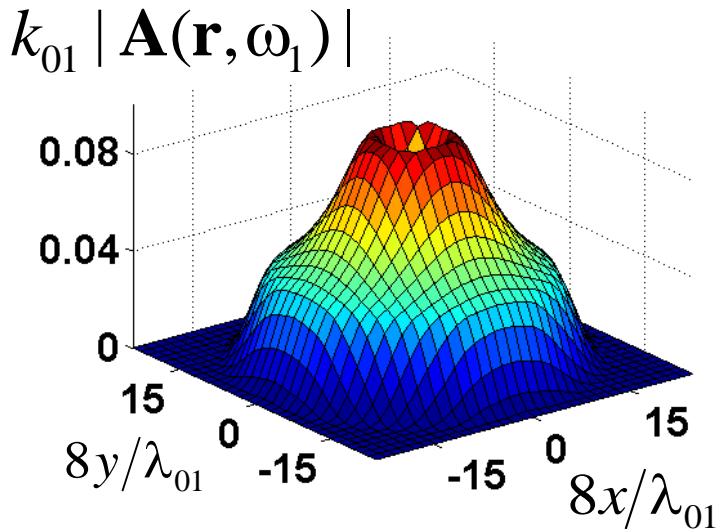


Crosssections of model and result



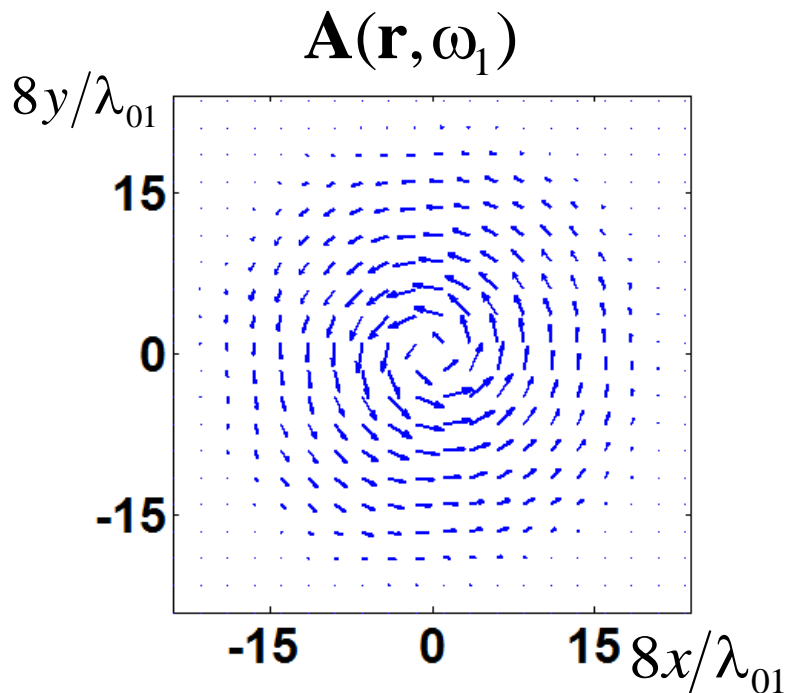
Reconstruction of vector inhomogeneities

Vector inhomogeneity of the vortex form

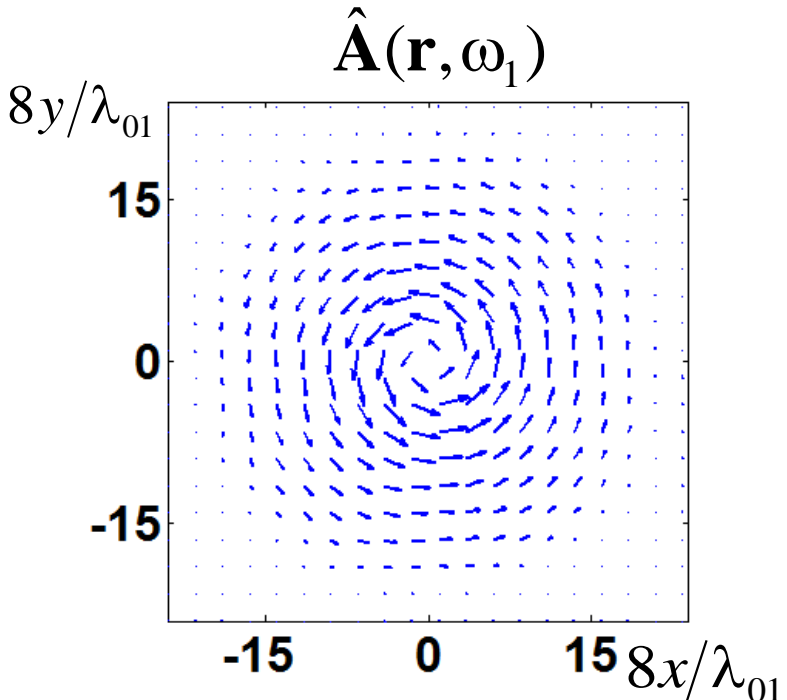


$$\mathbf{A}(\mathbf{r}, \omega_j) = \frac{\omega_j}{c^2(\mathbf{r})} \mathbf{v}(\mathbf{r}) \quad v(\mathbf{r}, \omega_j) \equiv 0$$

$$\operatorname{div} \mathbf{A}(\mathbf{r}, \omega_j) \cong 0$$

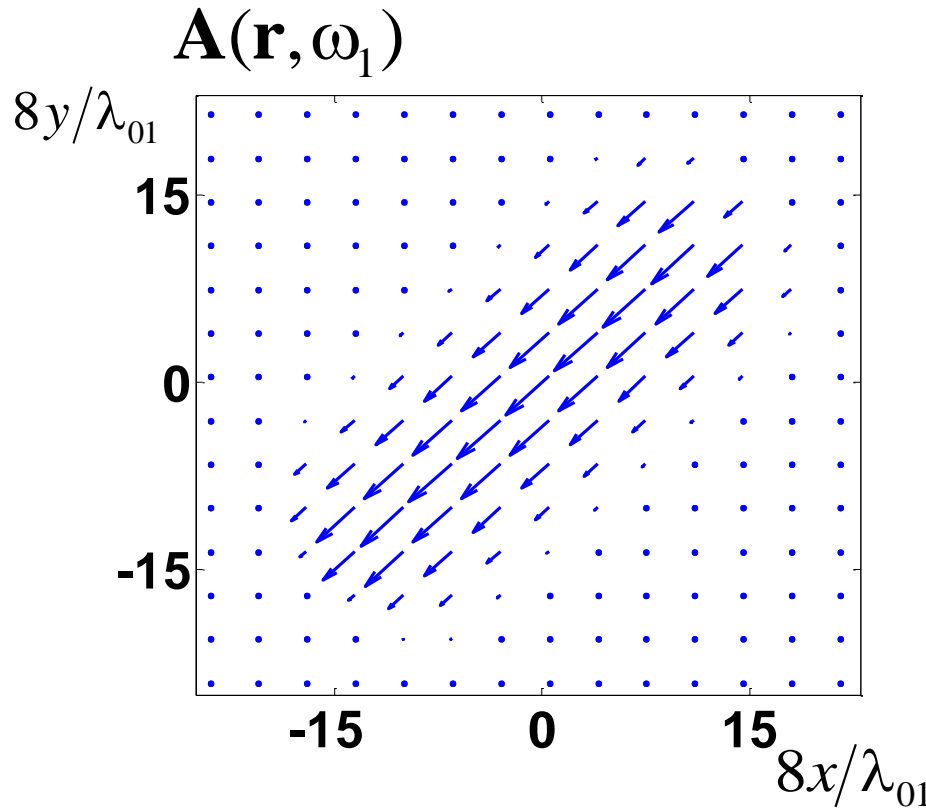


Model
Reconstruction
results

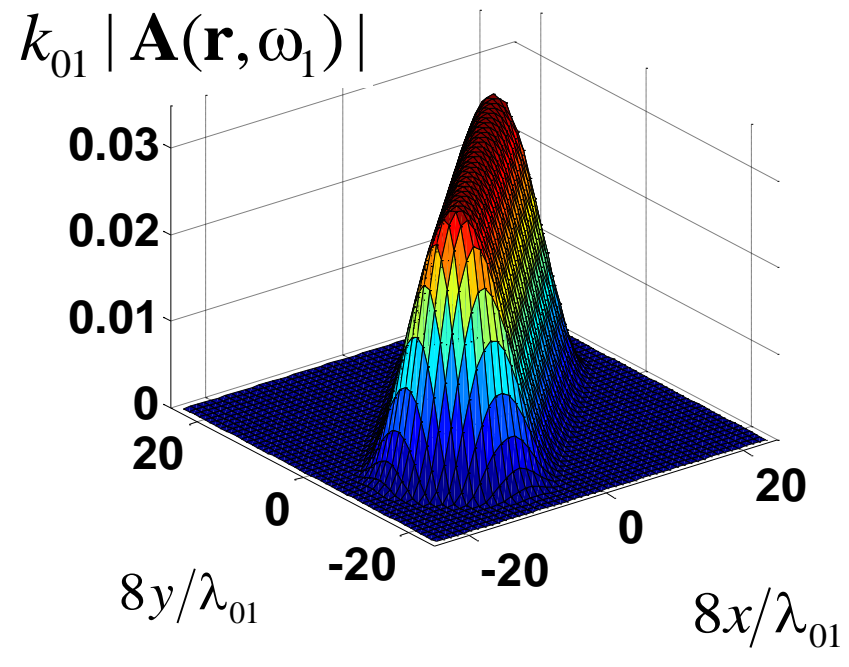


Vector inhomogeneity in the form of localized plane flow

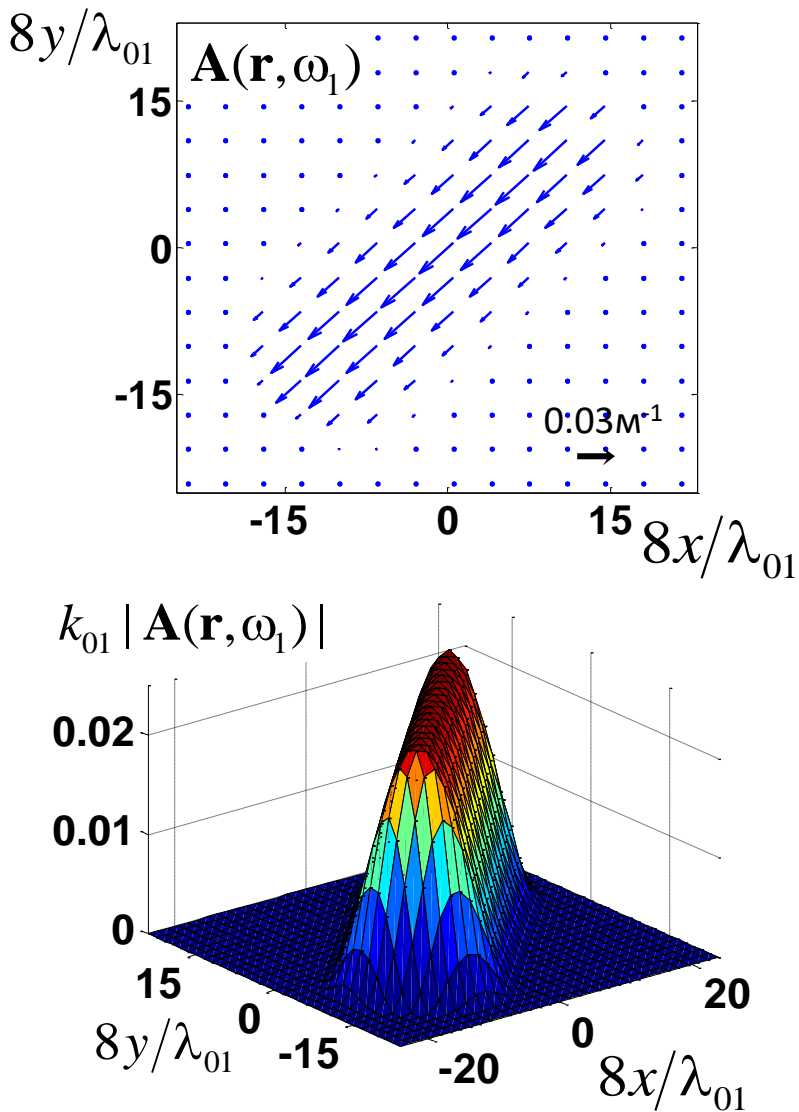
$$\operatorname{div} \mathbf{A}(\mathbf{r}, \omega_j) \neq 0$$



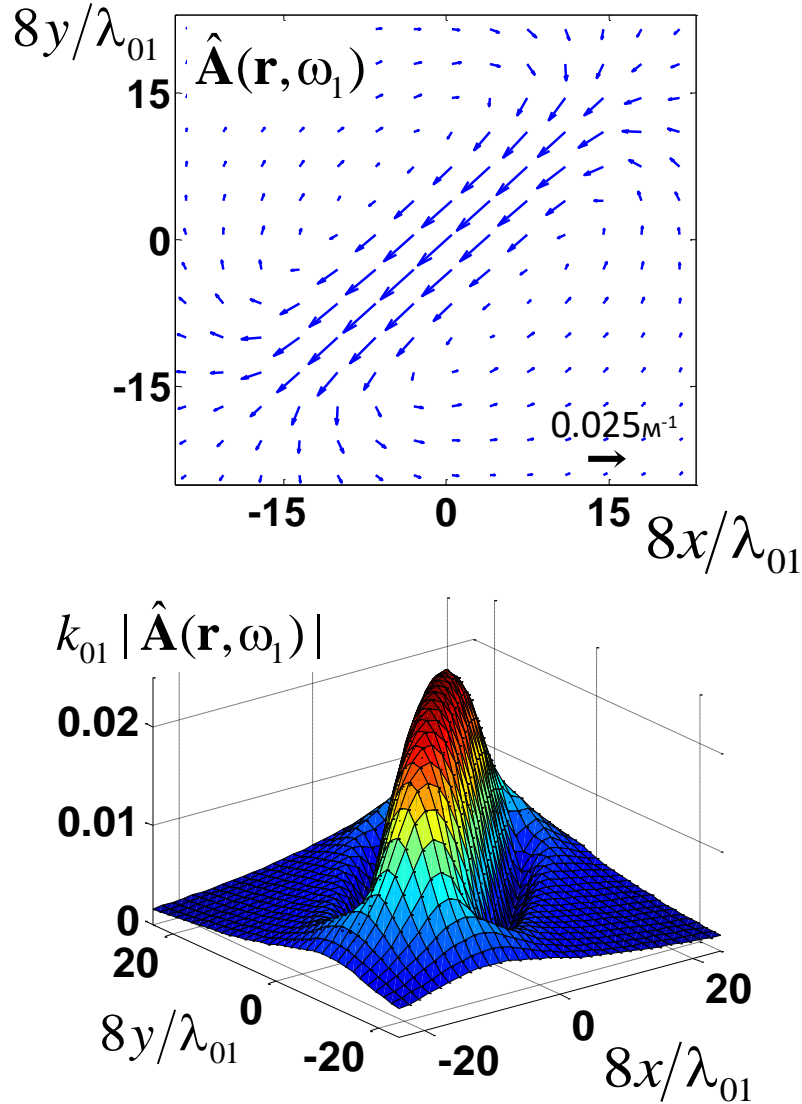
$$\eta_A = \sqrt{\frac{\sum_d |\mathbf{A}(\mathbf{r}_d) - \hat{\mathbf{A}}(\mathbf{r}_d)|^2}{\sum_d |\mathbf{A}(\mathbf{r}_d)|^2}}$$



Reconstruction results from the considered algorithm



Reconstruction results
|epow|



Reconstruction of the total vector field by using data on 2 frequencies (*)

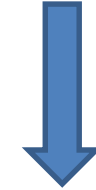
$$\left\{
 \begin{array}{l}
 \mathbf{A}(\mathbf{r}, \omega_j) = \mathbf{A}^{\text{div}}(\mathbf{r}, \omega_j) - \nabla \Phi(\mathbf{r}, \omega_j) = \mathbf{A}^{\text{div}}(\mathbf{r}, \omega_j) + \mathbf{A}^{\text{rot}}(\mathbf{r}, \omega_j), \\
 v(\mathbf{r}, \omega_j) = v^{\text{div}}(\mathbf{r}, \omega_j) + i \nabla^2 \Phi(\mathbf{r}, \omega_j) - (\nabla \Phi(\mathbf{r}, \omega_j))^2 - 2 \mathbf{A}(\mathbf{r}, \omega_j) \nabla \Phi(\mathbf{r}, \omega_j).
 \end{array}
 \right.$$

(3)



$$\nabla^2 \Phi(\mathbf{r}, \omega_j) = -\text{div } \mathbf{A}(\mathbf{r}, \omega_j) = -\omega_j \text{div} \left\{ \frac{\mathbf{v}(\mathbf{r})}{c^2(\mathbf{r})} \right\}$$

(1)



$$\text{Im } v^{\text{div}}(\mathbf{r}, \omega_j) = \text{Im } v(\mathbf{r}, \omega_j) - \nabla^2 \Phi(\mathbf{r}, \omega_j) = -2 \omega_j \frac{\alpha(\mathbf{r}, \omega_j)}{c(\mathbf{r})} + \omega_j \text{div} \left\{ \frac{\mathbf{v}(\mathbf{r})}{c^2(\mathbf{r})} \right\}$$

(2)



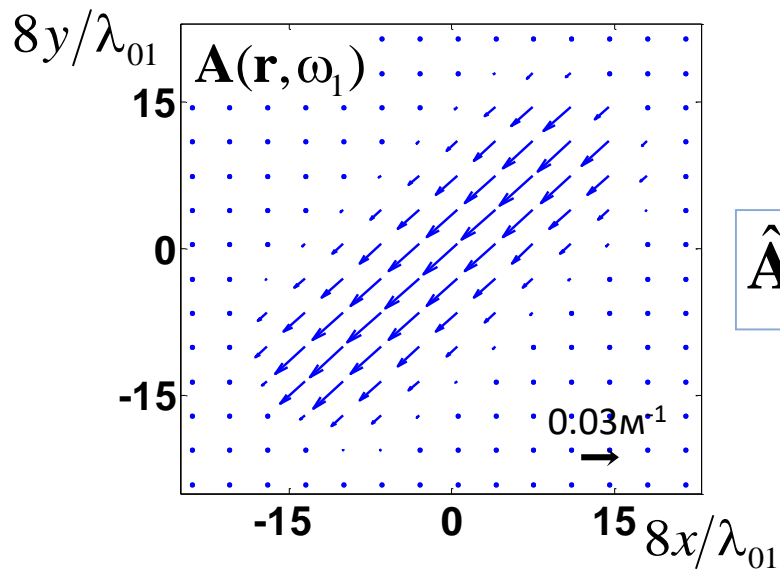
$$\left\{
 \begin{array}{l}
 \text{Im } v^{\text{div}}(\mathbf{r}, \omega_1) = -2 \frac{\omega_1^{\zeta(\mathbf{r})+1}}{\omega_0^{\zeta(\mathbf{r})}} \frac{\alpha(\mathbf{r}, \omega_0)}{c(\mathbf{r})} + \omega_1 \text{div} \left\{ \frac{\mathbf{v}(\mathbf{r})}{c^2(\mathbf{r})} \right\}, \\
 \text{Im } v^{\text{div}}(\mathbf{r}, \omega_2) = -2 \frac{\omega_2^{\zeta(\mathbf{r})+1}}{\omega_0^{\zeta(\mathbf{r})}} \frac{\alpha(\mathbf{r}, \omega_0)}{c(\mathbf{r})} + \omega_2 \text{div} \left\{ \frac{\mathbf{v}(\mathbf{r})}{c^2(\mathbf{r})} \right\}, \\
 \dots
 \end{array}
 \right.$$

$$\alpha(\mathbf{r}, \omega_j) = \left(\frac{\omega_j}{\omega_0} \right)^{\zeta(\mathbf{r})} \alpha(\mathbf{r}, \omega_0)$$

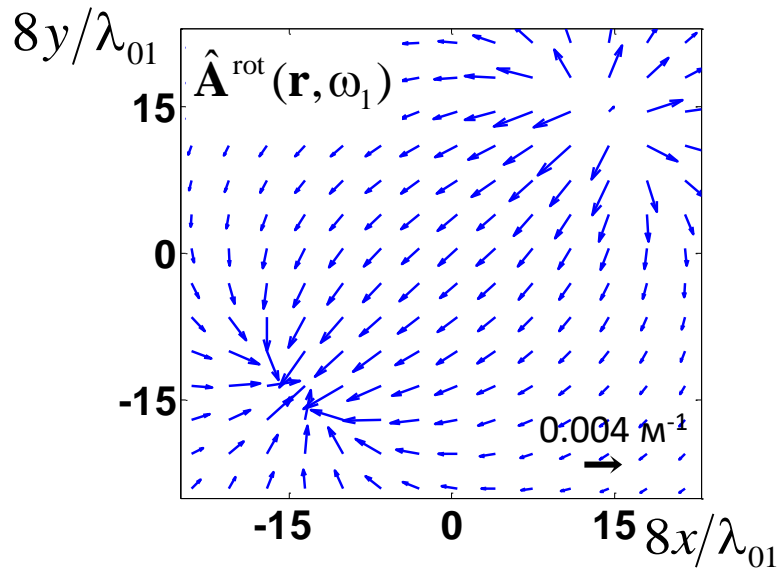
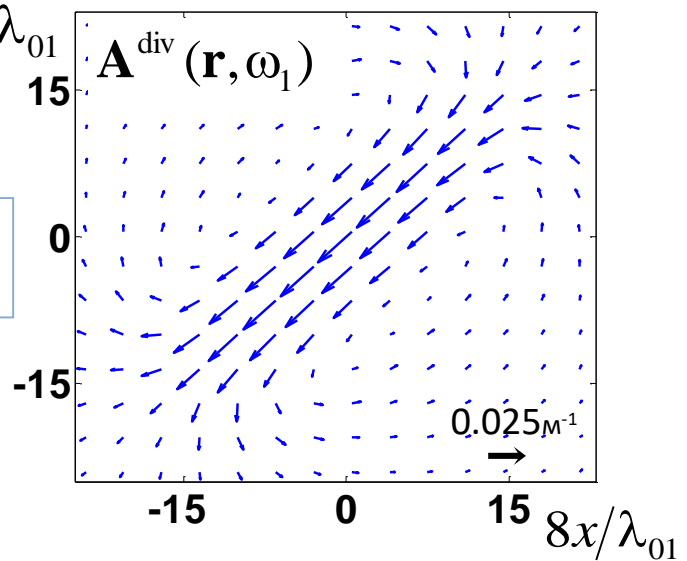
$\omega_0 > 0$ - typical frequency in the operational frequency range

(*) Agaltsov A.D. On the reconstruction of parameters of a moving fluid from the Dirichlet-to-Neumann map // Eurasian Journal of Mathematical and Computer Applications. 2016. V. 4. N 1. P. 4–11.

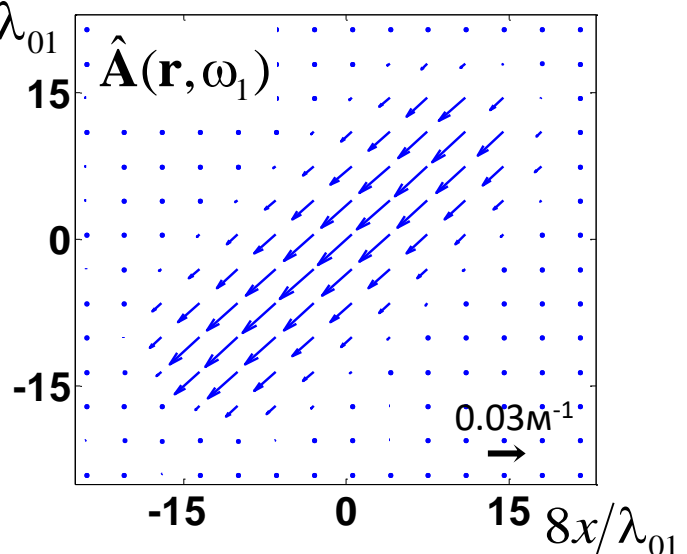
Reconstruction of the plane flow by using data on 2 frequencies



$$\hat{\mathbf{A}} = \hat{\mathbf{A}}^{\text{div}} + \hat{\mathbf{A}}^{\text{rot}}$$



$$\eta_A = 0.008$$

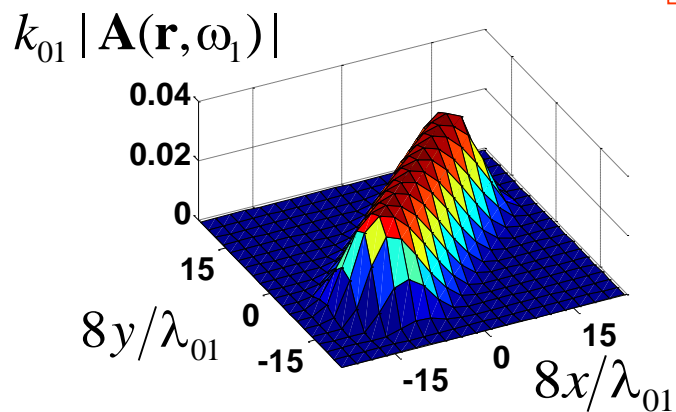


Influence of noise on reconstruction results

Normally distributed noise with
rms amplitude deviation

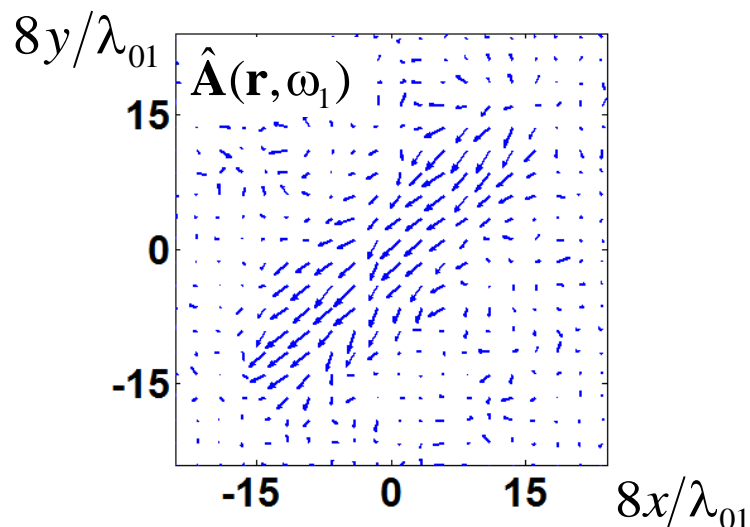
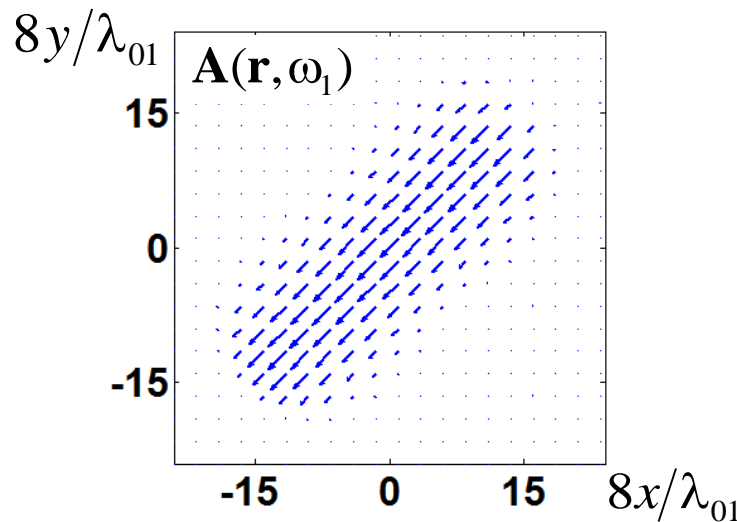
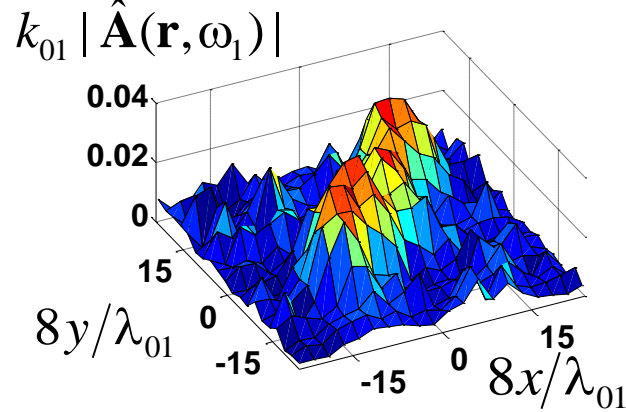
$$0.03 * \sqrt{\int_{\gamma} d\mathbf{x} \int_{\gamma} dy \left| G_{sc}(\mathbf{y}, \mathbf{x}; \omega_j) \right|^2} \Bigg/ \int_{\gamma} d\mathbf{x} \int_{\gamma} dy$$

Model



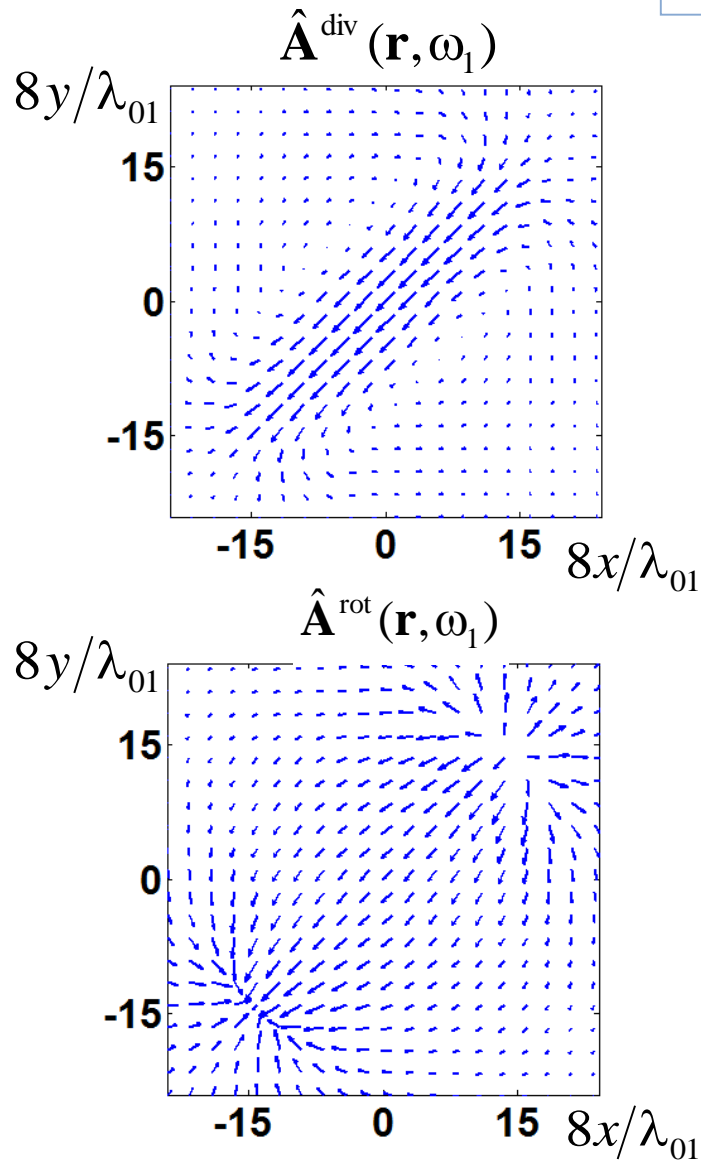
$$\eta_A = 0.55$$

Reconstruction results by
using data on 2 frequencies



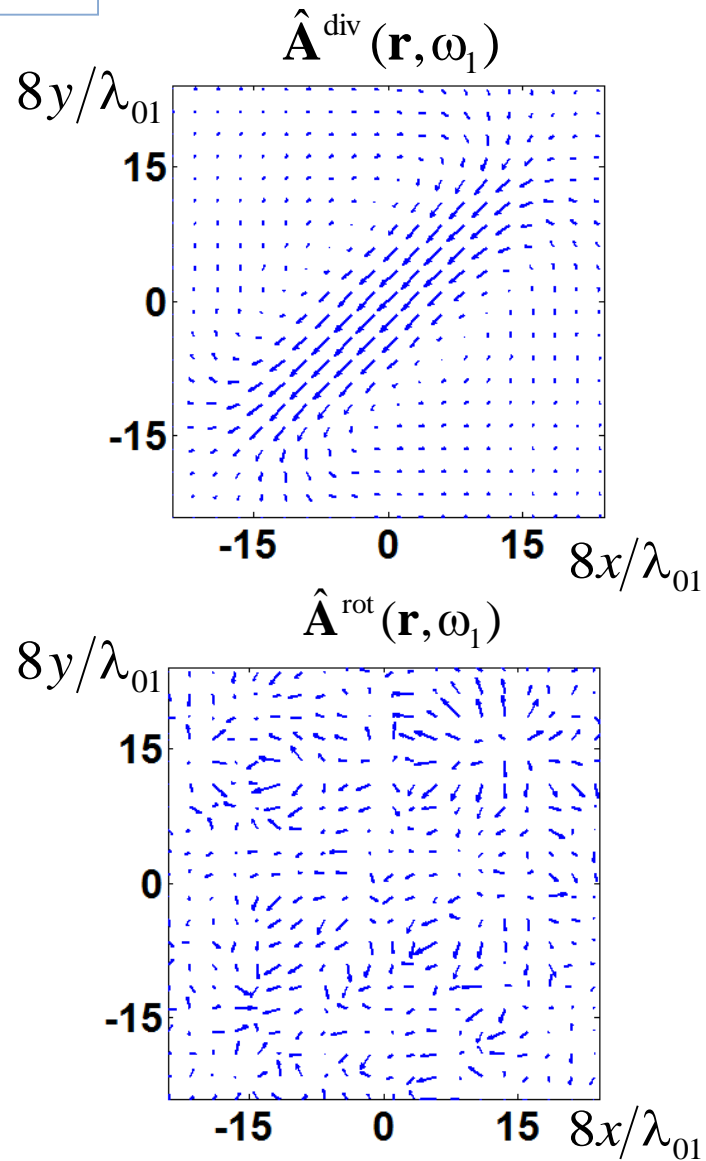
Reconstruction results by using data on 2 freqs

Without noise



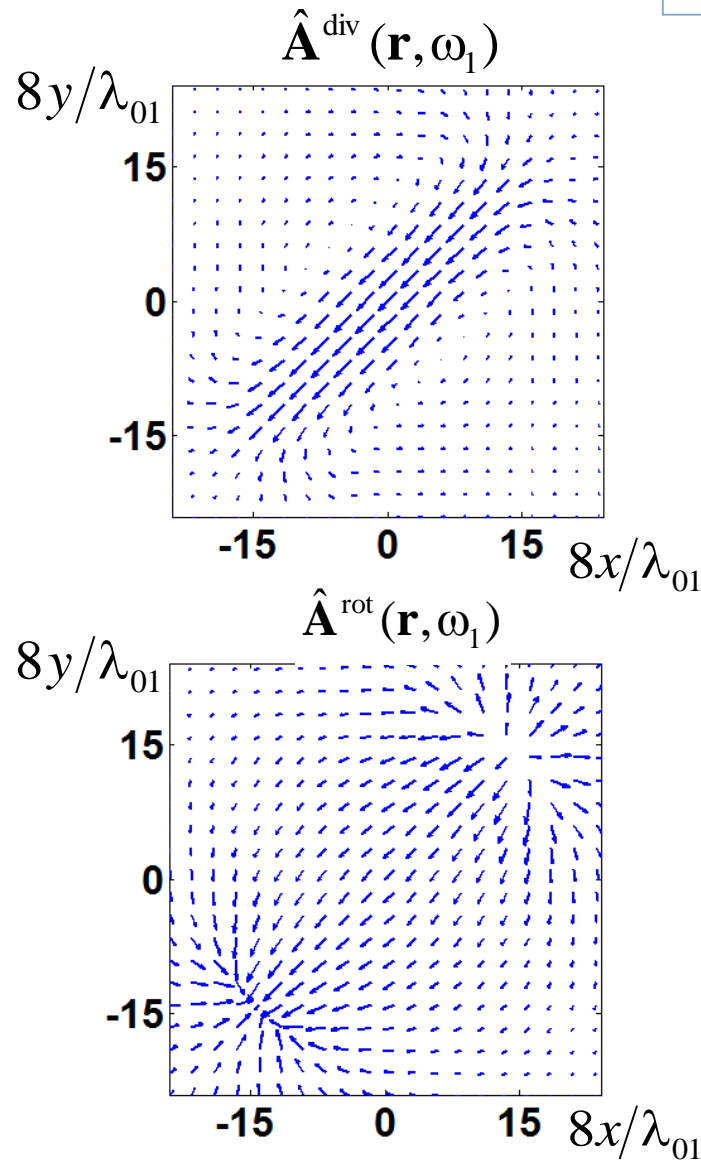
$$\hat{\mathbf{A}} = \hat{\mathbf{A}}^{\text{div}} + \hat{\mathbf{A}}^{\text{rot}}$$

With noise



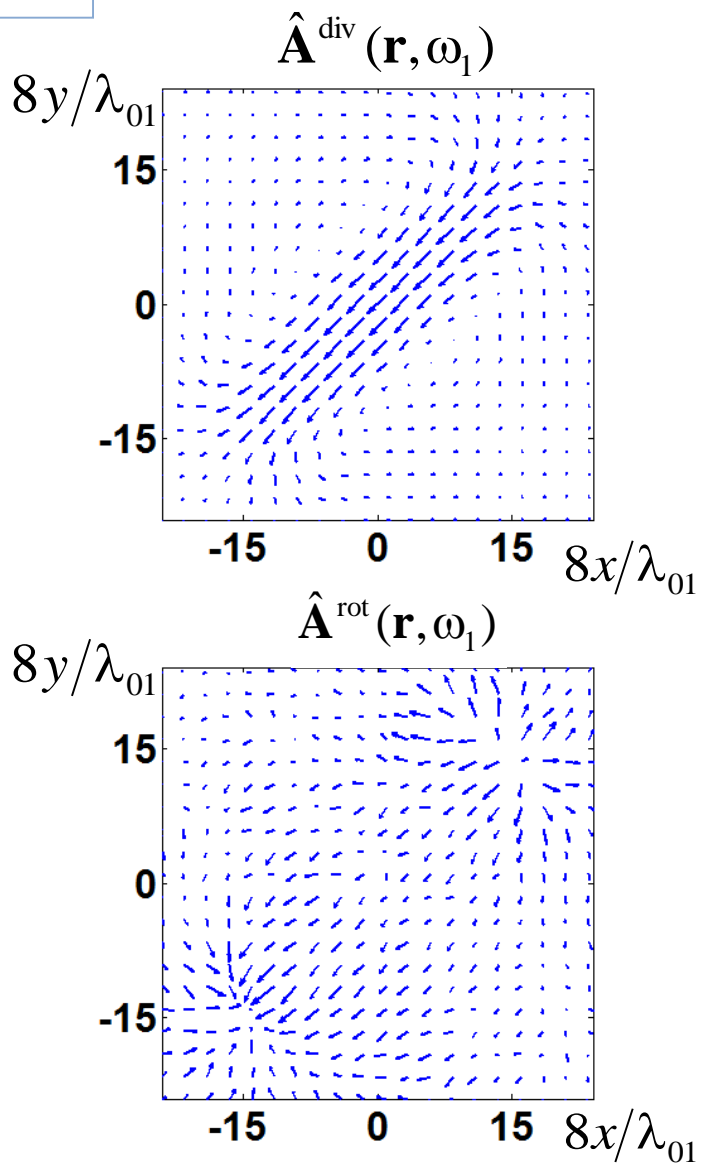
Reconstruction results by using data on 21 freqs

Without noise



$$\hat{\mathbf{A}} = \hat{\mathbf{A}}^{\text{div}} + \hat{\mathbf{A}}^{\text{rot}}$$

With noise

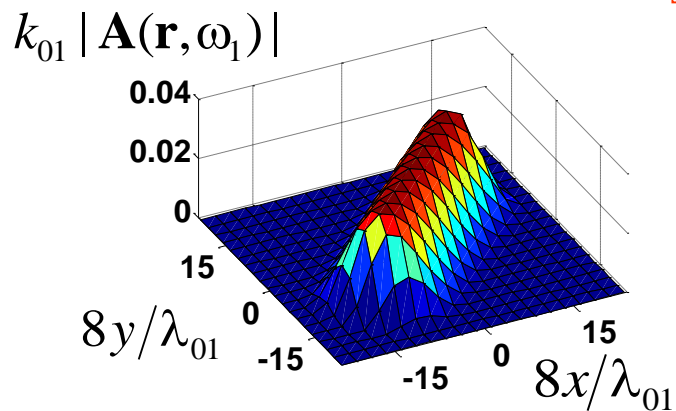


Influence of noise on reconstruction results

Normally distributed noise with
rms amplitude deviation

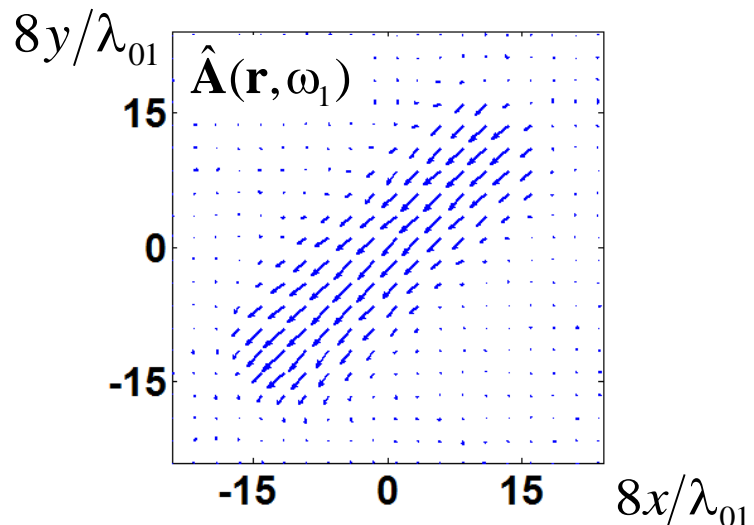
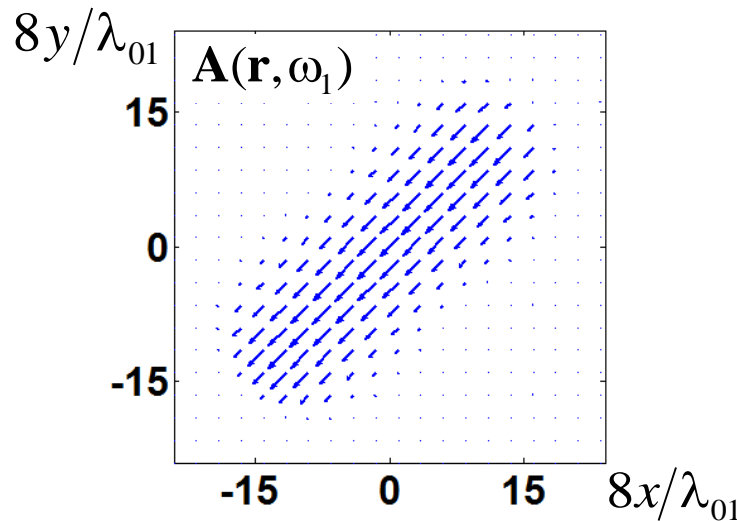
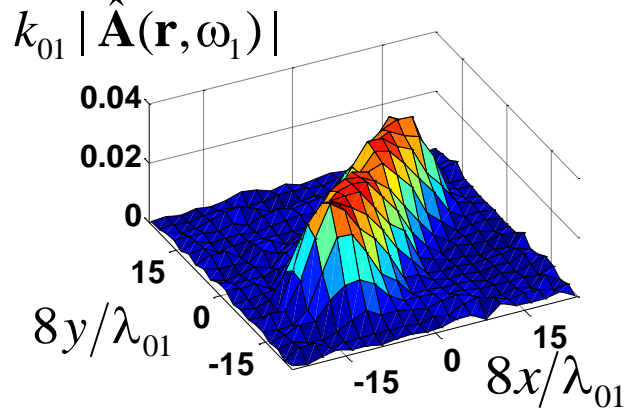
$$0.03 * \sqrt{\int_{\gamma} d\mathbf{x} \int_{\gamma} dy \left| G_{sc}(\mathbf{y}, \mathbf{x}; \omega_j) \right|^2} / \int_{\gamma} d\mathbf{x} \int_{\gamma} dy$$

Model



$$\eta_A = 0.16$$

Reconstruction results by
using data on 21 frequencies

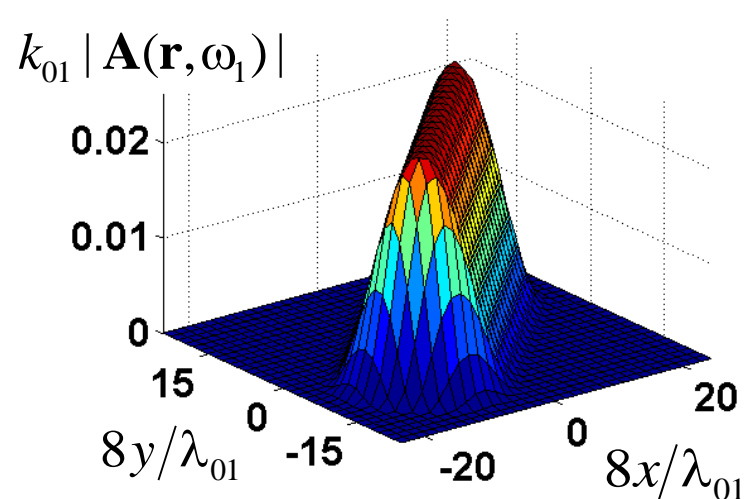
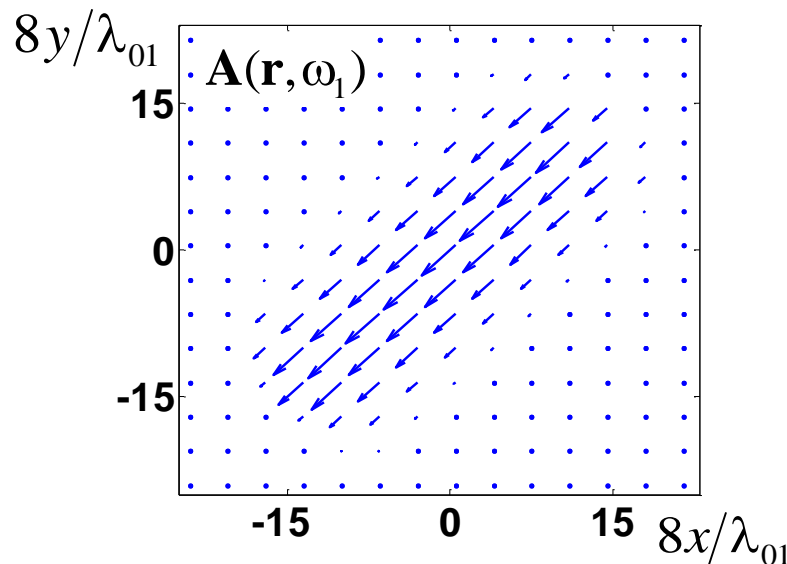
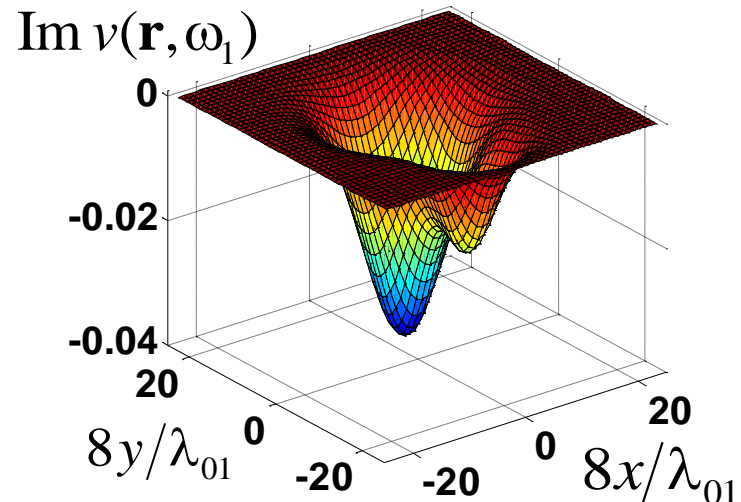
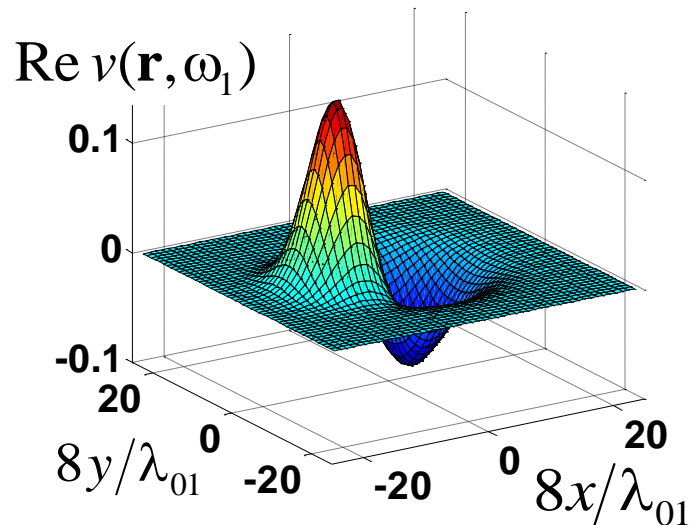


Reconstruction of combined scalar-vector inhomogeneity

$c(\mathbf{r})$, $\mathbf{v}(\mathbf{r})$, $\alpha(\mathbf{r}, \omega)$,

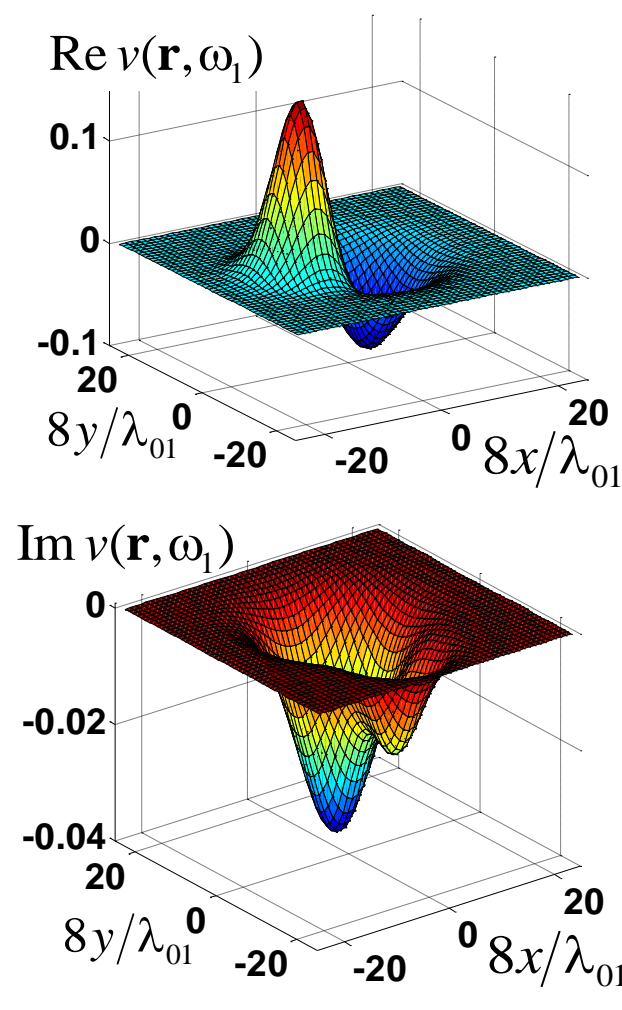
when $\nabla\rho(\mathbf{r}) \equiv 0$

Initial combined scalar-vector inhomogeneity

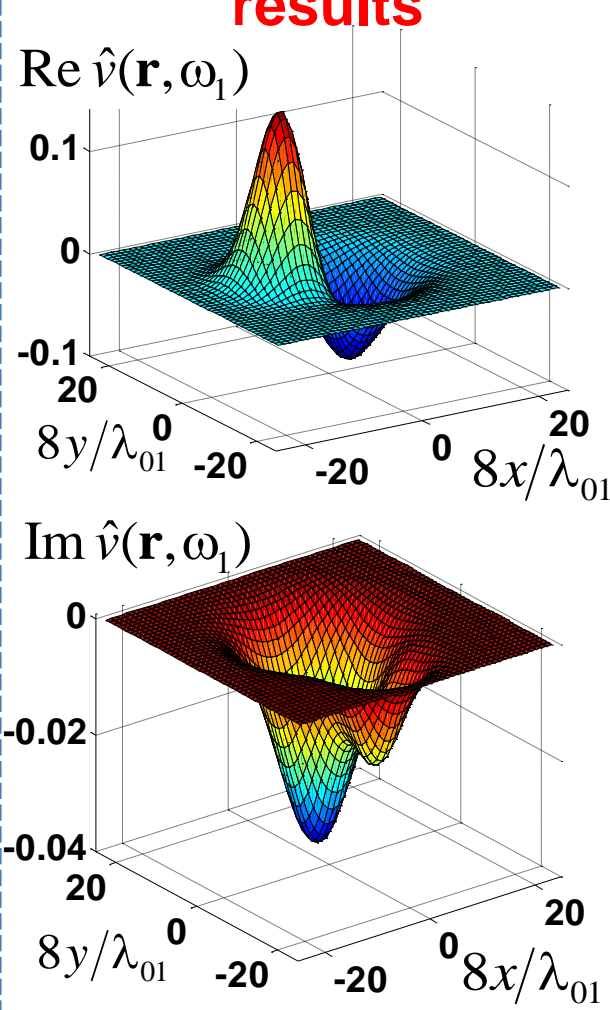


Reconstruction results of scalar component obtained by using 2 frequencies

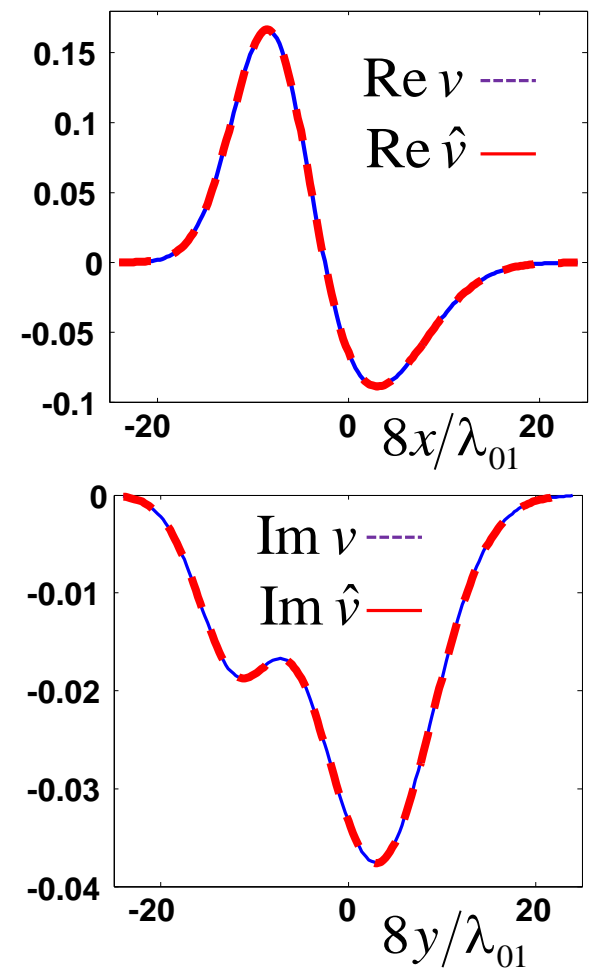
Model



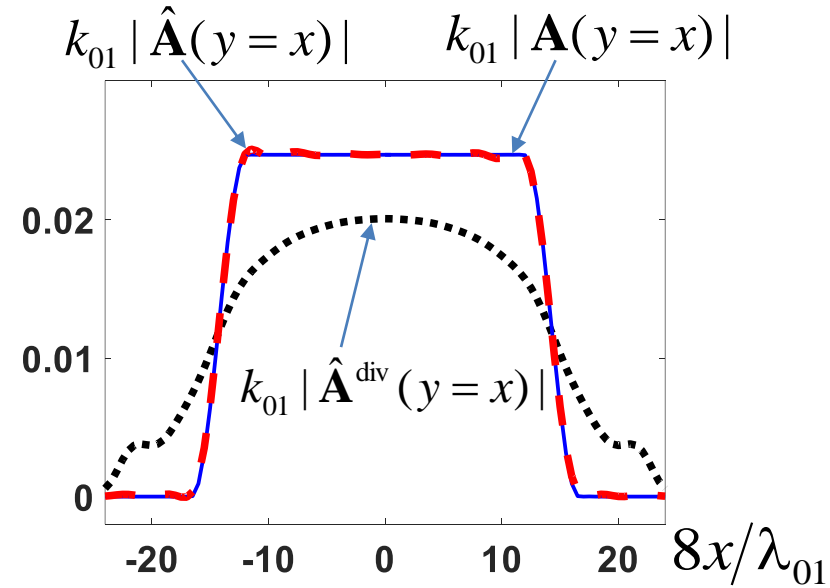
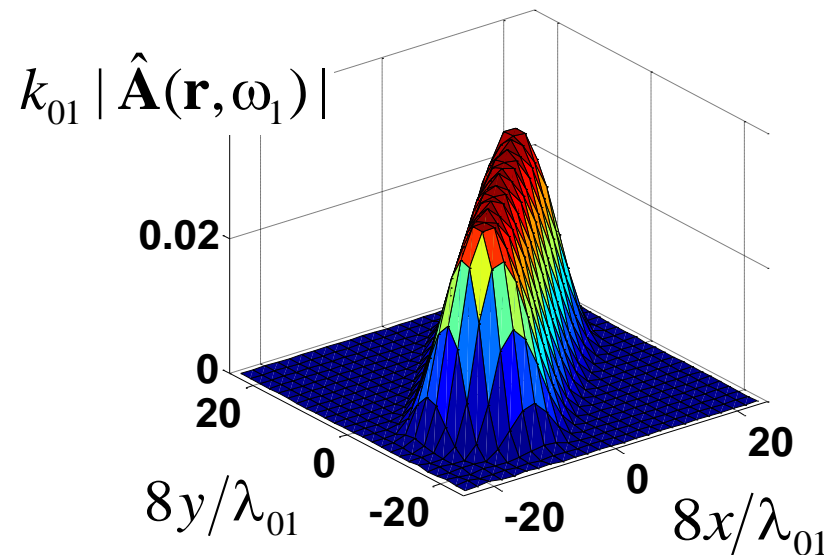
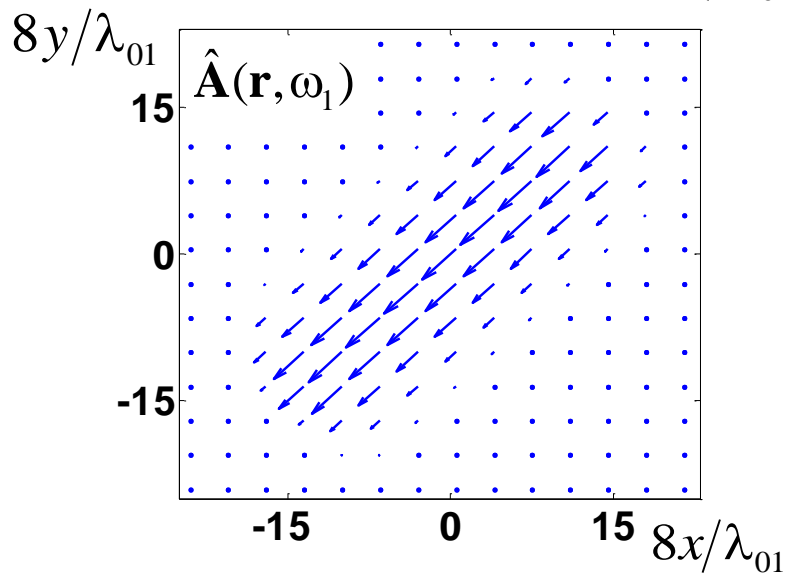
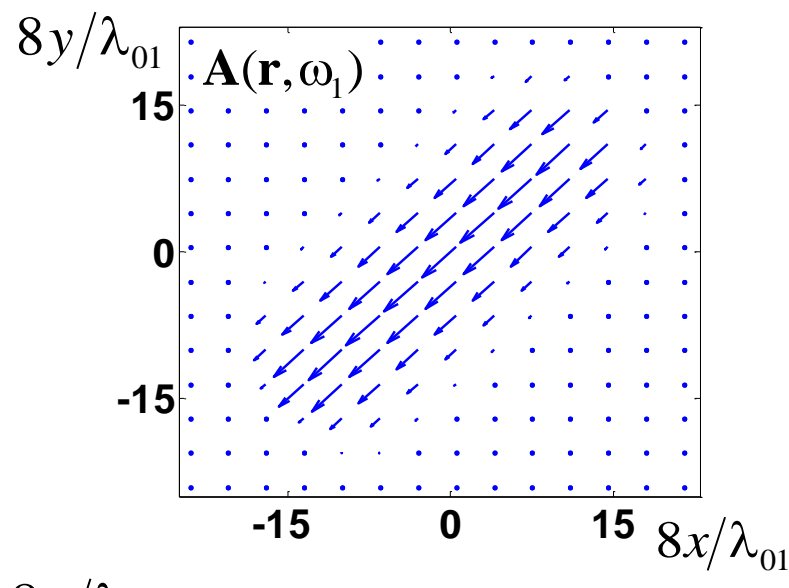
Reconstruction results



Crosssections of model and result

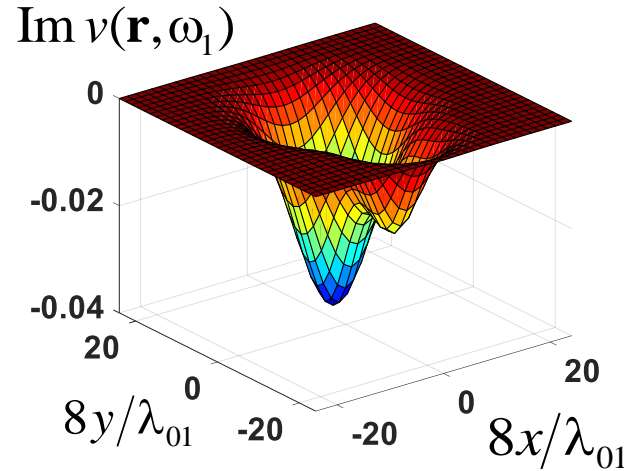
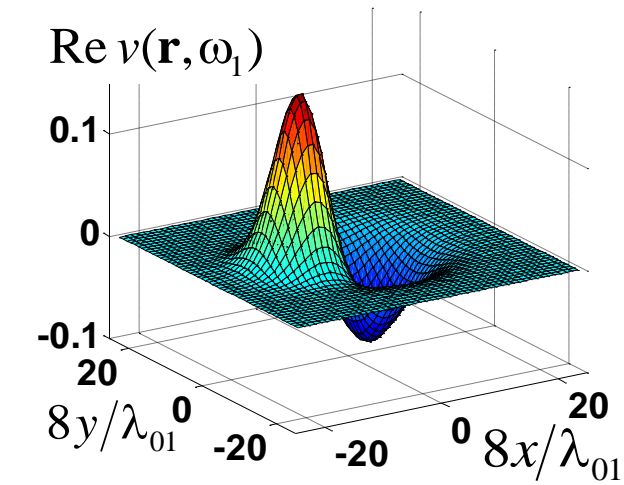


Reconstruction results of vector component obtained by using 2 frequencies

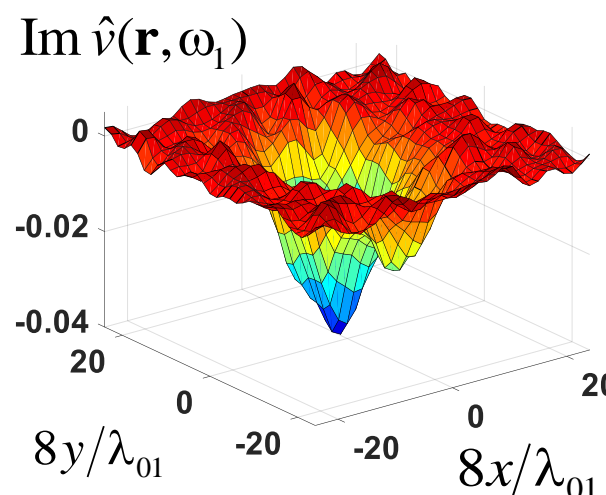
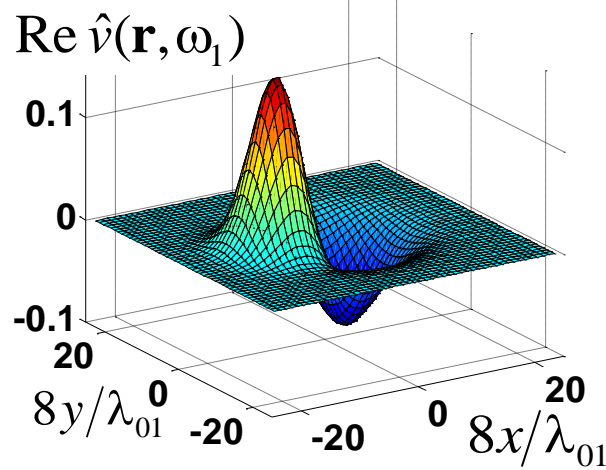


Influence of noise on reconstruction results (scattering data on 41 frequencies)

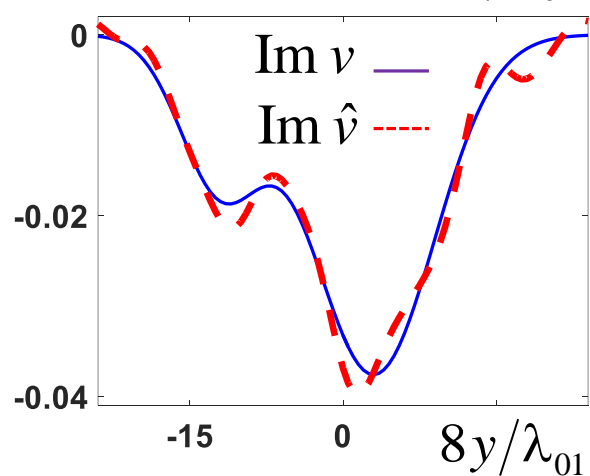
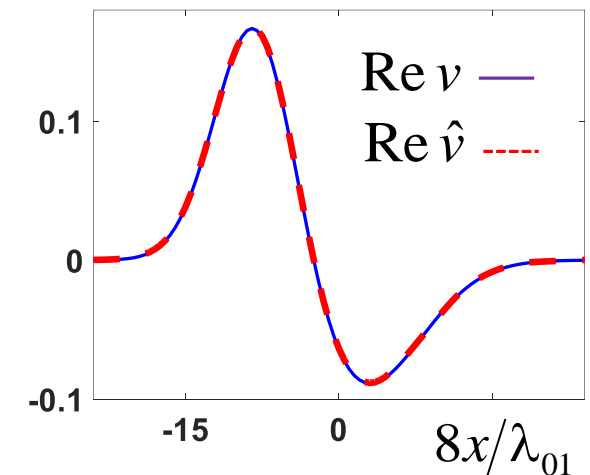
Model



Reconstruction results

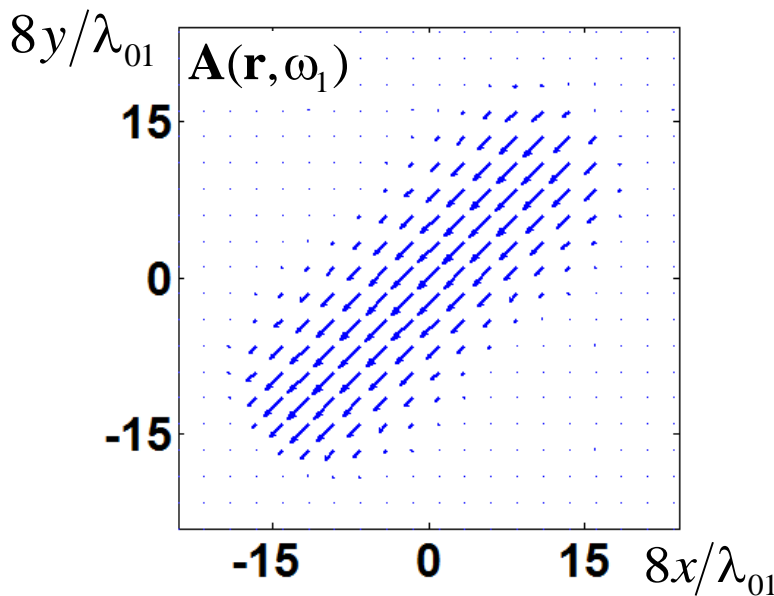
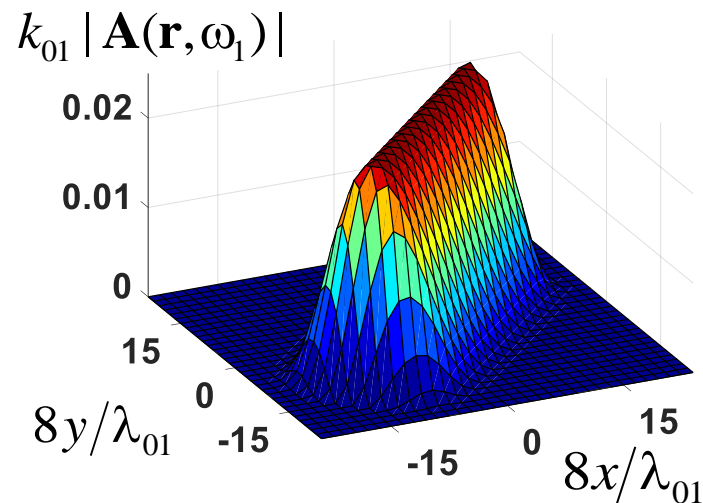


Crossections of model and result

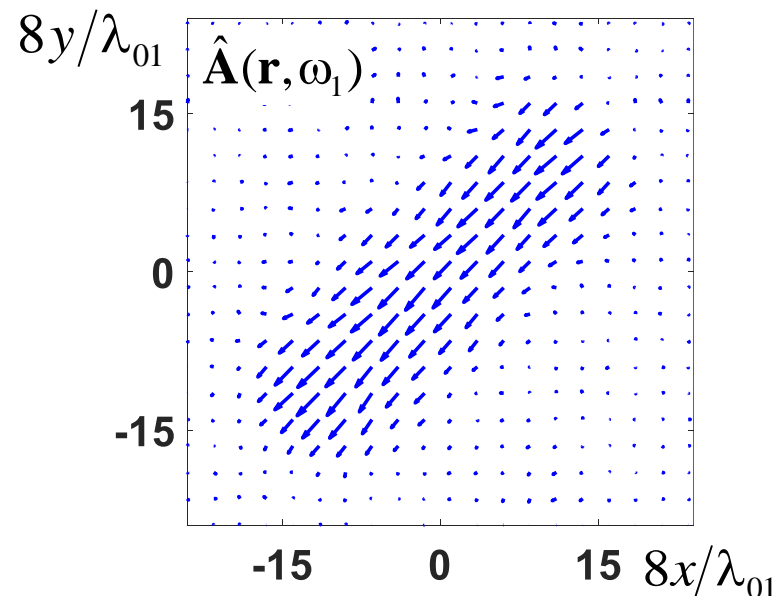
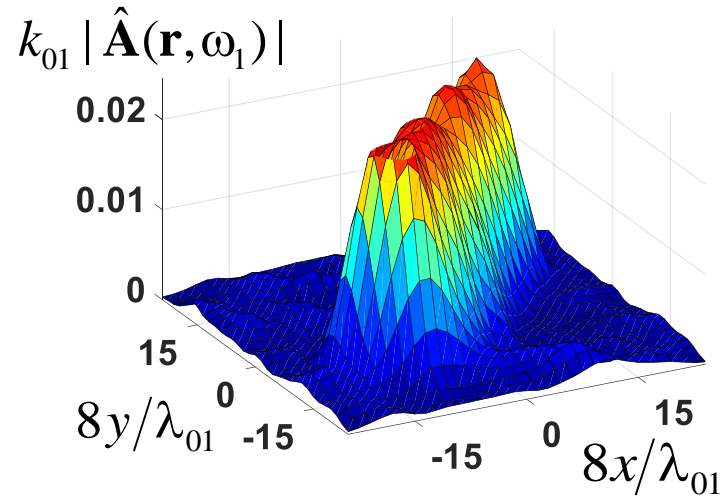


Influence of noise on reconstruction results

Model

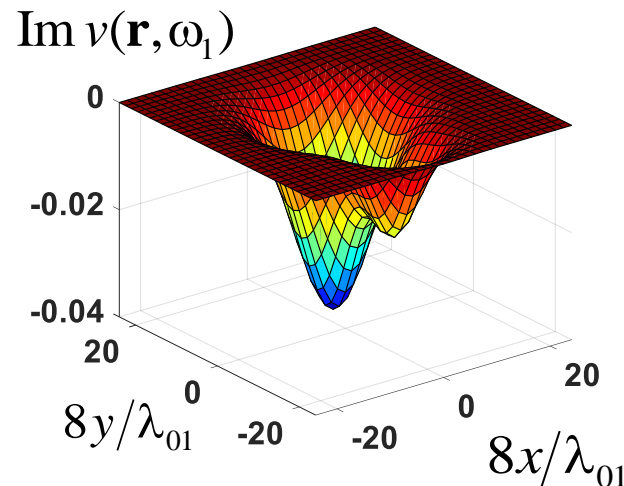
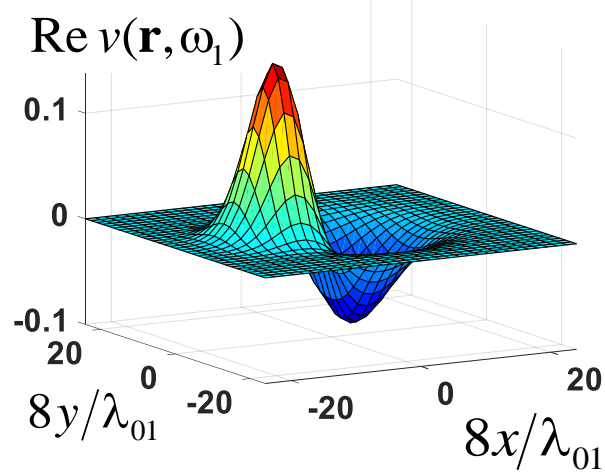


Reconstruction results by
using data on 41 frequencies

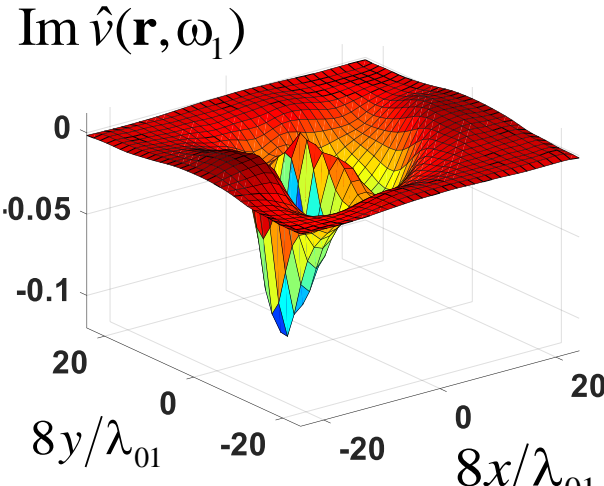
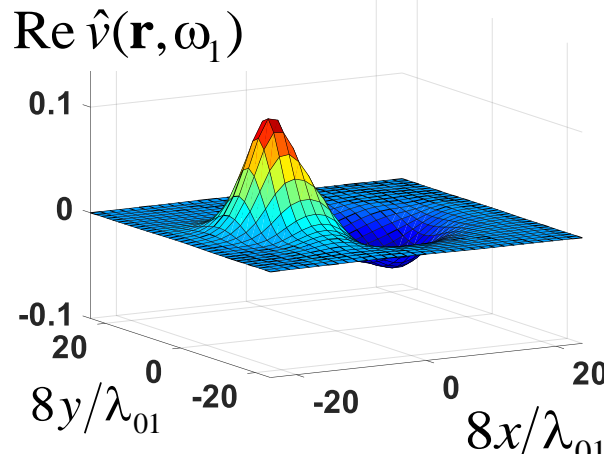


Attempt of reconstruction in Born's approximation (2 freqs, no noise)

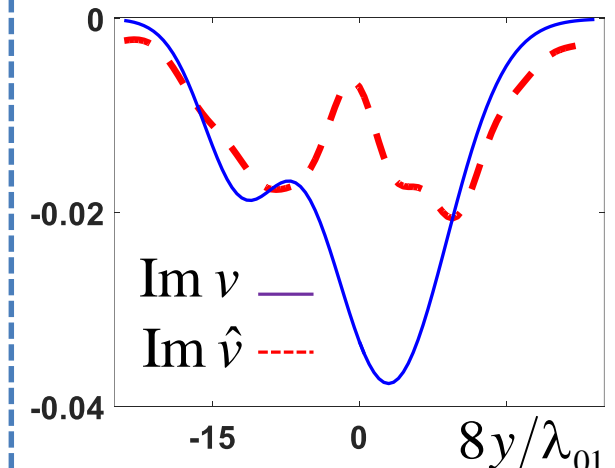
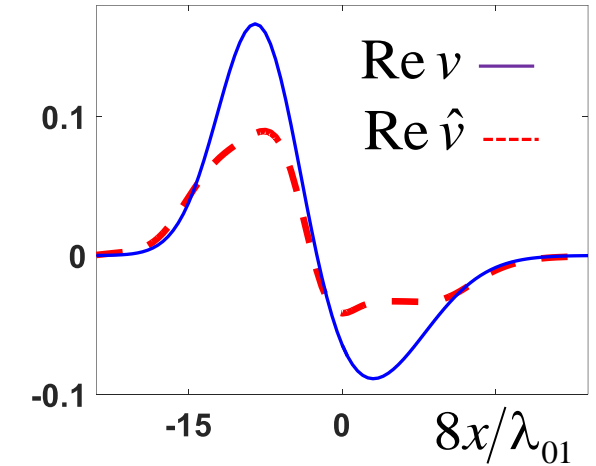
Model



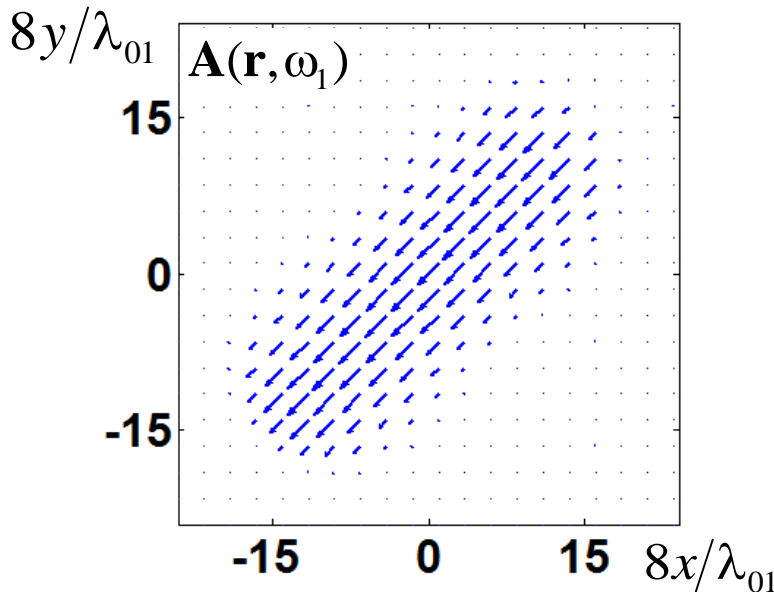
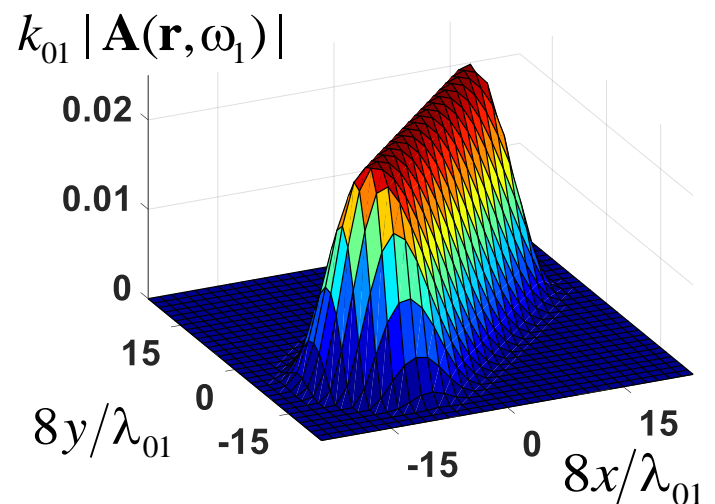
Reconstruction results



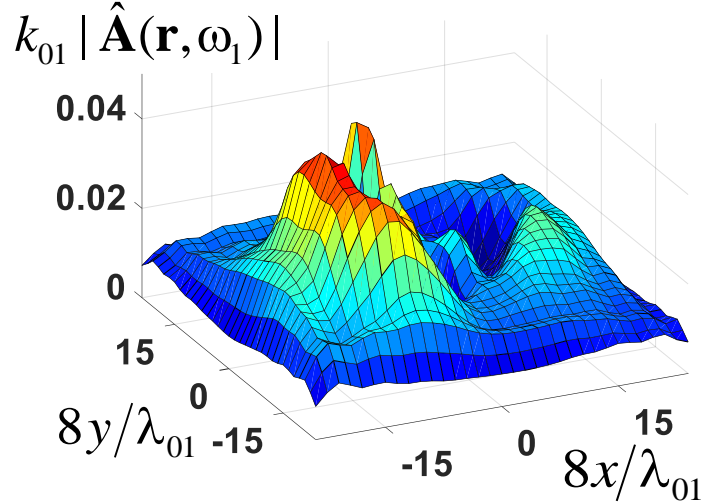
Crossections of model and result



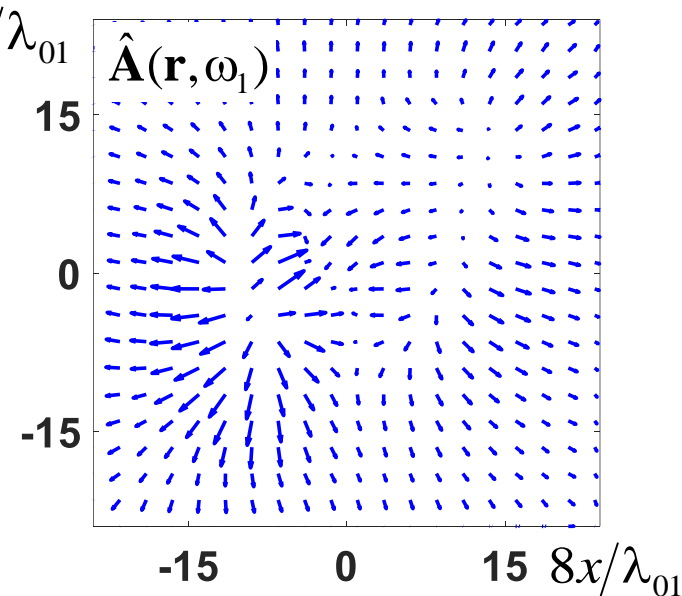
Attempt of reconstruction in Born's approximation (2 freqs, no noise)



Model

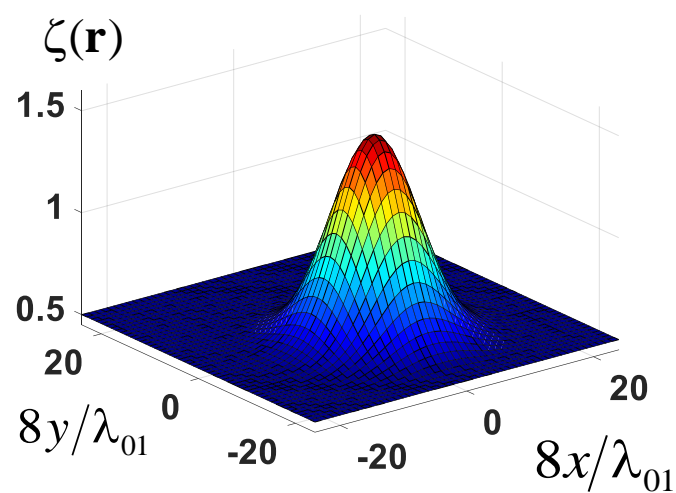
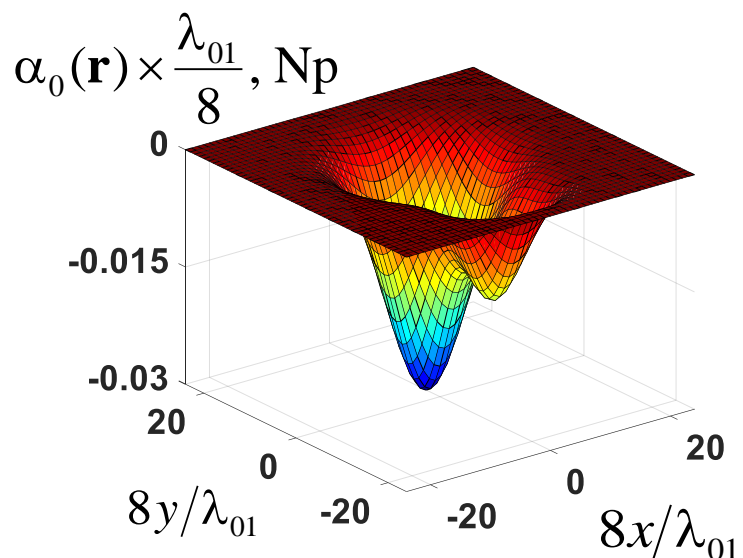
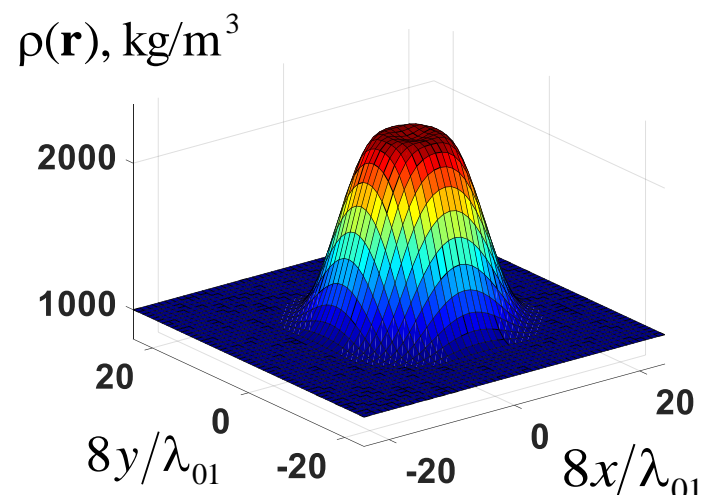
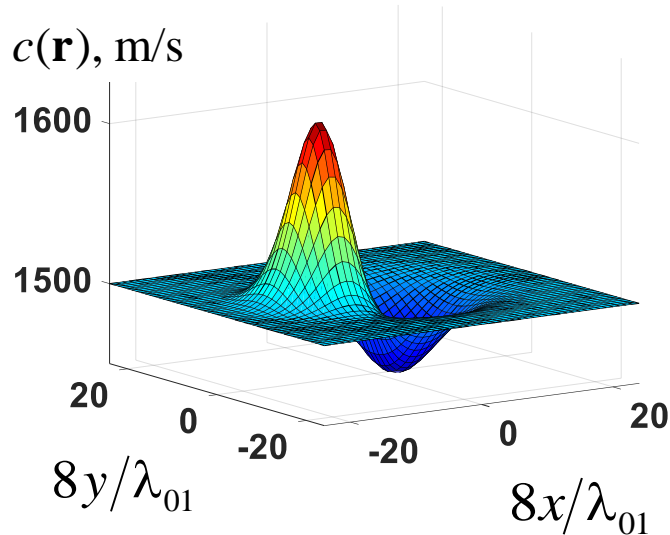


Reconstruction results



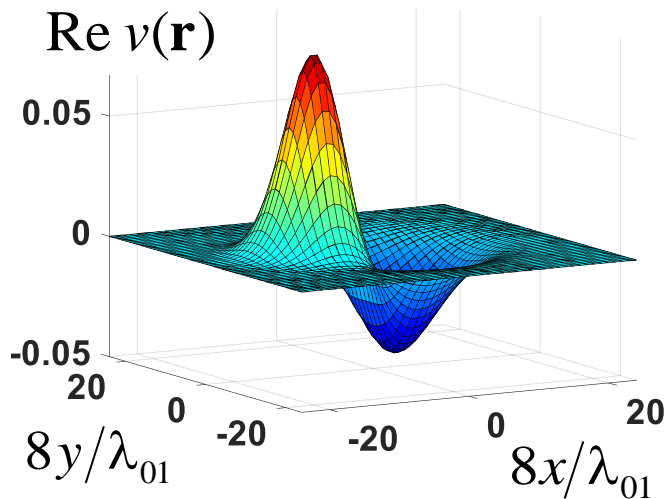
Reconstruction of
 $c(\mathbf{r}), \rho(\mathbf{r}), \alpha(\mathbf{r}, \omega_0), \zeta(\mathbf{r}),$
without flows $\mathbf{v}(\mathbf{r}) \equiv 0$

Parameters of the medium

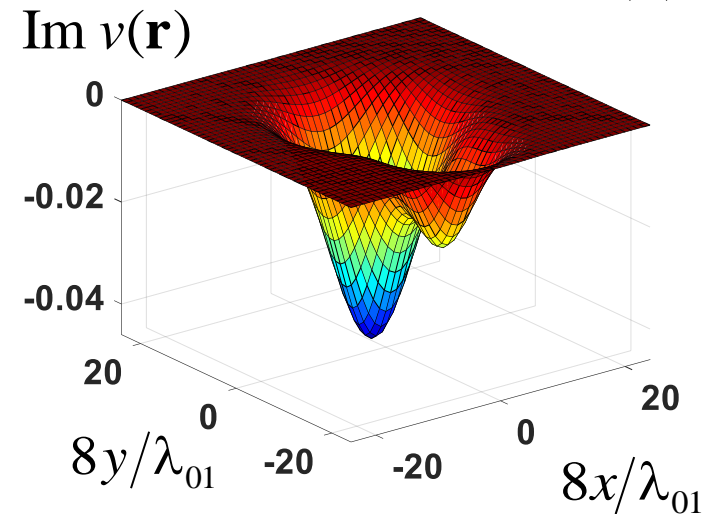


Scalar components of scatterer

$$\text{Re } v(\mathbf{r}, \omega_j) = \omega_j^2 \left(\frac{1}{c_0^2} - \frac{1}{c^2(\mathbf{r})} \right),$$



$$\text{Im } v(\mathbf{r}, \omega_j) = -2 \omega_j \frac{\alpha(\mathbf{r}, \omega_j)}{c(\mathbf{r})}.$$



This is scatterer of medium strength:

Additional phase shift along OX axis: for positive velocity contrast ($\text{Re } v > 0$)

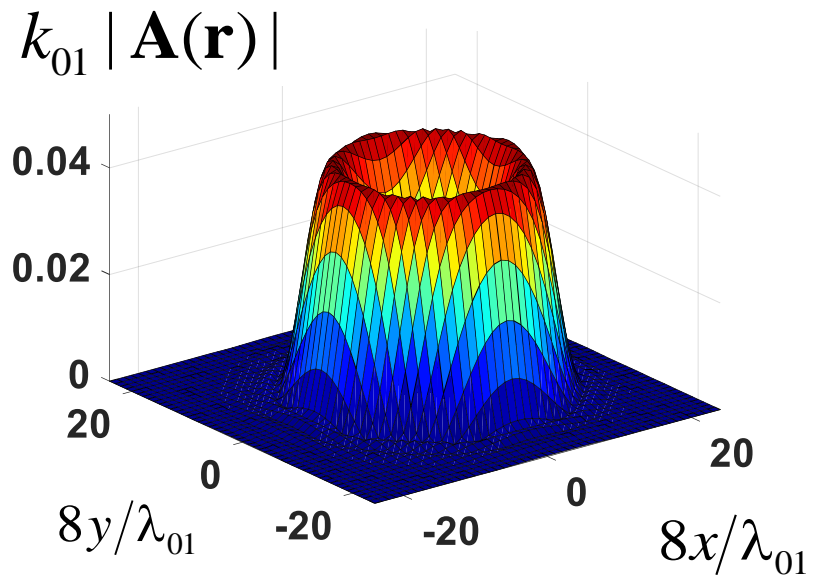
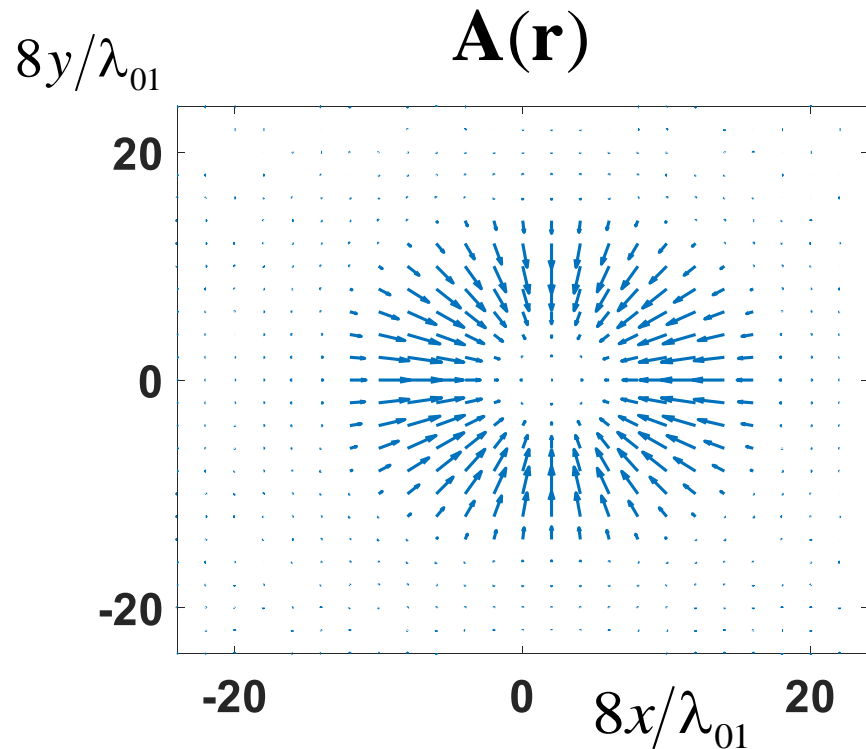
$\Delta\psi_{\text{pos}} \approx 0.29\pi$, for negative velocity contrast ($\text{Re } v < 0$) $\Delta\psi_{\text{neg}} \approx -0.19\pi$; amplitude attenuation is ≈ 1.99 (times).

The similar parameters along OY axis: $\Delta\psi_{\text{pos}} \approx 0$, $\Delta\psi_{\text{neg}} \approx -0.22\pi$; amplitude attenuation is ≈ 2.84 (times).

Vector component of scatterer

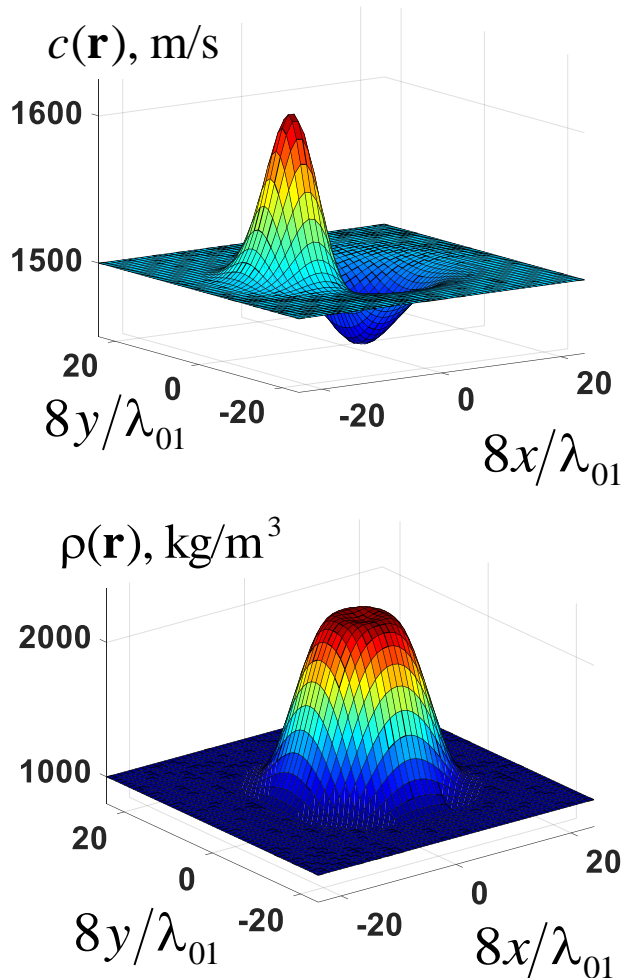
$$\mathbf{A}(\mathbf{r}) = i\nabla \ln \sqrt{\rho(\mathbf{r})}, \quad \text{rot } \mathbf{A}(\mathbf{r}) = 0$$

$$\mathbf{v}(\mathbf{r}) \equiv 0$$

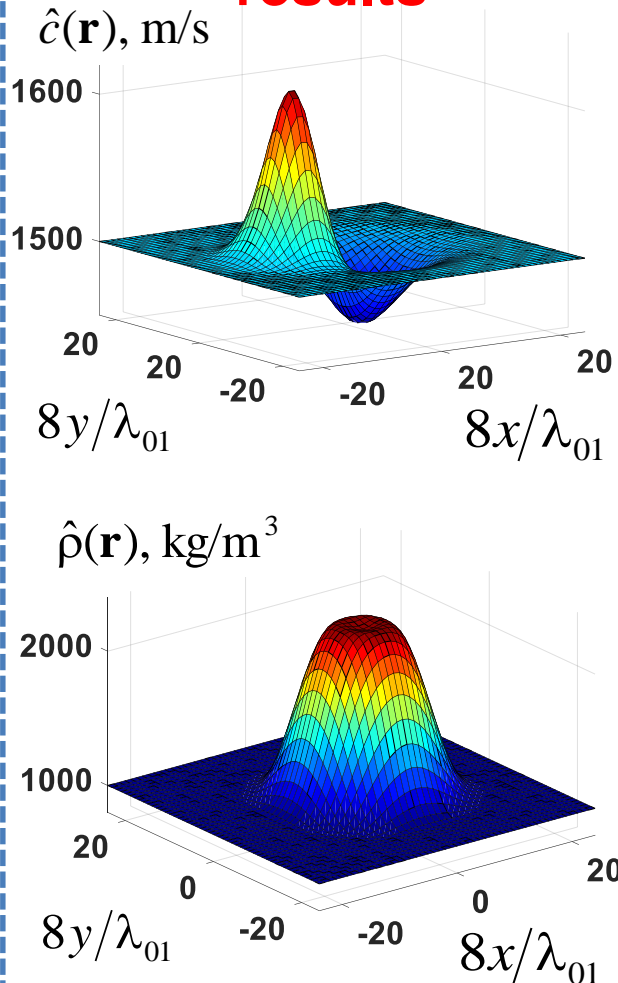


Reconstruction results obtained by using data on 2 frequencies, without noise

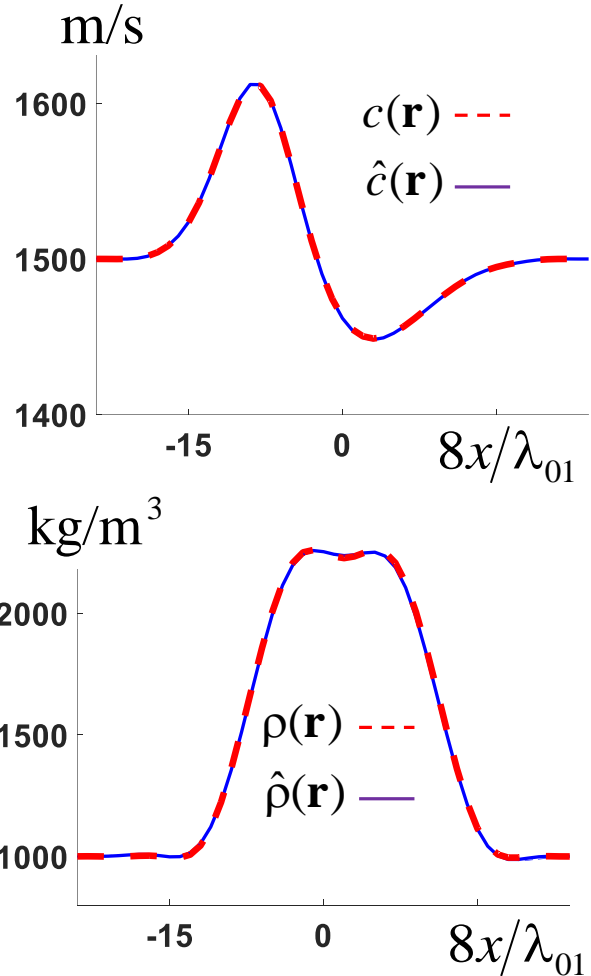
Model



Reconstruction results

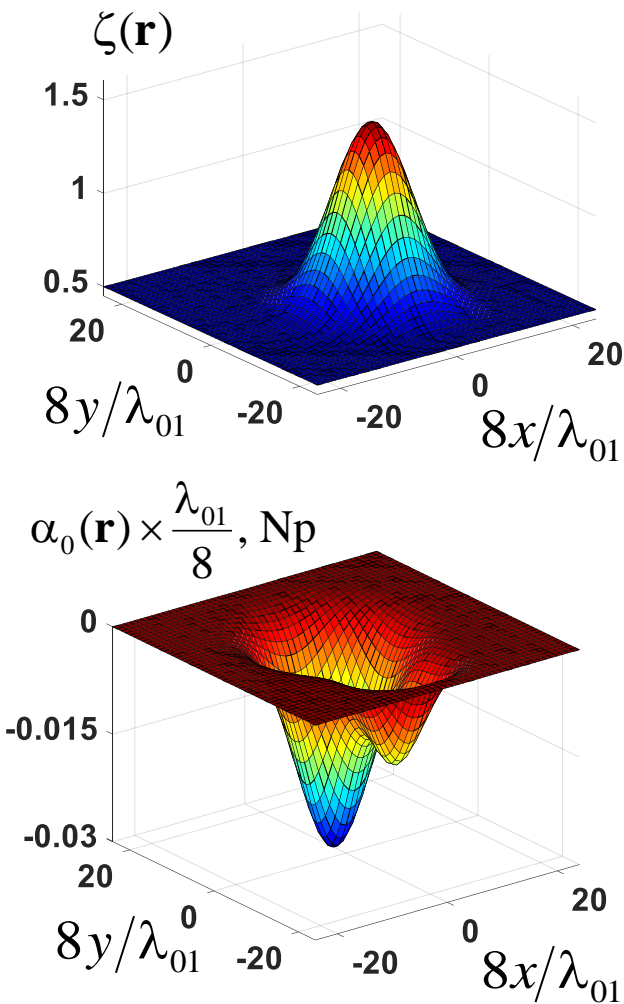


Crosssections of model and result

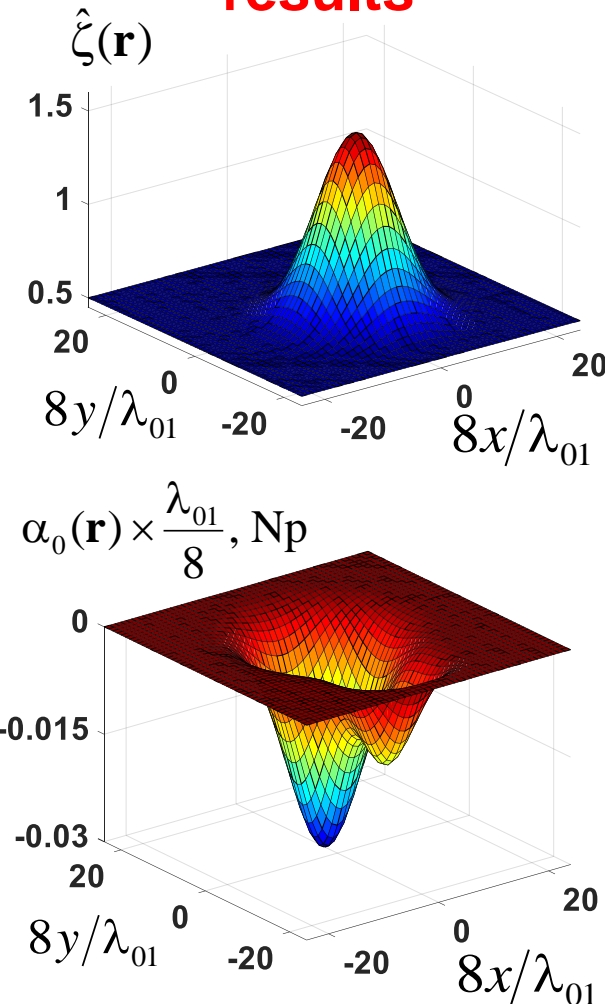


Reconstruction results obtained by using data on 2 frequencies, without noise

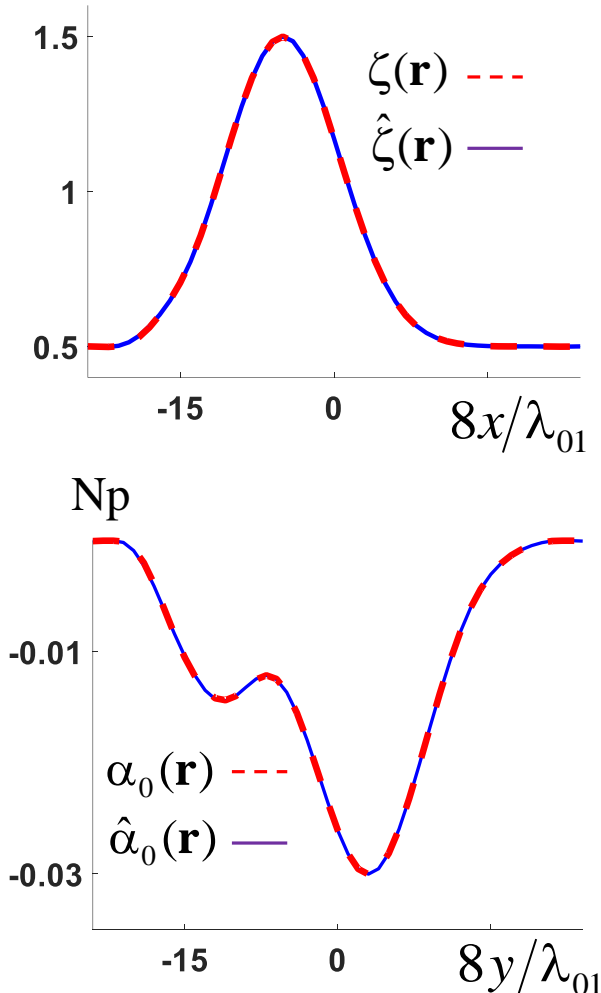
Model



Reconstruction results



Crosssections of model and result

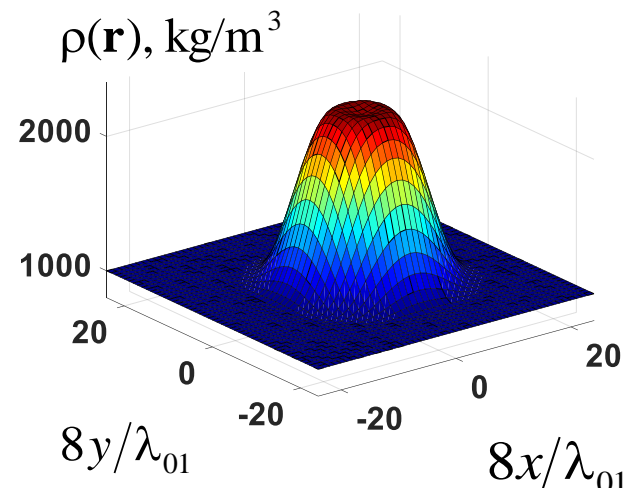
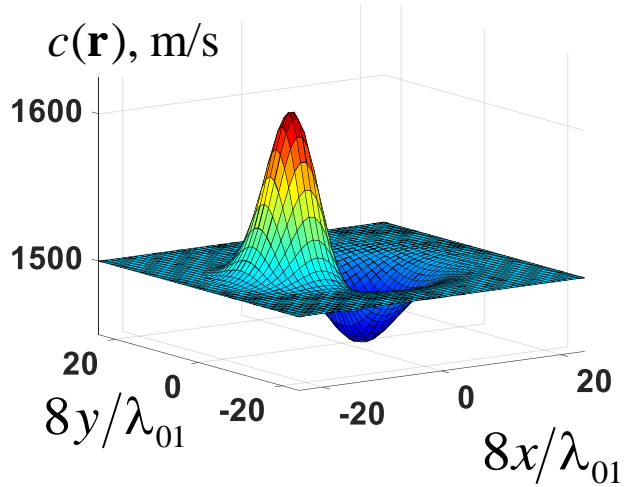


Influence of noise on reconstruction results

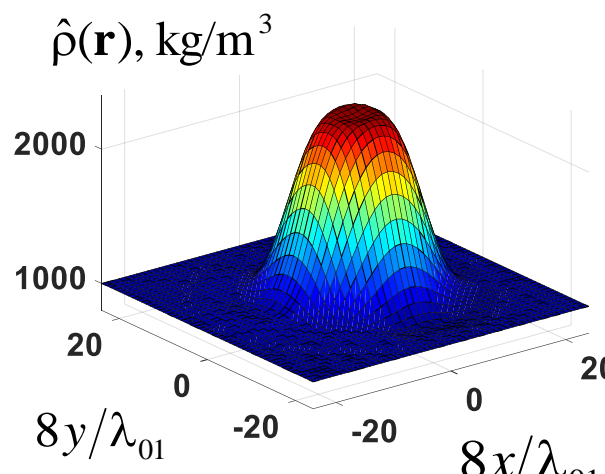
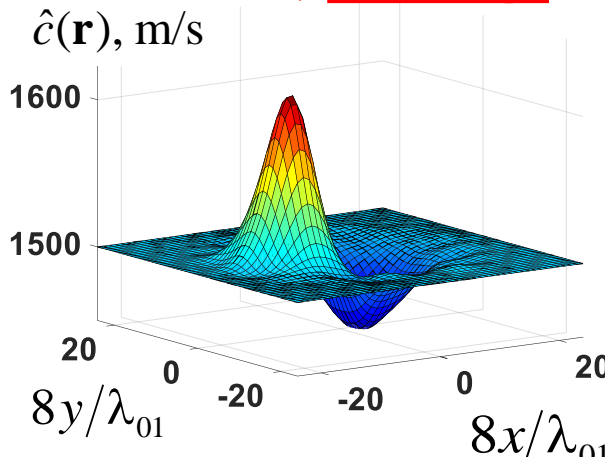
Normally distributed noise with
rms amplitude deviation

$$0.03 * \sqrt{\int_{\gamma} d\mathbf{x} \int_{\gamma} d\mathbf{y} \left| G_{sc}(\mathbf{y}, \mathbf{x}; \omega_j) \right|^2} / \int_{\gamma} d\mathbf{x} \int_{\gamma} d\mathbf{y}$$

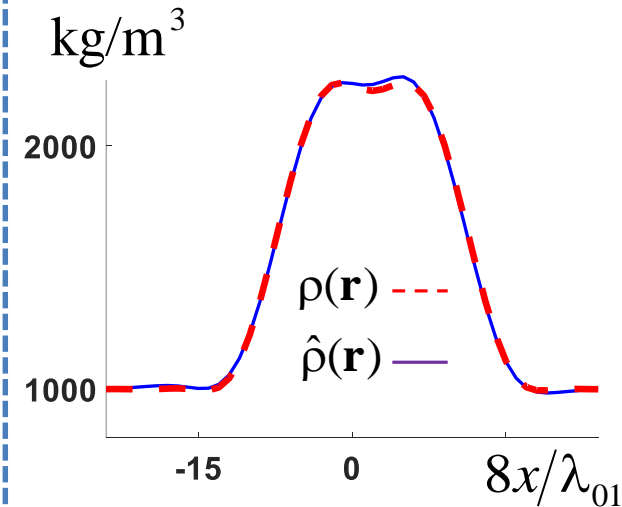
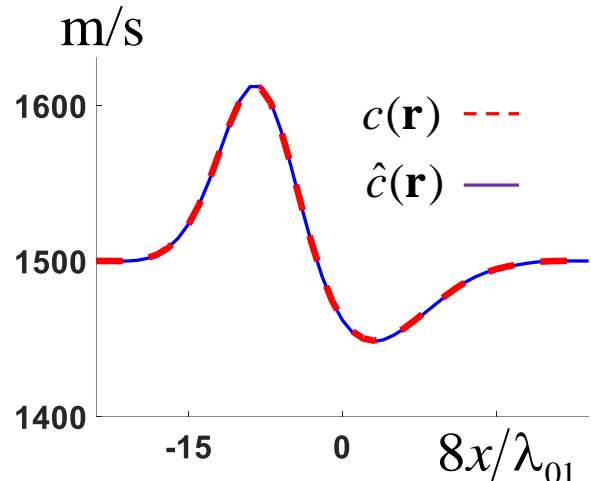
Model



Reconstruction results, 11 freqs

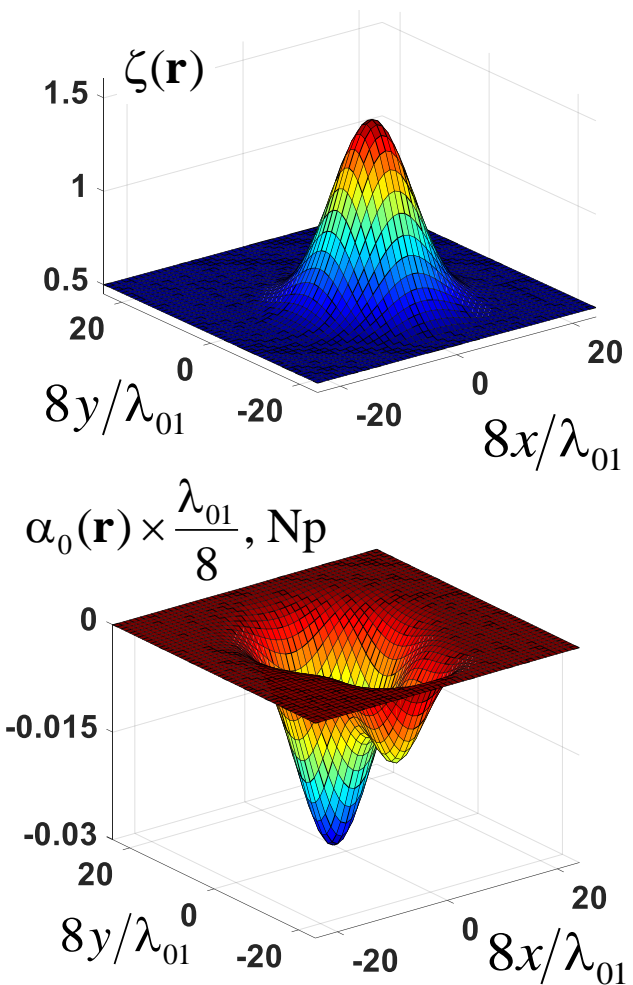


Crosssections of model and result

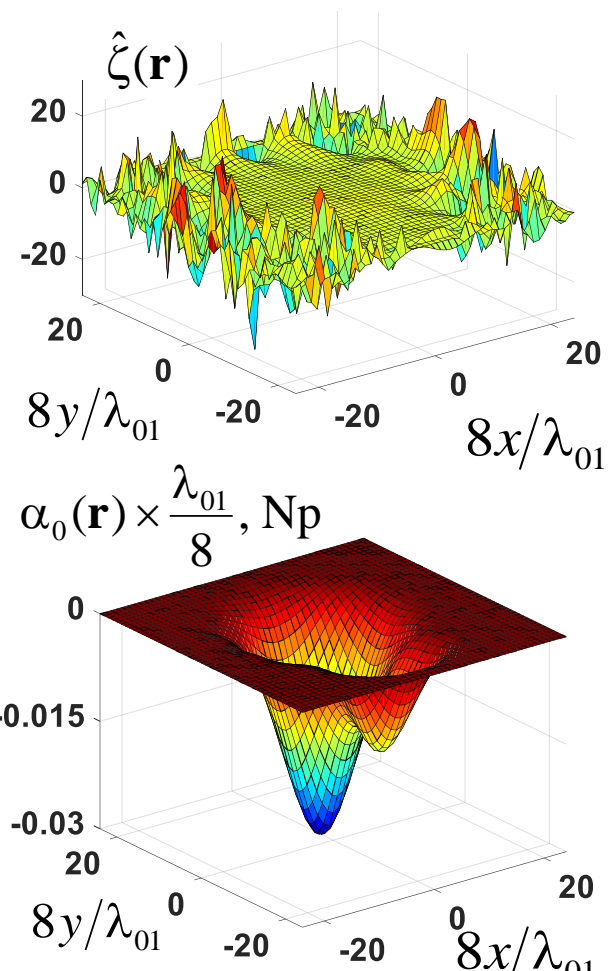


Reconstruction results obtained by using data on 11 frequencies, with noise

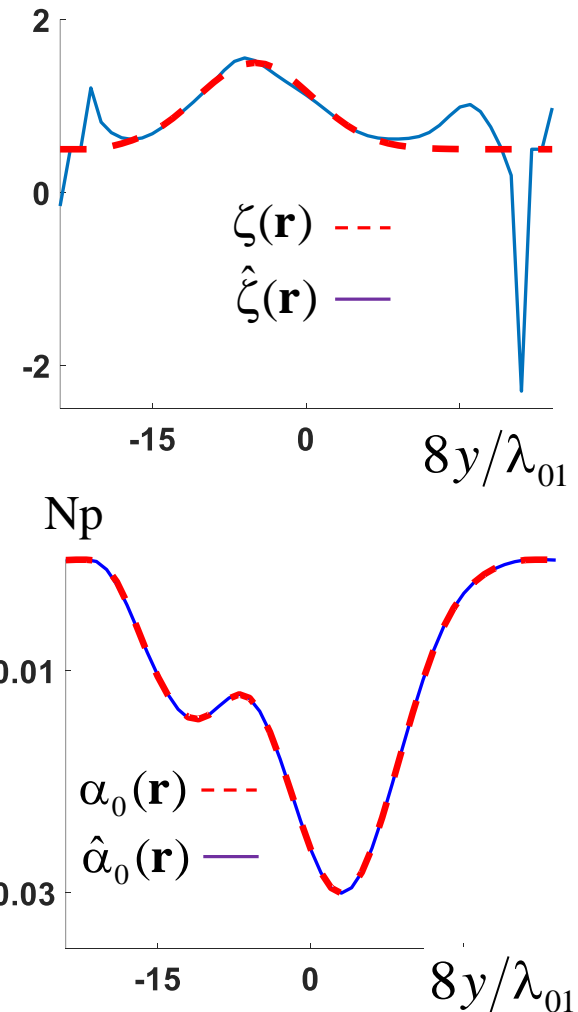
Model



Reconstruction results



Crossections of model and result



Improvements of $\zeta(\mathbf{r})$ reconstruction in multi frequency regime

$$\text{Im } Q(\mathbf{r}, \omega_j) = 2\omega_j \left(\frac{\omega_j}{\omega_0} \right)^{\zeta(\mathbf{r})} \frac{\alpha_0(\mathbf{r})}{c(\mathbf{r})}, \quad \rightarrow \quad \ln \left(\frac{\omega_j}{\omega_k} \right) [\zeta(\mathbf{r}) + 1] = \ln \left(\frac{\text{Im } Q(\mathbf{r}, \omega_j)}{\text{Im } Q(\mathbf{r}, \omega_k)} \right),$$

LSM estimation of $\zeta(\mathbf{r})$.

If $\alpha_0(\mathbf{r}) \rightarrow 0$, then it is impossible to reconstruct $\zeta(\mathbf{r})$ since

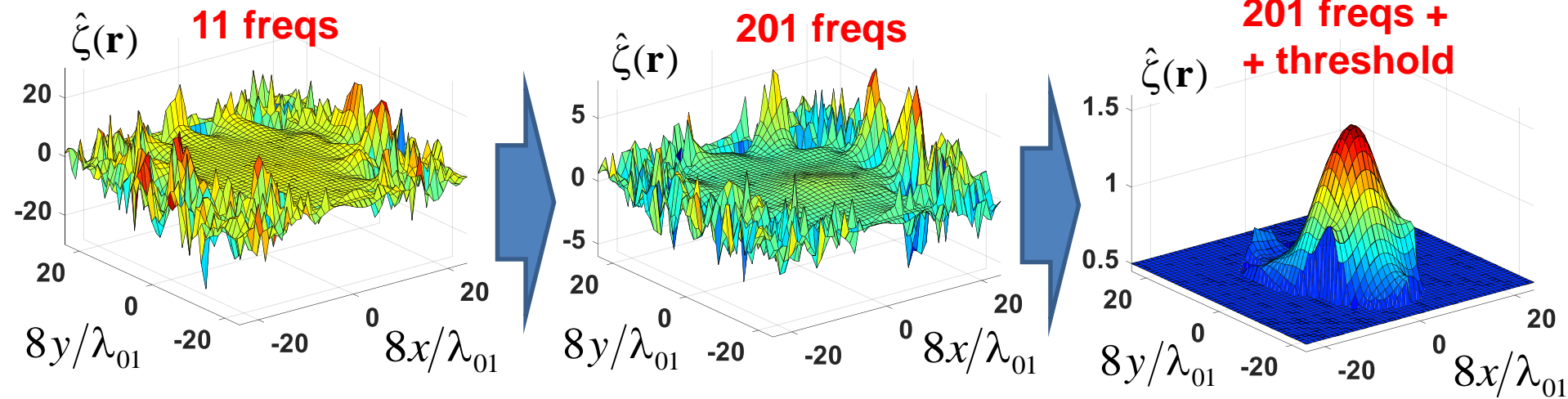
$$\frac{\text{Im } Q(\mathbf{r}, \omega_j)}{\omega_j} \cong \frac{\text{Im } Q(\mathbf{r}, \omega_k)}{\omega_k}, \text{ instabilities arrise in}$$

To exclude such points \mathbf{r} , the threshold Π can be applied:

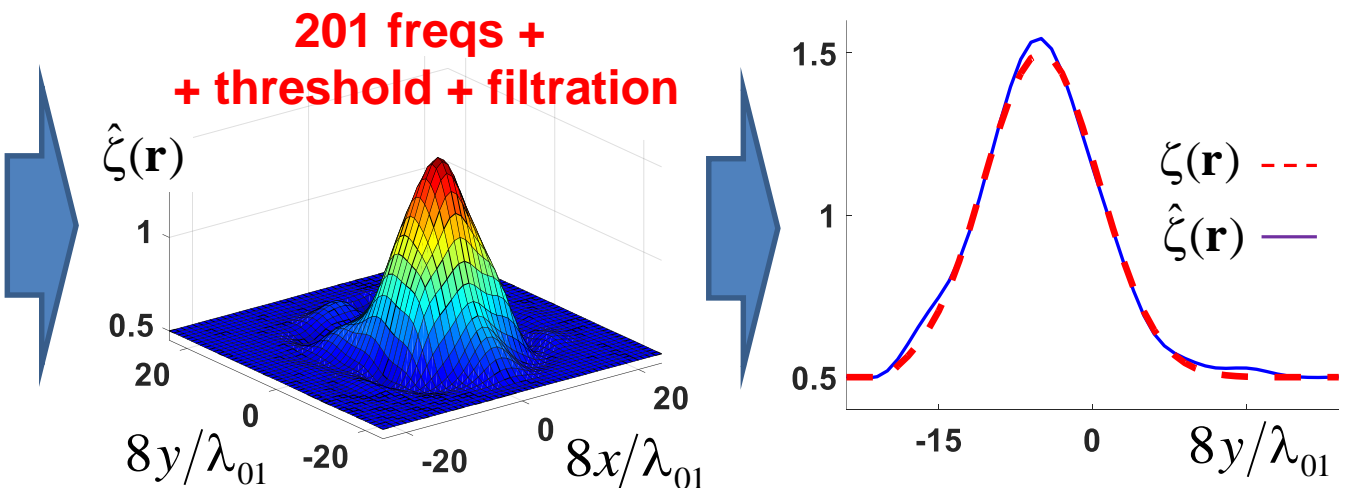
$$\left| \left\langle \frac{\text{Im } Q(\mathbf{r}, \omega_j)}{\omega_j} \right\rangle_j \right| \leq \Pi \cong 2 \frac{\bar{\alpha}_0^{\text{water}}}{c_0}$$

Acceptable reconstruction of $c(\mathbf{r})$
helps for acceptable reconstruction of $\alpha_0(\mathbf{r})$: $\alpha_0(\mathbf{r}) = \frac{c(\mathbf{r})}{2\omega_j} \text{ Im } Q(\mathbf{r}, \omega_j) \left(\frac{\omega_0}{\omega_j} \right)^{\zeta(\mathbf{r})}$

Improvements of $\zeta(\mathbf{r})$ reconstruction in multi frequency regime



Filtration:
• space-spectrum,
• background values.



*Reconstruction
of all medium properties*

$c(\mathbf{r})$, $\rho(\mathbf{r})$, $\alpha(\mathbf{r}, \omega_0)$, $\zeta(\mathbf{r})$, $\mathbf{v}(\mathbf{r})$

Reconstruction process

$$\begin{cases} \operatorname{Re} Q(\mathbf{r}, \omega_1) = f_1 - \omega_1^2 f_2, \\ \operatorname{Re} Q(\mathbf{r}, \omega_2) = f_1 - \omega_2^2 f_2, \\ \dots \end{cases} \quad \xrightarrow{\hspace{1cm}} \quad f_1, f_2 \quad \xrightarrow{\hspace{1cm}} \quad c(\mathbf{r}), \rho(\mathbf{r})$$

Procedure for the reconstruction of sound speed
and density is the same as for $c(\mathbf{r}), \rho(\mathbf{r}), \alpha(\mathbf{r}, \omega)$.

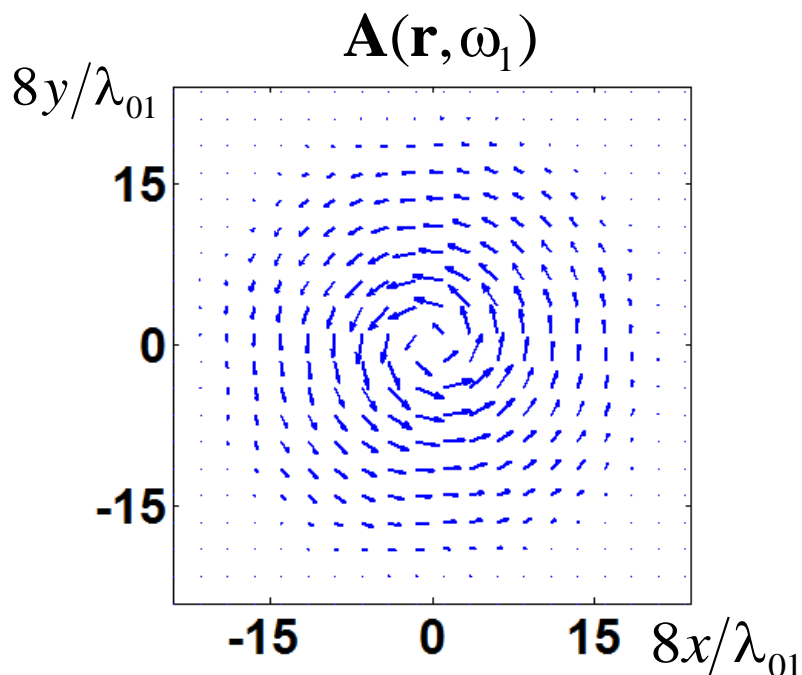
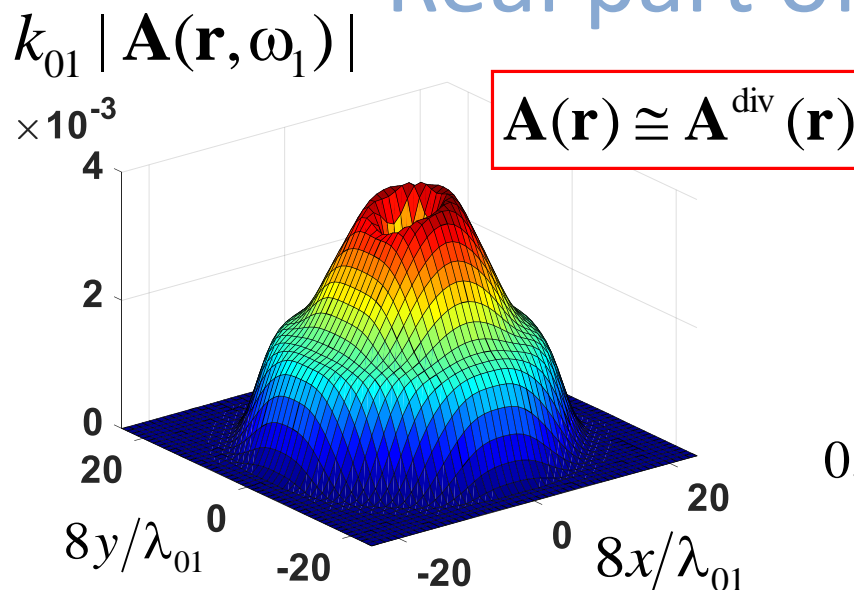
$$\mathbf{v}(\mathbf{r}) = \mathbf{v}^{\text{div}}(\mathbf{r}) + \mathbf{v}^{\text{rot}}(\mathbf{r}), \quad \operatorname{div} \mathbf{v}^{\text{div}} \equiv 0, \quad \operatorname{rot} \mathbf{v}^{\text{rot}} \equiv 0, \quad \mathbf{v}^{\text{div}}(\mathbf{r}) = c^2(\mathbf{r}) \frac{\mathbf{A}^{\text{div}}(\mathbf{r}, \omega_j)}{\omega_j}$$

If $\mathbf{v}(\mathbf{r}) \approx \mathbf{v}^{\text{div}}(\mathbf{r})$, $\frac{|\mathbf{v}|}{c} \ll 1$ (for example, this is valid in ocean applications),
then:

$$1. \quad \mathbf{v}(\mathbf{r}) \approx c^2(\mathbf{r}) \frac{\mathbf{A}^{\text{div}}(\mathbf{r}, \omega_j)}{\omega_j},$$

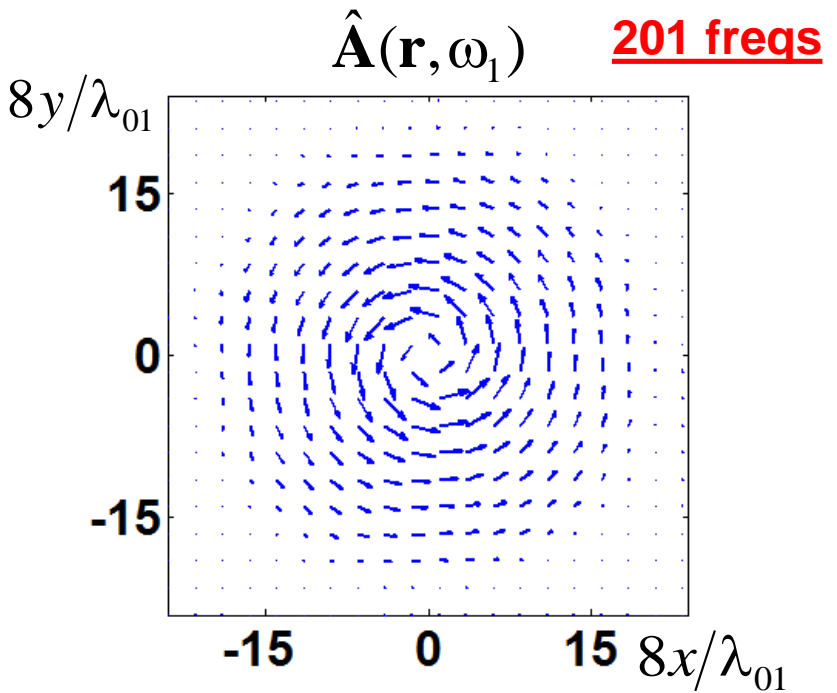
$$2. \quad \alpha_0(\mathbf{r}) \approx \frac{c(\mathbf{r})}{2\omega_j} \operatorname{Im} Q(\mathbf{r}, \omega_j) \left(\frac{\omega_0}{\omega_j} \right)^{\bar{\zeta}}, \quad \text{if} \quad \nabla \cdot \frac{\mathbf{v}(\mathbf{r})}{c^2(\mathbf{r})} - \frac{\mathbf{v}(\mathbf{r}) \cdot \nabla \ln \rho(\mathbf{r})}{c^2(\mathbf{r})} \ll \frac{\alpha(\mathbf{r}, \omega)}{c(\mathbf{r})}$$

Real part of vector inhomogeneity with the vortex form



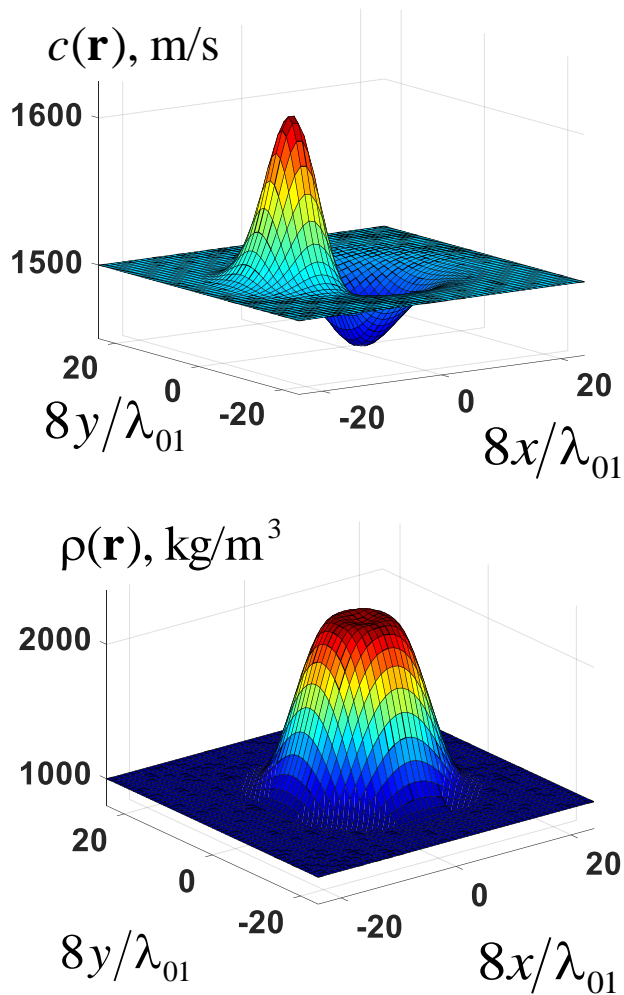
Model
Reconstruction
results

$$0.03 * \sqrt{\int_{\gamma} d\mathbf{x} \int_{\gamma} d\mathbf{y} |G_{sc}(\mathbf{y}, \mathbf{x}; \omega_j)|^2} / \int_{\gamma} d\mathbf{x} \int_{\gamma} d\mathbf{y}$$

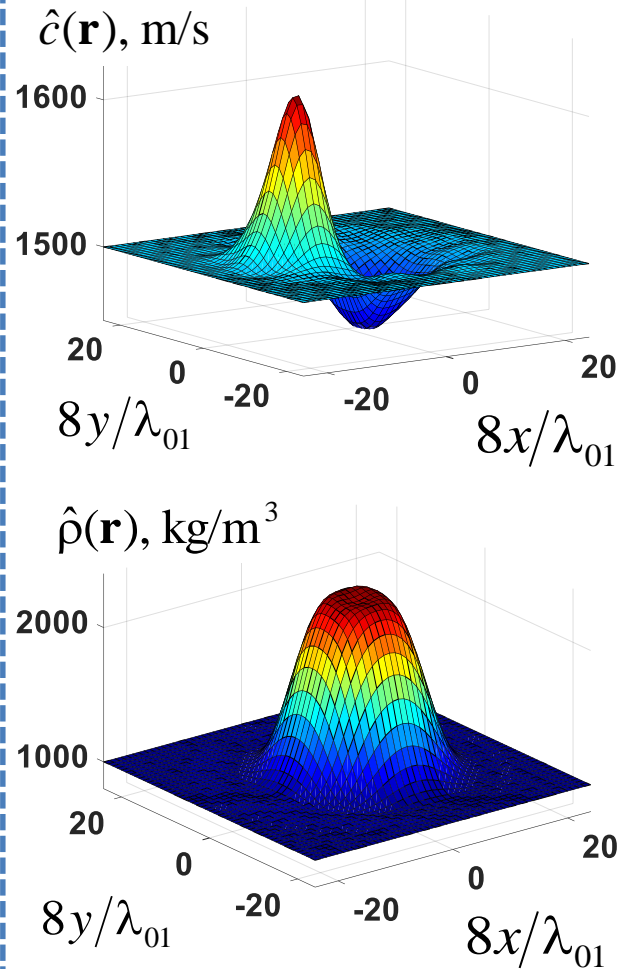


Reconstruction results obtained by using data on 201 frequencies, with noise

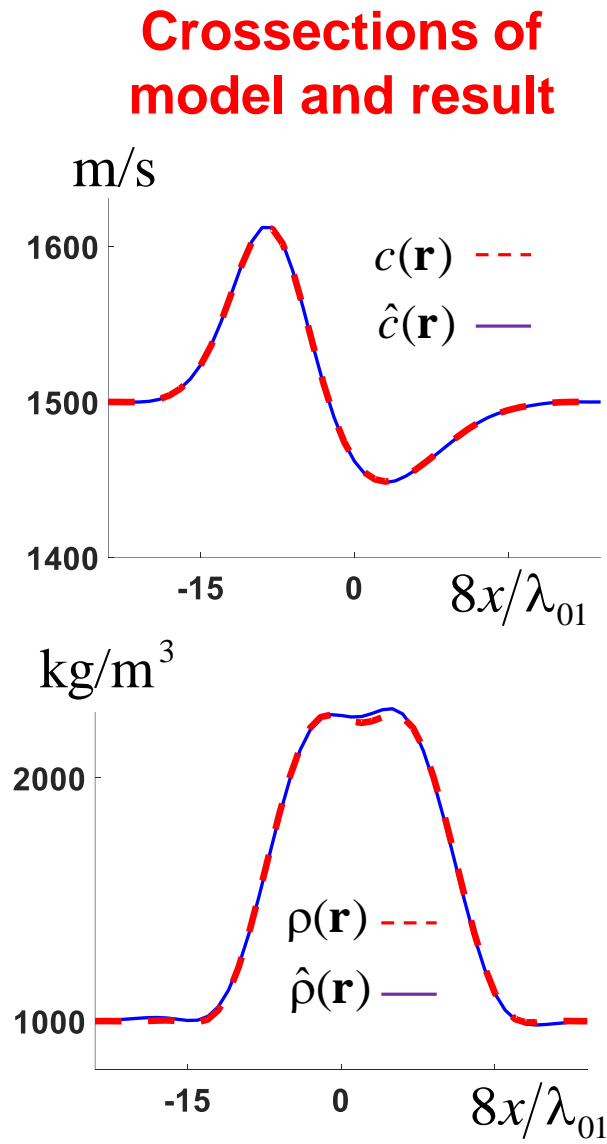
Model



Reconstruction results

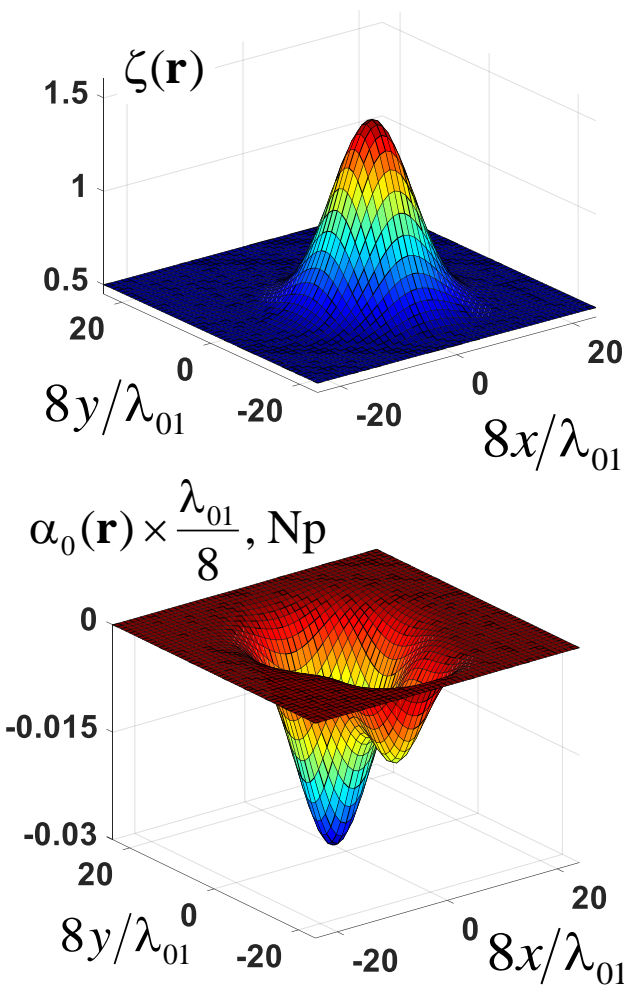


Crossections of model and result

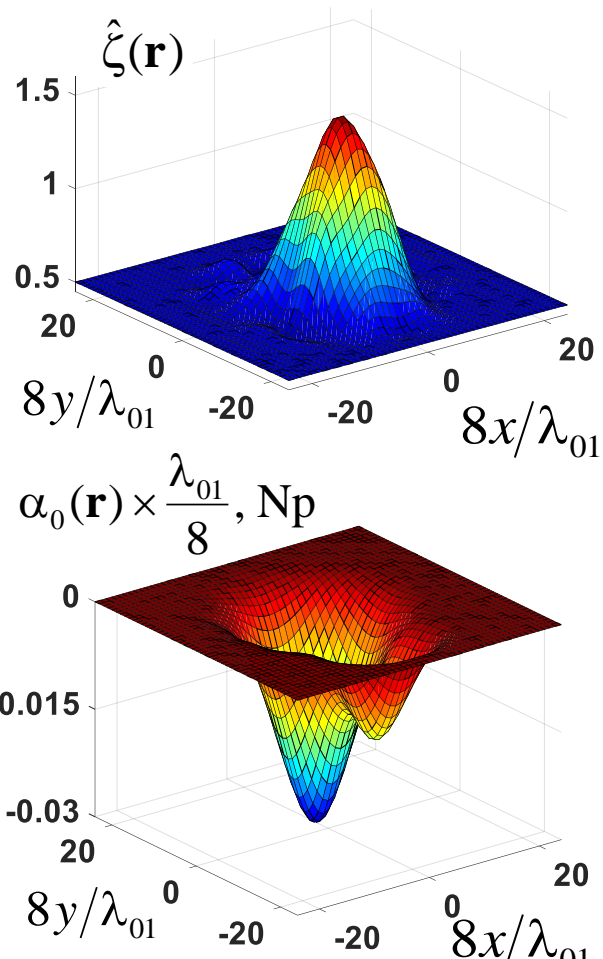


Reconstruction results obtained by using data on 201 frequencies, with noise

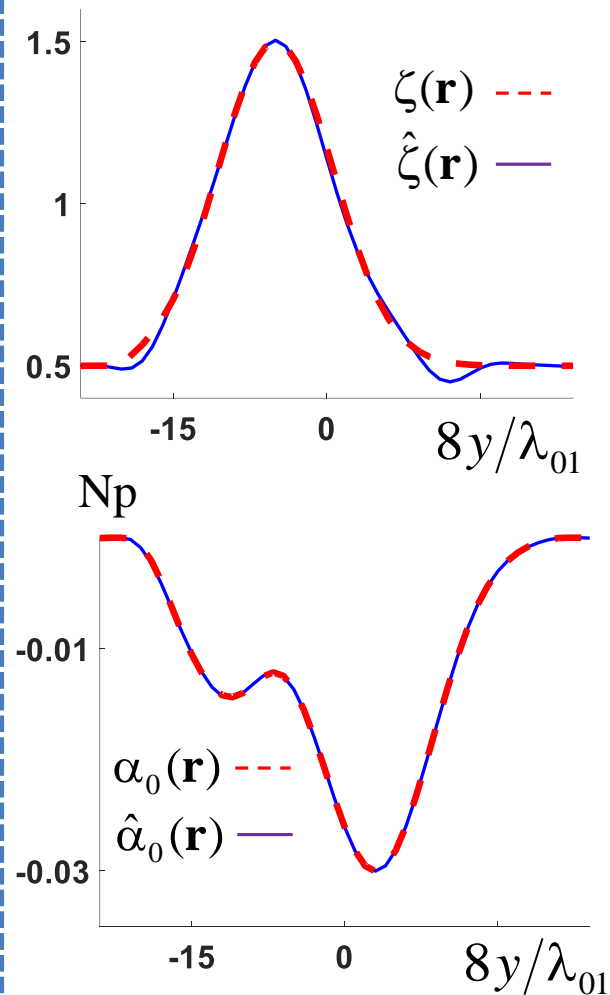
Model



Reconstruction results



Crosssections of model and result



Conclusions for 2D problem

1. The considered algorithm of the joint reconstruction of different scatterer's components based on the Novikov-Agaltsov algorithm, shows a high resolution and good noise stability, that makes it perspective for the development of practical schemes of acoustic tomography in different applications such as:
 - reconstruction of $c(\mathbf{r})$, $\rho(\mathbf{r})$, $\alpha_0(\mathbf{r})$, $\zeta(\mathbf{r})$ in medical diagnostics, when influence of flows can be negligible,
 - reconstruction of $c(\mathbf{r})$, $\rho(\mathbf{r})$, $\alpha_0(\mathbf{r})$, $\zeta(\mathbf{r})$, $\mathbf{v}(\mathbf{r})$ in ocean applications, when $\mathbf{v}(\mathbf{r}) \approx \mathbf{v}^{\text{div}}(\mathbf{r})$, $|\mathbf{v}|/c \ll 1$.
2. Numerical modeling shows the better noise stability for the reconstruction of $c(\mathbf{r})$, $\rho(\mathbf{r})$, $\alpha_0(\mathbf{r})$, $\mathbf{v}^{\text{div}}(\mathbf{r})$, while $\zeta(\mathbf{r})$, $\mathbf{v}^{\text{rot}}(\mathbf{r})$ requires additional multi frequency scattering data and a priory information about reconstructed functions.

3D inverse problem.
Ocean Acoustic Tomography

Acoustic field in ocean waveguide as a sum of normal modes

$$\nabla^2 p(\mathbf{r}, z) + k_0^2 p(\mathbf{r}, z) = 0$$

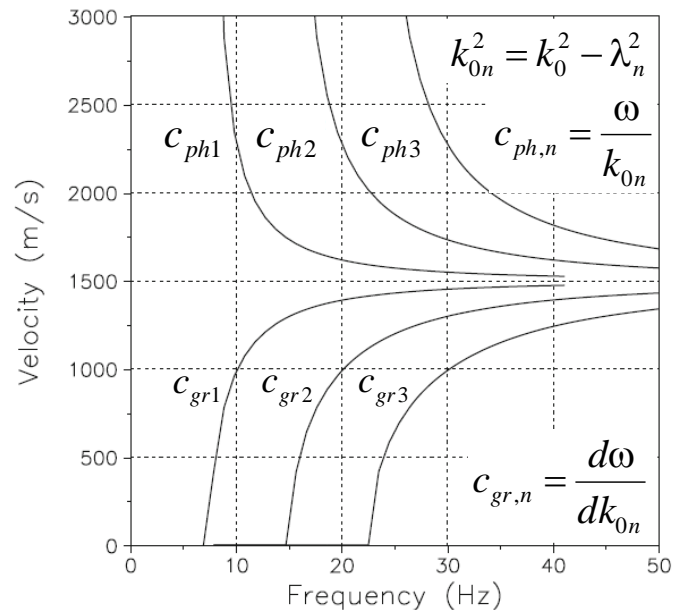
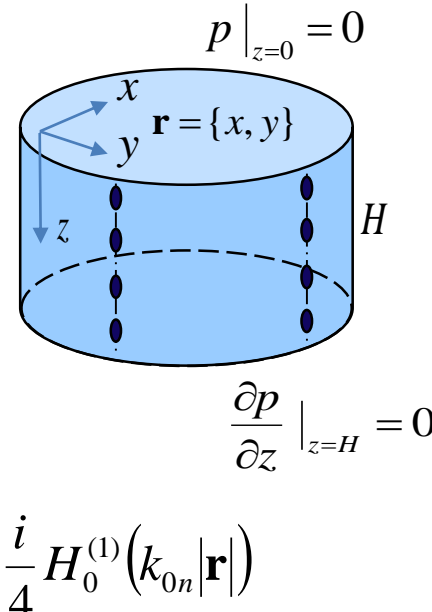
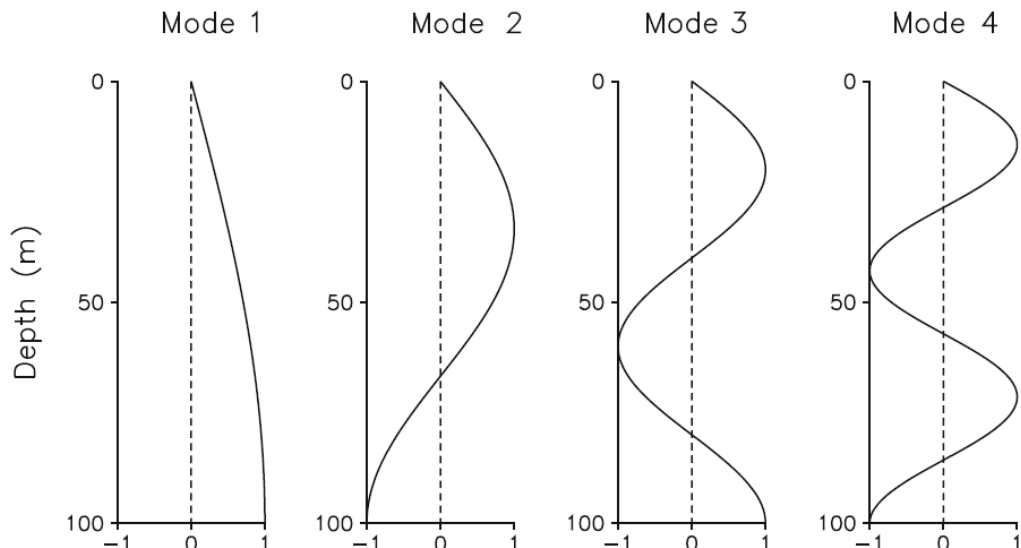
$$p(\mathbf{r}, z) = \sum_{n=1}^{\infty} \psi_n(\mathbf{r}) \phi_n(z)$$

$$\begin{cases} \frac{d\phi_n}{dz} + \lambda_n^2 \phi_n = 0, \\ + b.c. \end{cases}$$

$$\phi_n(z) = \sqrt{\frac{2}{H}} \sin(\lambda_n z)$$

$$\lambda_n = \frac{\pi}{H} \left(n - \frac{1}{2} \right), \quad n = 1, 2, \dots$$

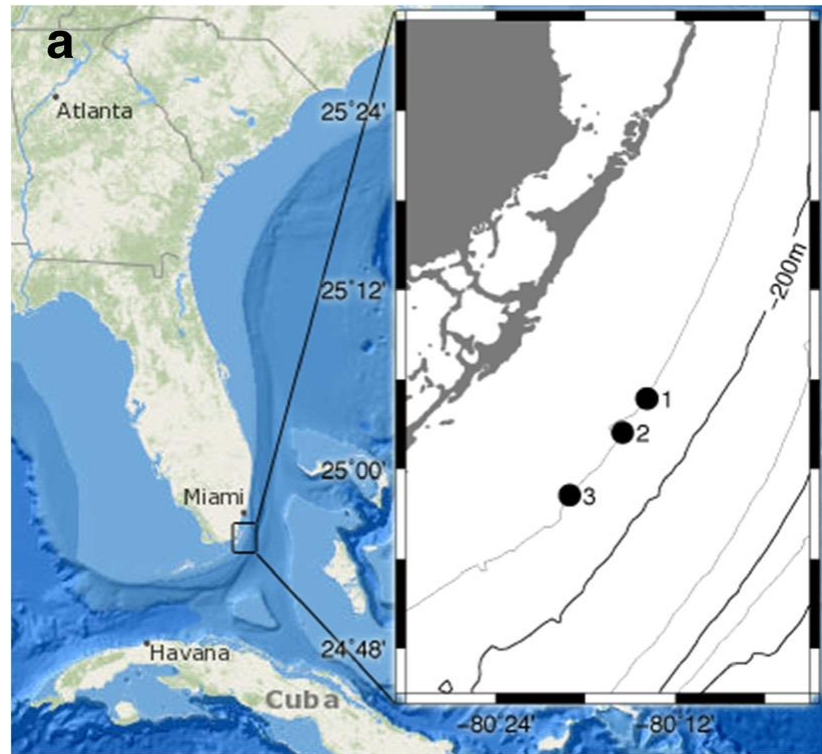
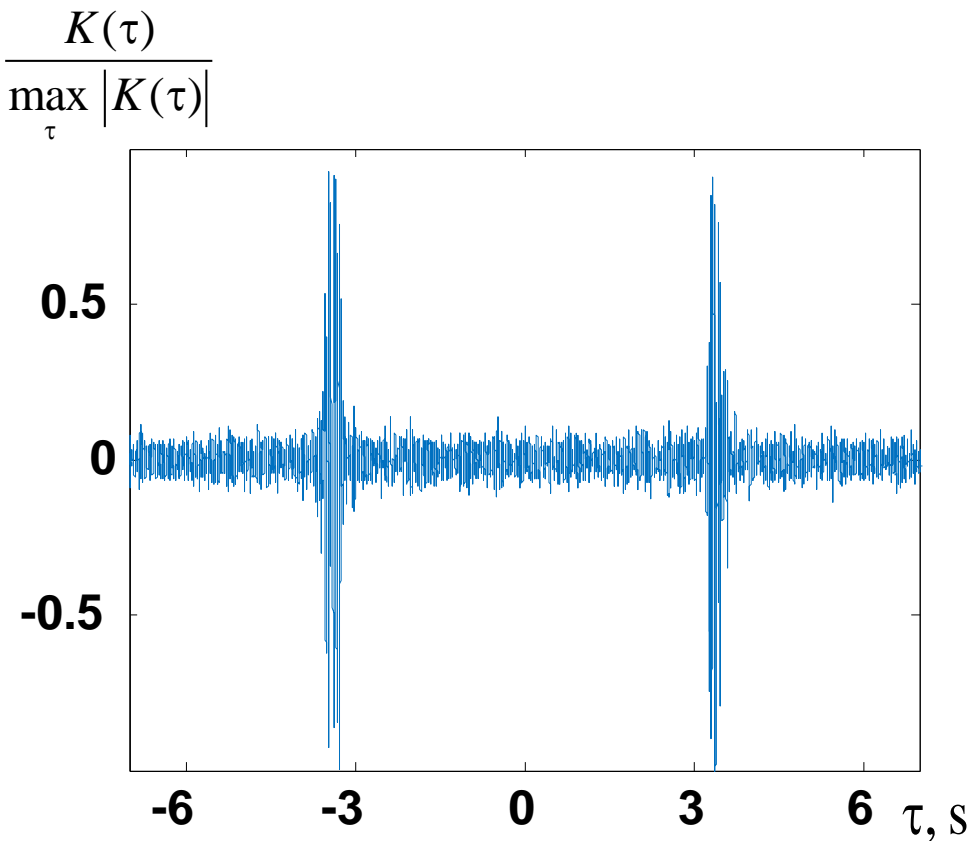
$$-\frac{i}{4} H_0^{(1)}(k_{0n} |\mathbf{r}|)$$



Experimental observations of hydroacoustic modes

Mode selection in the **Experiment in Florida Straits (*)**

Cross-correlation function between two hydrophones in frequency branch 10-110 Hz. Accumulation time – 6 days



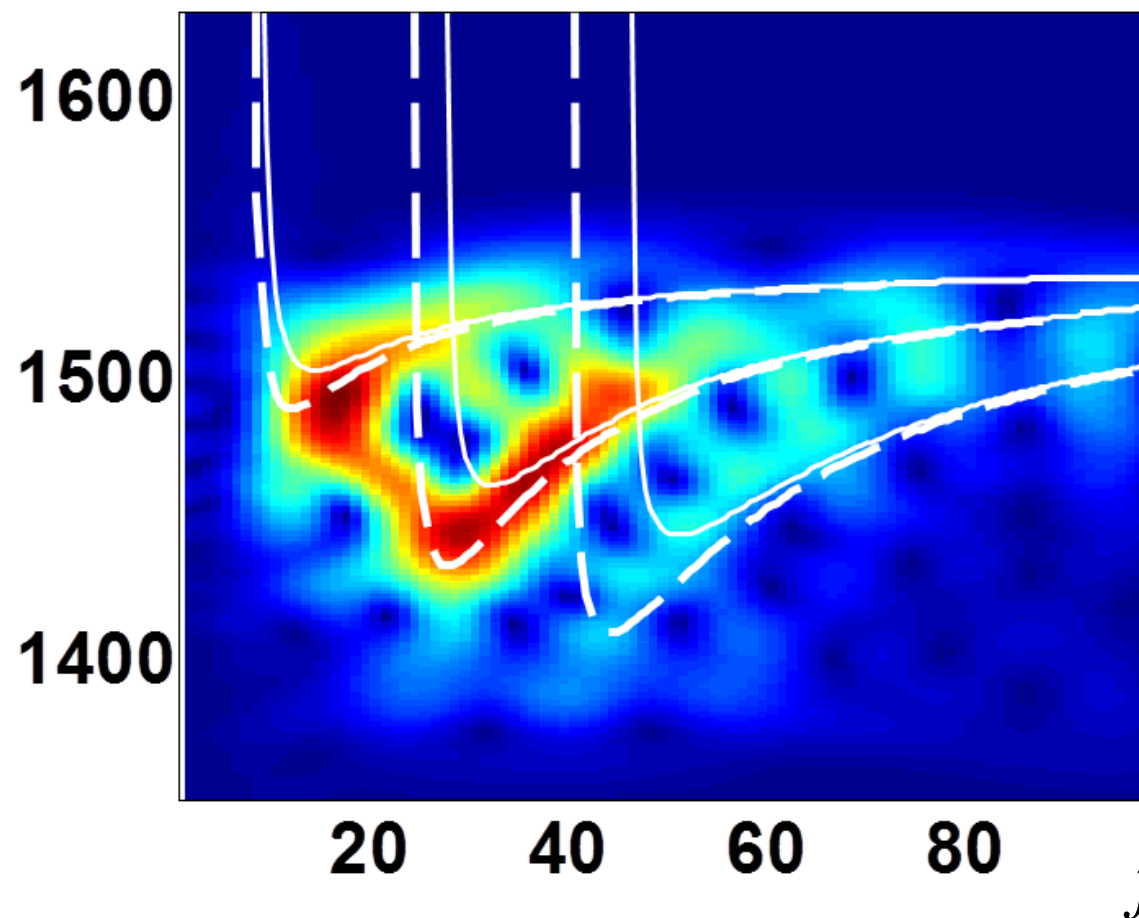
Peaks of cross-correlation function correspond to acoustic signals as if they were emitted and received by receivers.

(*) Sergeev S.N., Shurup A.S., Godin O.A., Vedenev A.I., Goncharov, etc. *Acoustical Physics*. 2017. V. 63. N 1. P. 76-85.

Spectrogram of correlation function

$$K_{\text{sp}}(\tau', f) = \int_{-T}^{+T} K(\tau) \underbrace{h(\tau - \tau')}_{0.1 \text{ s}} \exp(-i 2\pi f \tau) d\tau$$

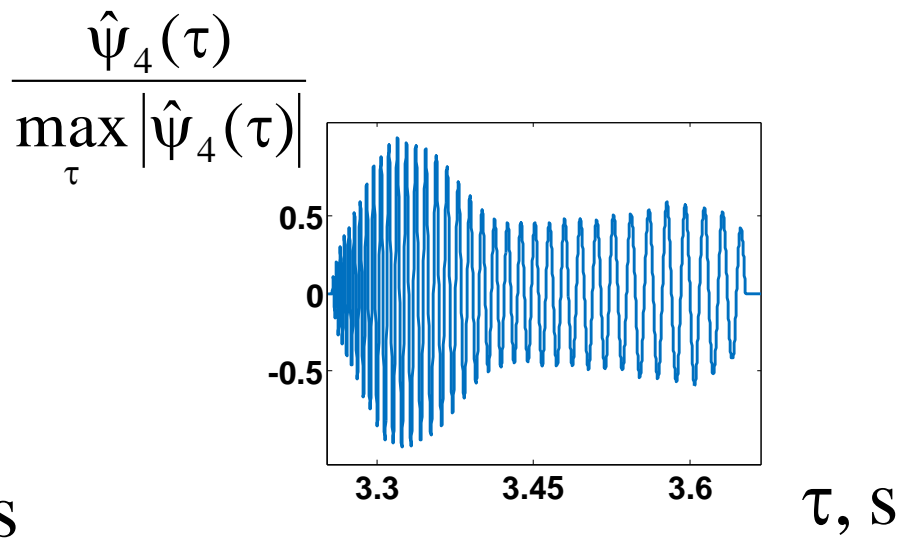
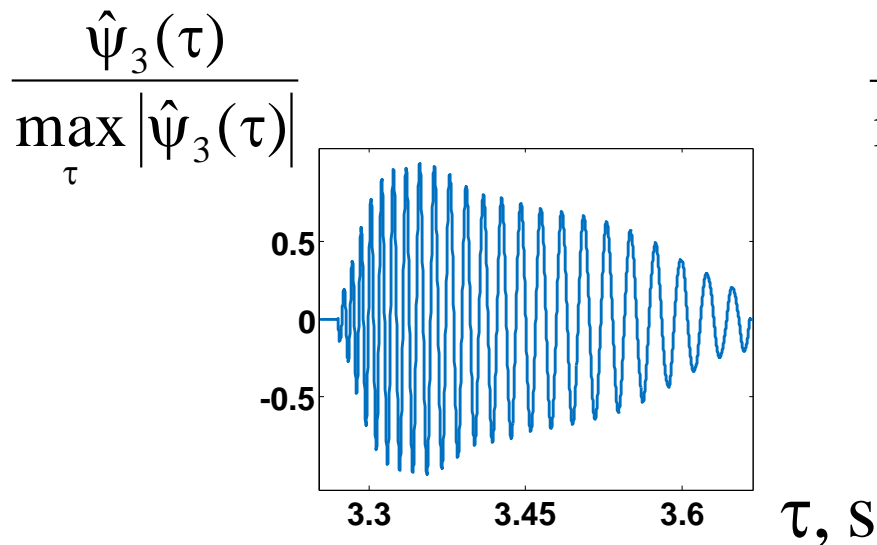
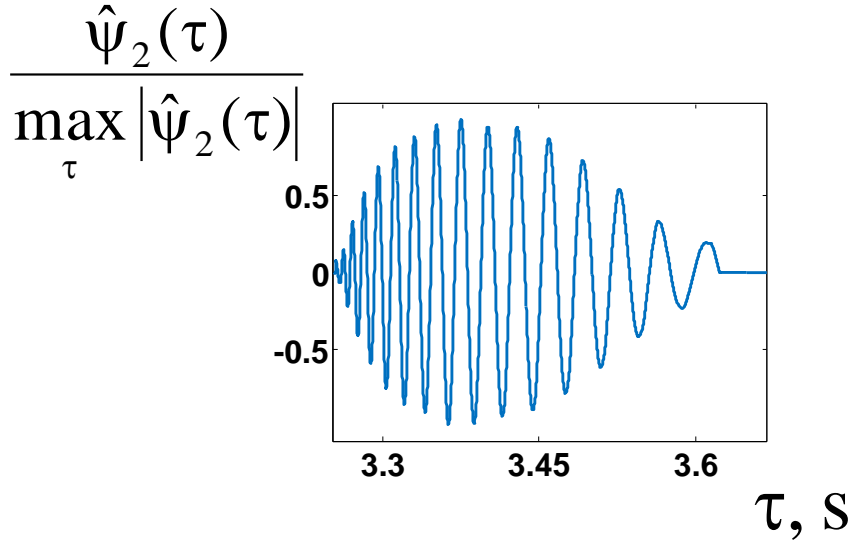
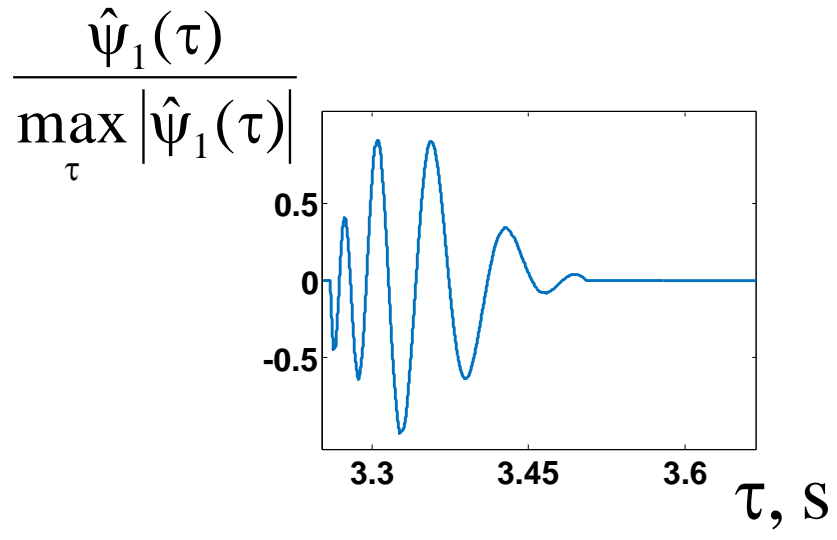
c' , m/s



$$\frac{|K_{\text{sp}}(c', f)|}{\max_{c', f} |K_{\text{sp}}(c', f)|}$$

The white lines show theoretical dispersion curves calculated for the expected parameters of ocean waveguide.

Signals in time of different modes normalized on its maximum values



Adiabatic approximation and nonadiabatic (multi-channel) propagation

$$\nabla^2 p(\mathbf{r}, z) + k_0^2 p(\mathbf{r}, z) = v(\mathbf{r}, z) p(\mathbf{r}, z)$$

$$v(\mathbf{r}, z) = \omega^2 \left(\frac{1}{c_0^2} - \frac{1}{c^2(\mathbf{r}, z)} \right)$$

$$p(\mathbf{r}, z) = \sum_{n=1}^{\infty} \psi_n(\mathbf{r}) \phi_n(z)$$

$$\begin{cases} \frac{d\phi_n}{dz} + \lambda_n^2 \phi_n = 0, \\ + b.c. \end{cases} \quad \Rightarrow \quad \phi_n(z) = \sqrt{\frac{2}{H}} \sin(\lambda_n z)$$

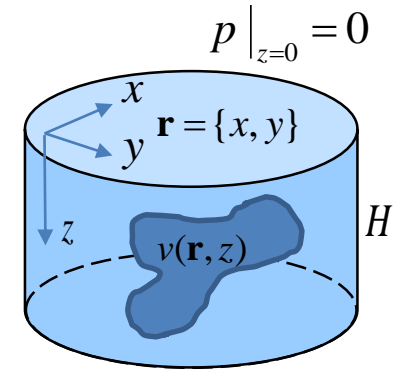
$$\lambda_n = \frac{\pi}{H} \left(n - \frac{1}{2} \right), \quad n = 1, 2, \dots, \quad k_{0n}^2 = k_0^2 - \lambda_n^2$$

$$\nabla^2 \psi_n(\mathbf{r}) + k_{0n}^2 \psi_n(\mathbf{r}) = S_{nm}(\mathbf{r}) \psi_m(\mathbf{r}), \quad S_{nm}(\mathbf{r}) = \int_0^H \phi_n(z) v(\mathbf{r}, z) \phi_m(z) dz$$

multi-channel scattering

If $S_{nm}(\mathbf{r}) = 0$, for $n \neq m$, then each mode propagates independently.

In this case 3D problem of acoustic signal propagation is splitted into 2D problems for individual modes - **adiabatic approximation**.



Statement of 3D scalar problem

It is assumed that the investigated area is surrounded over perimeter by the vertical antennas (quasi-point in horizontal plane) emitting and receiving acoustic modes $\psi_n(\mathbf{r})$ of different numbers.

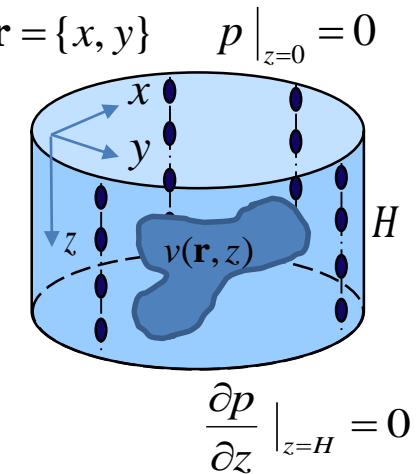
Others ways of emitting and receiving of modes are also possible.

In the tomographic area there is an unknown **scalar inhomogeneity**

$$v(\mathbf{r}, z, \omega_j) = \omega_j^2 \left(\frac{1}{c_0^2} - \frac{1}{c^2(\mathbf{r}, z)} \right),$$

ω – circular frequency, c_0 – known background sound speed value,
 $c(\mathbf{r}, z)$ – unknown sound speed space distribution.

How to reconstruct inhomogeneity $v(\mathbf{r}, z, \omega_j)$, if we know sufficiently large number of acoustic modes $\psi_n(\mathbf{r})$?



Solution of 3D problem

Acoustic modes in the considered area satisfy Helmholtz equation

$$\nabla^2 \psi_n(\mathbf{r}) + k_{0n}^2 \psi_n(\mathbf{r}) = S_{nm}(\mathbf{r}) \psi_m(\mathbf{r}), \quad S_{nm}(\mathbf{r}) = \int_0^H \phi_n(z) v(\mathbf{r}, z) \phi_m(z) dz$$

which can be rewritten in the form

$$\nabla^2 \psi_n(\mathbf{r}) + k_0^2 \psi_n(\mathbf{r}) = V_{nm}(\mathbf{r}) \psi_m(\mathbf{r}), \quad V_{nm}(\mathbf{r}) = [k_0^2 - k_{0n}^2] \delta_{nm} + S_{nm}(\mathbf{r})$$

The algorithm how to get the approximate solution of this rewritten equation is regarded in (*). This algorithm allows us to estimate the inhomogeneity $V_{nm}(\mathbf{r})$ by using **the similar integral equations as in 2D algorithm** considered in details before.

The main difference with 2D problem is that in 3D problem all functions used in reconstruction are matrix-valued.

(*) Novikov R.G., Santacesaria M. International Mathematics Research Notices. 2013. V. 2013. N 6. P. 1205–1229.

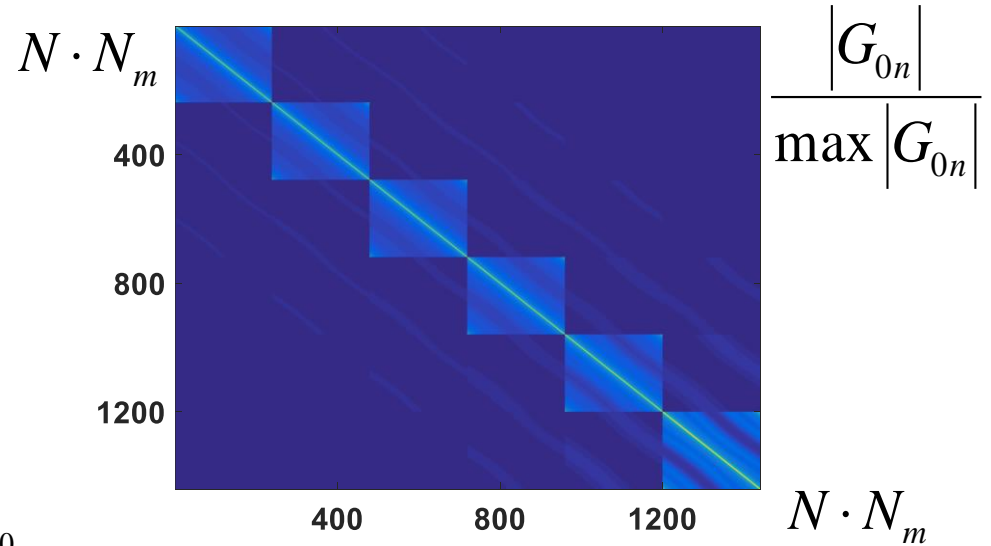
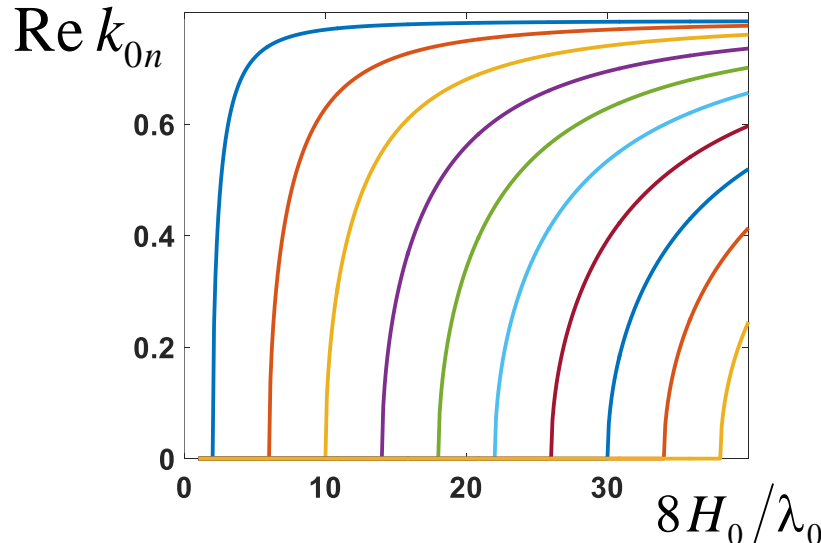
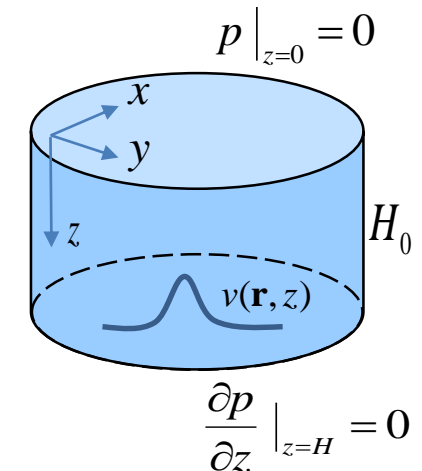
Numerical modeling of Nonadiabatic Mode Tomography with functional algorithm

Inhomogeneity in the form of a mount on the bottom:

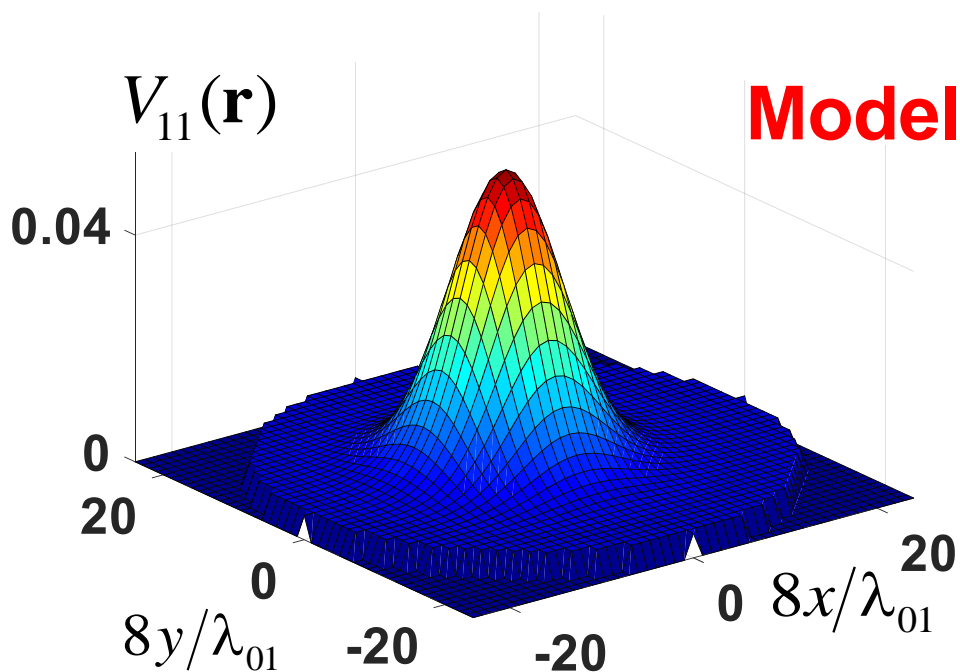
$$H = H(x, y) \rightarrow S_{nm}(\mathbf{r}) = k_0^2 \int_{H(x,y)}^{H_0} \phi_n(z) \phi_m(z) dz$$

$\lambda_0 = 2\pi/k_0 = 8$ relative units of length,

$H_0/\lambda_0 = 3 \rightarrow 6$ propagating modes (i.e. 6 channels are open)



Numerical modeling of Nonadiabatic Mode Tomography with functional algorithm

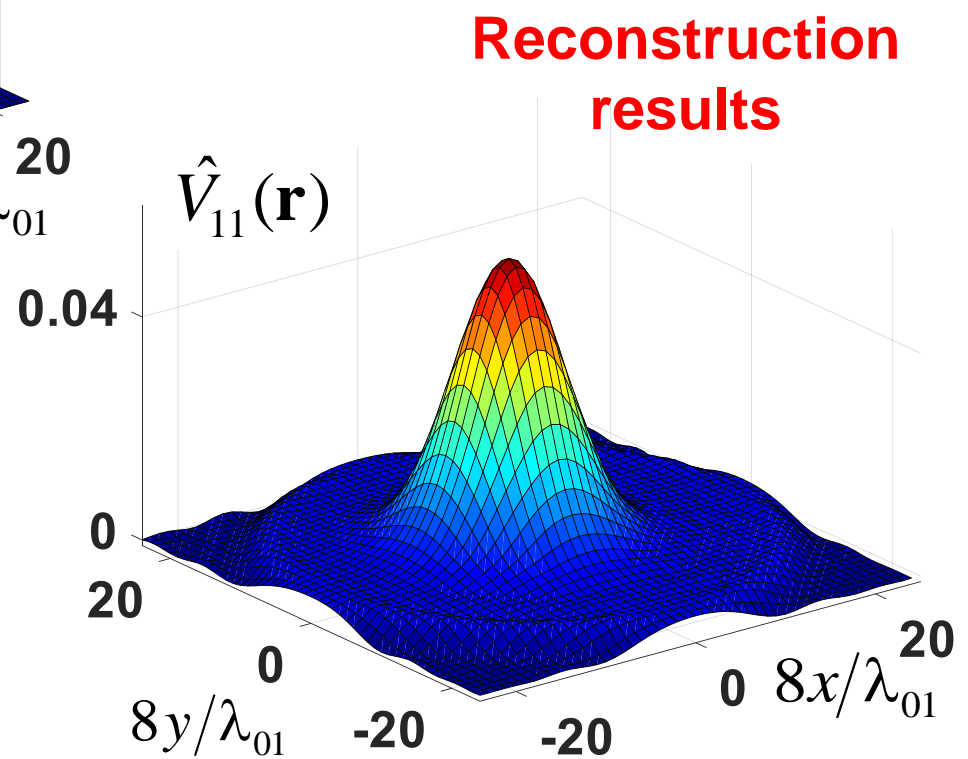


Model

Additional phase shifts:

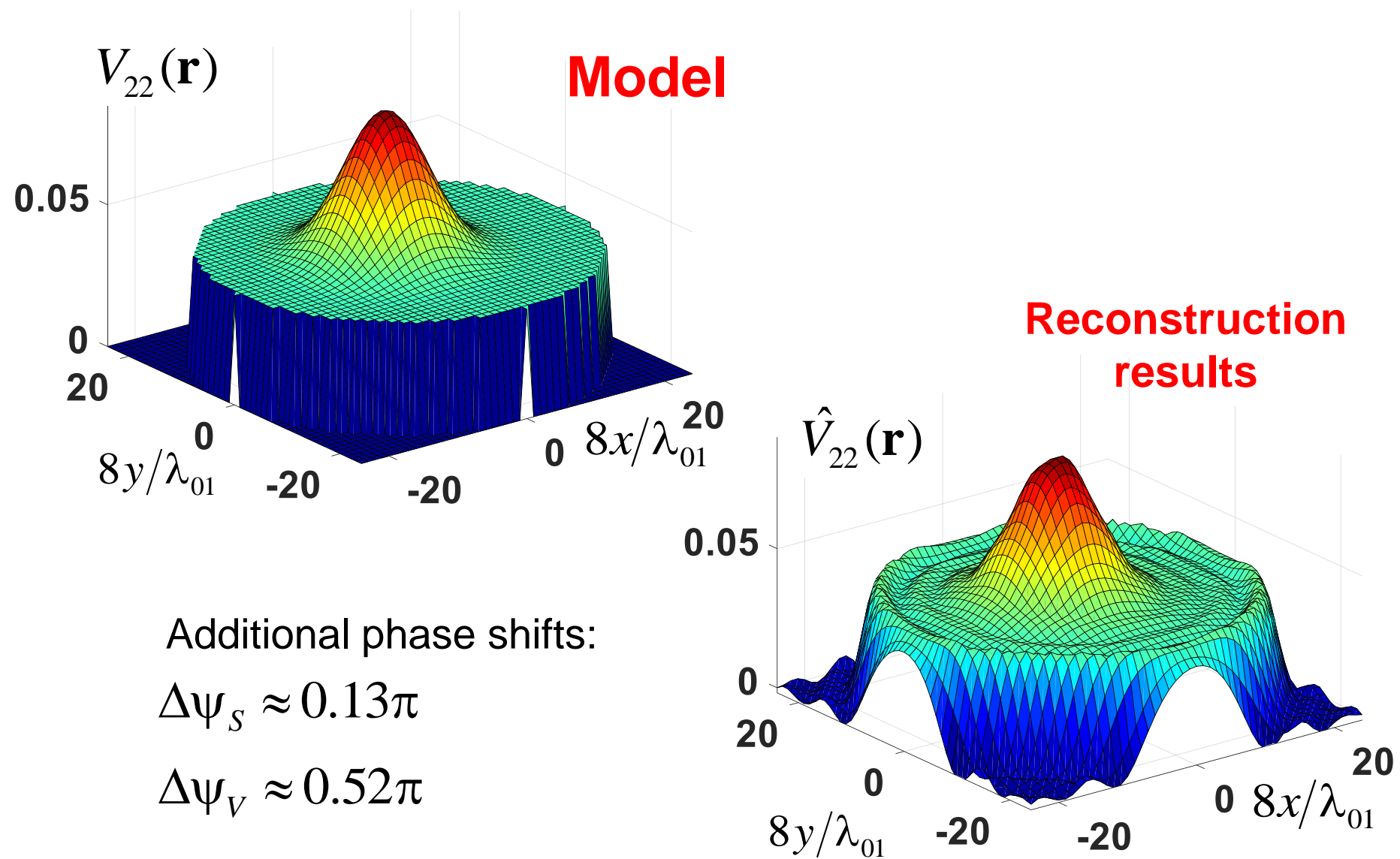
$$\Delta\psi_s \approx 0.13\pi$$

$$\Delta\psi_v \approx 0.17\pi$$

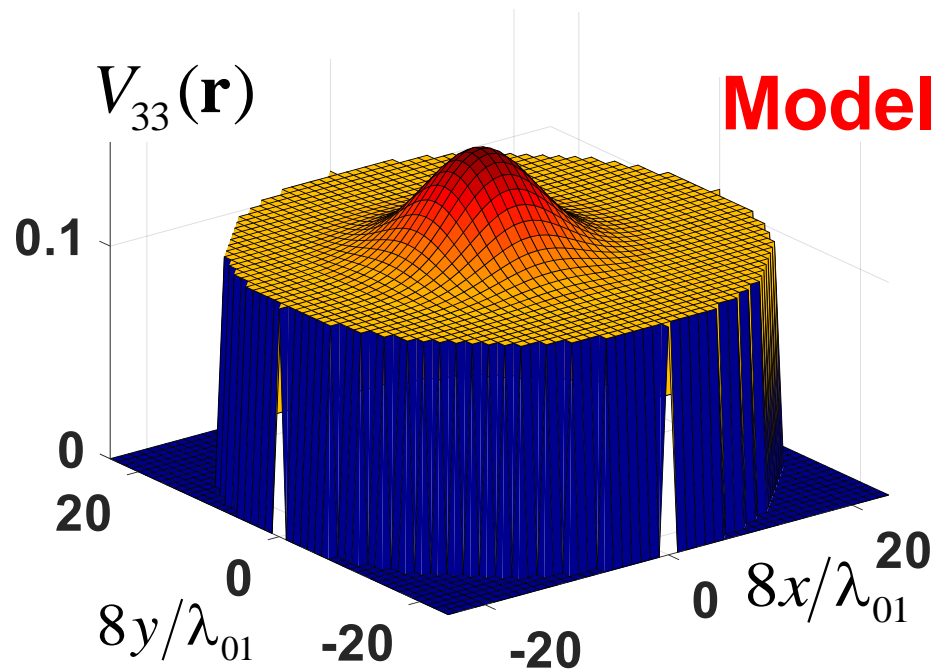


Reconstruction
results

Numerical modeling of Nonadiabatic Mode Tomography with functional algorithm



Numerical modeling of Nonadiabatic Mode Tomography with functional algorithm

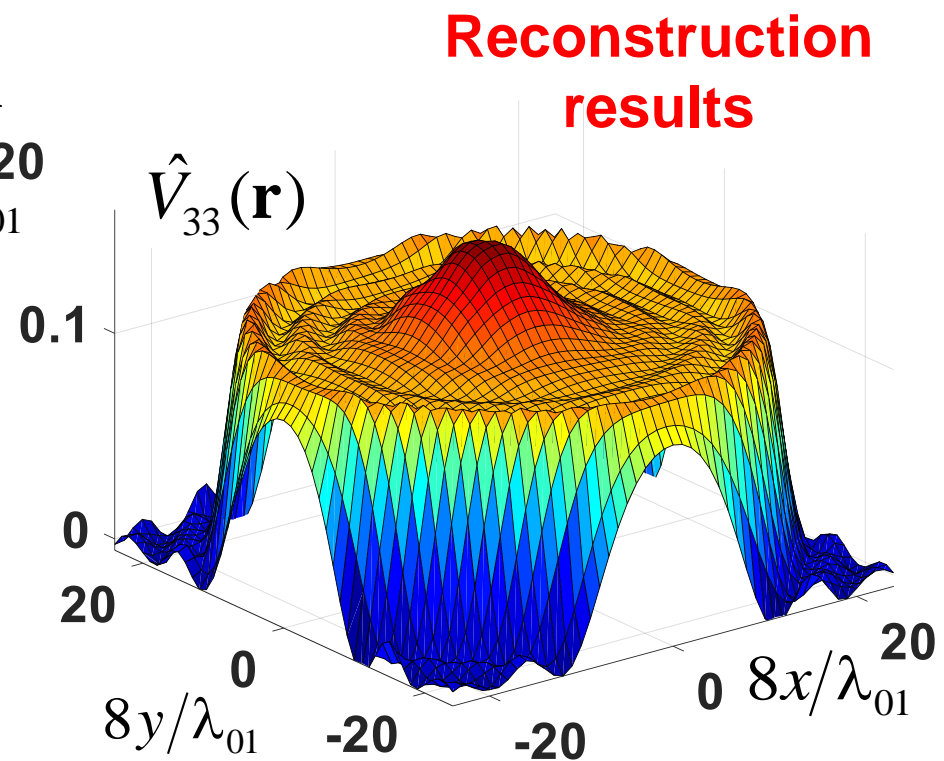


Model

Additional phase shifts:

$$\Delta\psi_s \approx 0.13\pi$$

$$\Delta\psi_v \approx 1.23\pi$$



Reconstruction
results

Conclusions

1. The considered functional algorithm has a high resolution and good noise stability, which can be acceptable for practical purposes, for example, in ultrasonic acoustic tomography of the scalar and vector inhomogeneities.
2. The use of the considered functional algorithm is well combined with the geometry and the measurement abilities of the developing acoustic tomograph.
3. Computational operations of this algorithm is well parallelized and allow acceleration of the data processing, which gives opportunities to solve practical problems with real dimensions at acceptable times.
4. Both monochromatic and multifrequency regimes for the considered algorithm are possible that is important for the practical applications in the acoustic tomography.
5. The further detailed numerical investigation is required for 3D algorithm for understanding its perspectives and limitations in nonadiabatic ocean tomography problems.

THANK YOU FOR YOUR ATTENTION!